

TECHNISCHE UNIVERSITÄT MÜNCHEN

Fachgebiet Molekulare Katalyse

**Organorhenium and Organomolybdenum Oxides:
Synthesis and Application as Olefin Epoxidation Catalysts**

Simone Antonia Hauser

Vollständiger Abdruck der von der Fakultät für Chemie der Technischen Universität
München zur Erlangung des akademischen Grades eines

Doktors der Naturwissenschaften

genehmigten Dissertation.

Vorsitzender: Univ. – Prof. Dr. K. Köhler

Prüfer der Dissertation: 1. Univ. – Prof. Dr. F. E. Kühn
2. Prof. Dr. J. Mink, Research Centre for Natural Sciences,
Hungarian Academy of Sciences, Budapest/Ungarn

Die Dissertation wurde am 26. September 2012 bei der Technischen Universität München eingereicht und durch die Fakultät für Chemie am 13. November 2012 angenommen.

Die vorliegende Arbeit entstand in der Zeit von Juni 2009 bis September 2012 am Anorganisch-Chemischen Institut, Fachgebiet Molekulare Katalyse, der Technischen Universität München

Mein ganz besonderer Dank gilt meinem Doktorvater

Herrn Professor Dr. Fritz E. Kühn

für die Aufnahme in seinen Arbeitskreis, den wertvollen wissenschaftlichen Gesprächen, sowie das uneingeschränkte Vertrauen, das er mir und meiner Arbeit entgegenbrachte.

Diese Arbeit wurde durch das Elitenetzwerk Bayern, Doktorandenkolleg NanoCat, gefördert.

*Für meine Eltern,
Isabelle und Regula,
und Benoît.*

In Liebe und Dankbarkeit.

*In diesen heil'gen Hallen,
Kennt man die Rache nicht.
Und ist ein Mensch gefallen;
Führt Liebe ihn zur Pflicht.
Dann wandelt er an Freundeshand,
Vergnügt und froh ins bess're Land.*

aus „Die Zauberflöte“ von Wolfgang Amadeus Mozart

Acknowledgments

I would not have had such exciting years at the Chair of Inorganic Chemistry/Group of Molecular Catalysis without all of you other Ph.D. students, thank you all very much!

I would also like to thank...

Dr. Mirza Cokoja for proof-reading my written work and his valuable support and inputs concerning experimental work.

Dr. Markus Drees for the calculations of all the possible mechanistic pathways in the Mo – catalysed olefin epoxidation.

Dr. Eberhardt Herdtweck and **Dr. Alexander Pöthig** for the single-crystal X-ray diffraction data collection and structure solution of my complexes.

Dr. Gabriele Raudaschl-Sieber for the measurement of the solid MAS NMR spectra.

Georgeta Krutsch and **Jürgen Kudermann** for recording my numerous liquid NMR samples. Thank you for your confidence and letting me perform many measurements on my own.

Ulrike Ammari, **Petra Ankenbauer** and **Maria Weindl** for the elemental analysis of all my samples.

Christina, **Jenny**, **Marlene**, **Philipp**, **Sophie** and **Stefan**, I always enjoyed our coffee breaks.

Marlene and **Sophie** for sharing the lab with me, I could not have wished for a more pleasant company!

I sincerely acknowledge **Professor Dr. Janos Mink** for welcoming me at his laboratories in Budapest and Veszprem and for his help in interpreting the IR and Raman spectra, as well as the calculations of the bond force constants in the organomolybdenum tricarbonyl complexes.

Contents

| | | |
|----------|--|-----------|
| 1 | Epoxidation of Olefins with Homogeneous Catalysts - <i>quo vadis?</i> | 1 |
| 1.1 | Background | 2 |
| 1.2 | Epoxidation of <i>cis</i> -cyclooctene | 3 |
| 1.3 | More demanding substrates | 4 |
| 1.3.1 | 1-Octene | 4 |
| 1.3.2 | Styrene | 6 |
| 1.4 | Terpenes | 6 |
| 1.4.1 | Limonene | 7 |
| 1.4.2 | α -Pinene | 8 |
| 1.4.3 | Camphene | 8 |
| 1.4.4 | Geraniol | 8 |
| 1.5 | Prochiral olefins | 9 |
| 1.5.1 | Aryl-substituted olefins | 9 |
| 1.5.2 | Cyclic alkenes | 11 |
| 1.5.3 | α,β -Unsaturated ketones | 12 |
| 1.6 | Epoxidation of industrially relevant bulk olefins | 13 |
| 1.6.1 | Ethylene | 13 |
| 1.6.2 | Propylene | 13 |
| 1.7 | Conclusion | 14 |
| 1.8 | References | 16 |
| 2 | Objectives | 21 |
| 2.1 | Methyltrioxorhenium | 22 |
| 2.2 | Molybdenum complexes | 22 |
| 2.3 | References | 24 |
| 3 | Chromophoric Lewis Base Adducts of Methyltrioxorhenium: Synthesis, Catalysis and Photochemistry | 25 |
| 3.1 | Background | 26 |
| 3.2 | Results and Discussion | 26 |
| 3.2.1 | Synthesis and spectroscopic characterisation | 26 |
| 3.2.2 | X-ray crystal structure of ligand 5 and complexes 8-14 | 28 |
| 3.2.3 | Determination of formation constants | 29 |
| 3.2.4 | Application in epoxidation catalysis | 30 |
| 3.2.5 | Photostability of the synthesised compounds | 31 |
| 3.3 | Conclusion | 33 |
| 3.4 | Experimental Section | 33 |
| 3.4.1 | Materials and methods | 33 |
| 3.4.2 | Ligand synthesis | 34 |

| | | |
|----------|---|-----------|
| 3.4.3 | Typical procedure for the preparation of the chromophoric Lewis base adducts of MTO | 34 |
| 3.4.4 | Single-crystal X-ray structure determination | 34 |
| 3.4.5 | Formation constant measurements | 36 |
| 3.4.6 | Catalysis | 36 |
| 3.4.7 | Testing the photostability of the complexes | 36 |
| 3.5 | References | 37 |
| 4 | Catalytic Olefin Epoxidation with a Fluorinated Organomolybdenum Complex | 39 |
| 4.1 | Background | 40 |
| 4.2 | Results and Discussion | 41 |
| 4.2.1 | Olefin epoxidation with a fluorinated organomolybdenum catalyst | 41 |
| 4.2.2 | Catalytic investigations | 45 |
| 4.2.3 | Catalysis in ionic liquids | 50 |
| 4.3 | Conclusion | 51 |
| 4.4 | Experimental Section | 51 |
| 4.4.1 | Materials and methods | 51 |
| 4.4.2 | Synthesis of the complexes | 52 |
| 4.4.3 | Kinetic studies | 52 |
| 4.4.4 | Computational details | 53 |
| 4.5 | References | 54 |
| 5 | The Quest of the Mechanism of Olefin Epoxidation Catalysed by Monomeric Organomolybdenum Complexes | 59 |
| 5.1 | Background | 60 |
| 5.2 | Experimental approach | 63 |
| 5.3 | Results and Discussion | 63 |
| 5.3.1 | Activity of the catalyst precursors – [Cp'Mo(CO) ₃ R] | 63 |
| 5.3.2 | Catalytic activity of the chloro derivatives | 65 |
| 5.3.3 | Comparison of [Cp'Mo(O ₂)(O)R]-type complexes | 66 |
| 5.3.4 | Mechanistic studies with [CpMo(O) ₂ Cl] | 69 |
| 5.3.5 | Mechanistic investigations by means of ¹³ C NMR spectroscopy | 71 |
| 5.4 | Conclusion | 72 |
| 5.5 | Experimental Section | 73 |
| 5.5.1 | Materials and methods | 73 |
| 5.5.2 | Synthesis of the complexes | 73 |
| 5.5.3 | Catalysis studies | 73 |
| 5.6 | References | 74 |
| 6 | The [η⁵-(C₅H₅)Mo(CO)₃R] Compound Class: Similarities and Differences | 77 |
| 6.1 | Background | 78 |
| 6.2 | Results and Discussion | 78 |
| 6.2.1 | Vibrational spectra | 79 |
| 6.2.2 | Molecular structures | 85 |
| 6.3 | Conclusion | 87 |
| 6.4 | Experimental Section | 88 |
| 6.5 | References | 89 |

| | | |
|----------|--------------------------------|------------|
| 7 | Summary | 91 |
| 7.1 | Methyltrioxorhenium | 92 |
| 7.2 | Molybdenum complexes | 92 |
| 8 | Appendix A | 95 |
| 9 | Appendix B | 109 |

Preface

Nearly every day, contributions on how to approach the challenges of preserving natural resources and exploring novel energy feedstocks can be found in the media. Sustainability has become an important goal in chemical industry. Great effort is put into the development of alternative technologies which are designed to respect the principles of sustainable chemistry, *i.e.* (i) minimising transport and storage of chemicals through integrated chemical processes, (ii) designing new synthetic strategies for one-pot reactions instead of multistep processes, and (iii) using alternative reactants that are less toxic or hazardous.

Catalysis, originating from the Old Greek word *κατάλυσις*, can be translated as a "putting down",¹ which, transferred into the present context, means: a lowering of the energy barrier. This is indeed the key for the development of future sustainable industrial processes. The revision of existing industrial productions to meet today's ecological and economical standards, all the while keeping up the productivity, would not be achievable without designing new catalysts and enhancing the performance of existing ones. Catalysts allow accessing naturally abundant raw materials that are hardly used nowadays due to their inertness, *e.g.* carbon dioxide and methane. Moreover, they open new possibilities for reaction pathways that require less energy input in form of heat or pressure, and that save resources through higher selectivity towards the product and reduced waste production, with by-products that eventually even serve as feedstock for other processes, in both bulk and fine chemical synthesis. In particular, epoxidation catalysis plays a crucial role in industry, as epoxides are important building blocks in chemical synthesis. Their derivatives appear in nearly every part of daily life, their range of application reaching from disinfectants via materials (*e.g.* polyester fibres, foils and bottles), antifreeze in cars and airplanes and biodegradable detergents to pharmaceuticals and cosmetics. The need to develop processes that are working under more benign conditions is apparent.

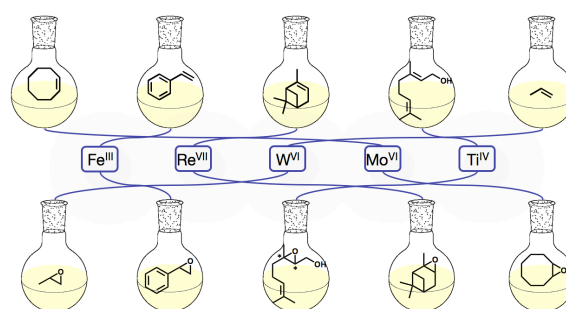
This thesis presents the results of experimental investigations of two catalytic systems. On the one hand, the influence of novel chromophoric nitrogen-donor ligands on the methyltrioxorhenium (MTO) catalysed olefin epoxidation with hydrogen peroxide as an oxidant was examined. The photochemistry of these kind of MTO adducts had been previously unknown, and we expected a beneficial effect through weakening bonds that have to be broken during the catalytic cycle. On the other hand, organomolybdenum compounds were studied functioning as olefin epoxidation catalysts. They were being used for exploring how the mechanism of this reaction works. Numerous computational studies provided the basis for controversial debates on this mechanism. This thesis now provides experimental studies for a better insight.

¹from Liddell / Scott / Jones, "A Greek-English Lexicon" (1996), Bath.

Abbreviations

| | |
|---------------------------|---|
| Å | Ångström |
| acac | acetylacetonate |
| [bmim][NTF ₂] | 1-butyl-3-methylimidazolium bis(trifluoromethylsulfonyl)imide |
| Cp | cyclopentadienyl |
| Cp* | pentamethylcyclopentadienyl |
| Cp' | substituted cyclopentadienyl ring |
| CP MAS | cross polarization magic angle spinning |
| δ | chemical shift (ppm) |
| d | doublet |
| DCM | dichloromethane |
| GC | gas chromatography |
| <i>e.g.</i> | <i>exempli gratia</i> (for the sake of example) |
| equiv. | equivalents |
| Et | ethyl |
| Et ₂ O | diethylether |
| EtOH | ethanol |
| <i>et al.</i> | <i>et alii</i> (and others) |
| h | hour |
| Hz | Hertz |
| <i>i.e.</i> | <i>id est</i> (that is) |
| IR | infrared spectroscopy |
| <i>J</i> | coupling constant |
| m | multiplet |
| M | molar mass |
| Me | methyl |
| min | minute |
| mL | milliliter |
| mol | mole |
| MTO | methyltrioxorhenium |
| NMR | nuclear magnetic resonance spectroscopy |
| Ph | phenyl |
| ppm | parts per million |
| q | quartet |
| RT | room temperature |
| RTIL | room temperature ionic liquid |
| s | singlet |
| t | triplet |
| TBHP | <i>tert</i> -butyl hydroperoxide |
| <i>t</i> BuOH | <i>tert</i> -butanol |
| THF | tetrahydrofurane |
| TOF | turn-over frequency |
| TON | turn-over number |
| XRD | X-ray diffraction |

1 Epoxidation of Olefins with Homogeneous Catalysts - *quo vadis?*



This chapter originated the following publication:
S. A. Hauser, M. Cokoja, F. E. Kühn, *Cat. Sci. Technol.*, **2013**, accepted.

1.1 Background

The epoxidation of olefins is a reaction of high relevance in both industry and academia. Epoxides are very important intermediates in the chemical industry, particularly for the synthesis of various polymers (polyglycols, polyamides, polyurethanes, etc.),¹ but they are also being used in the synthesis of fine chemicals, such as pharmaceuticals, food additives, or flavour and fragrance compounds.² The biggest market is propylene oxide, which is currently produced on a scale of 8 million tons/year with an expected annual increase of 5%.³ For ethylene and propylene oxide, heterogeneous catalysts, such as Ag@Al₂O₃ (for ethylene oxide) and titania-doped zeolite-type silicates (TS-1, for propylene oxide), developed by EniChem, Evonik, Dow and BASF are the state-of-the-art processes.³ Main reasons for their application are the catalyst recycling, which is intrinsically easier for heterogeneous catalysts, as well as their long-time stability, product selectivity and the type of oxidant. Whereas the heterogeneous catalysts usually rely on cheap oxygen, either used directly (in the case of ethylene oxide production), or indirectly (*e.g.* for the production of H₂O₂ or organic peroxides), homogeneous catalysts often require rather 'exotic' (from an industrial perspective) oxidants, such as NaOCl, iodosobenzene, amine- or pyridine-N-oxides. Thus, molecular epoxidation catalysts, such as the most prominent examples by Katsuki/Sharpless,⁴ Kochi/Jacobsen,⁵ Herrmann⁶ and others have so far mainly been used in the synthesis of more or less sophisticated organic molecules, as shown in several reviews.^{7,8} Asymmetric epoxidation of prochiral olefins is, of course, difficult to achieve with heterogeneous catalysts, and molecular catalysts are considered to be much more promising, by tuning the organic ligands at the metal, giving high enantiomeric excesses (*ee*). For these reactions, especially salen-type ligands appear to be the best choice;^{9,10} they, however, render the catalysts very expensive. Thus, a lot of effort has been devoted to the development of other molecular catalysts, such as dioxo molybdenum complexes and half-sandwich cyclopentadienyl molybdenum compounds.^{11–13} In the case of the very versatile catalyst methyltrioxorhenium (MTO), which utilises aqueous H₂O₂ as oxidant, all attempts to create a chiral version leading to high enantioselectivity in epoxidation have – so far – failed.^{14,15} Effective transmission of chirality can be obtained with lanthanide/1,1'-binaphthyl-2,2'-diol (BINOL) catalytic systems. They are, however, especially suited for enones.^{16,17} Meanwhile, also metal-free organocatalysts are used for asymmetric epoxidation of complex organic olefins, and they are successfully applied with a variety of oxidants: oxone (KHSO₅), aqueous hydrogen peroxide (H₂O₂), urea hydrogen peroxide (UHP) and even molecular oxygen (O₂).^{18–20} Nevertheless, these catalyst systems are usually applied for special organic substrates, where the epoxidation is normally one of many reaction steps towards a particular chemical.

Many reports on catalytic epoxidation in homogeneous phase notoriously do not comment on factors, which are important for an efficient, long-term (industrial) application, such as turnover frequencies (TOF) and numbers (TON), catalyst/product separation and recycling, and

catalyst stability. Further, the best known molecular epoxidation catalysts were not tested for ethylene and propylene epoxidation. In order to achieve an efficient catalyst separation, many groups focused on the immobilisation on solid supports,²¹ which is, however, often associated with a significant loss of catalytic activity. Another extensively studied possibility are two-phase reactions in ionic liquid (IL) media, where the catalyst is dissolved in the IL and substrate and product are immiscible.^{22,23}

Looking at the recent developments in epoxidation with molecular transition metal catalysts, the question can be raised, what the perspectives, *i.e.* the demands for an epoxidation catalyst are. In this chapter, the following two questions are discussed:

- 1) Which are the state-of-the-art catalysts for different types of olefins, such as cyclooctene, 1-octene, styrene, prochiral olefins, but also ethylene and propylene? To date, complexes of various metals bearing different ligands are known. Which of all those complexes is – among the plethora of available catalysts – the most widely applicable?
- 2) Do these catalysts exhibit a perspective to be used in industrial, large-scale epoxidation reactions, going well beyond being used for one of several (or many) synthesis steps in fine chemical synthesis? Do they exhibit a perspective for the epoxidation of ethylene and propylene; can they compete to the well-established industrial processes?

1.2 Epoxidation of *cis*-cyclooctene

Cis-cyclooctene is the most used test substrate in academic research. This olefin is particularly suitable for assessing the catalytic performance of a new compound, as it is easily epoxidised in presence of a catalyst. Hence, it is broadly used as benchmark substrate for catalyst comparison. However, the reaction conditions (temperature, catalyst concentration, duration, etc.) strongly influence the catalyst activity. Thus, it is of great importance to select a suitable reaction system for every catalyst and to bear in mind the conditions for the comparison of the catalyst performances. A specific characteristics exists that is intended to enable easy comparison, namely the turn-over frequency (TOF), which determines the amount of substrate (in mol) converted by the applied amount of catalyst (in mol) per unit time (usually given in hours). This number is usually calculated during the initial phase of the catalytic reaction, where the kinetics curve of product build-up shows a steep increase, substrate molecules are plentiful and diffusion is not a limiting factor. Unfortunately, the TOF is often not mentioned/determined in publications, so other features have to be considered: the faster a quantitative conversion is achieved, the better the catalyst appears to work. Another possibility of differentiation is the turn-over number (TON), which states the catalyst lifetime. It is calculated by the maximum amount of substrate (in mol) converted by the applied amount of catalyst (in mol) during its lifetime. Unfortunately, the published TONs are often calculated based on one single catalytic run, ignoring the remaining catalyst activity. There are three current benchmark catalysts (Figure 1.1), all of them showing very high TOFs. There

are two molybdenum-based complexes: $[\text{Mo}_2(\text{OtBu})_6]$ (**1**) reaches a TOF of above 50,000 h^{-1} , *i.e.* 25,000 h^{-1} per Mo centre, at a catalyst loading of 0.05 mol% with nearly quantitative yield.²⁴ The so-called ansa-complex $[\text{Mo}(\eta^5\text{-C}_5\text{H}_4(\text{CH}(\text{CH}_2)_3)\text{-}\eta^1\text{-CH})(\text{CO})_3]$ (**2**) even reaches a TOF of 44,000 h^{-1} (at a concentration of 0.05 mol% in a room temperature ionic liquid (RTIL)).²⁵ A TOF of almost 40,000 h^{-1} has been attained with 0.01 mol% methyltrioxorhenium (MTO, **3**), applied with an excess of pyrazole in hexafluoroisopropanol, and yielding full conversion of the substrate.²⁶

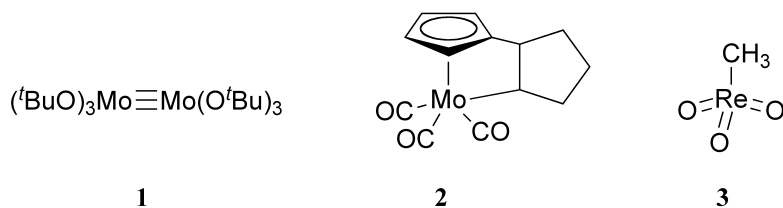


Figure 1.1 Three outstanding (pre-)catalysts for the epoxidation of cyclooctene.

Further (pre-)catalysts exhibit a TOF of above 4,000 h^{-1} (Table 1.1, Entries 4-8). Interestingly, these are all molybdenum-based complexes, working with *tert*-butyl hydroperoxide (TBHP) in decane as oxidant.^{27–31} The dioxomolybdenum catalyst **9** (Table 1.1, Entry 9) has a high catalytic activity,³² as well as the tungsten-based complexes **10** and **11** (that are applied with aqueous H_2O_2 as oxidant; Table 1.1, Entries 10-11). At low catalyst loadings, they reach quantitative substrate conversion within a reasonable time.^{33,34} Peracetic acid is used in the reaction with the dimeric Mn-catalyst **12**, which quantitatively converts cyclooctene to the epoxide within 3 min (at 3 mol% catalyst loading, Entry 12).³⁵

1.3 More demanding substrates

After a catalyst performance has been assessed in the epoxidation of cyclooctene, a range of aromatic or aliphatic substrates are available to show the catalyst potential. There are two model substrates, an aliphatic terminal olefin (1-octene) and an aromatic alkene (styrene). They both are more difficult to epoxidise and are prone to ring-opening by-product formation, thus allowing a more subtle distinction of the catalytic power of a catalyst.

1.3.1 1-Octene

MTO (**3**) confirms its great potential as epoxidation catalyst, as it shows the best performance in the epoxidation of 1-octene. Applied under similar reaction conditions as for cyclooctene, the catalytic system reaches a TOF of nearly 5,000 h^{-1} , yielding 89 % epoxide within 3 h.²⁶ Together with compound **1** (86 % yield in 16 h with 0.5 mol% catalyst), two other Mo-complexes presented in the previous section exhibit high catalytic activities for terminal olefins as well (Figure 1.2).^{32,35}

Table 1.1 Metal complexes with a good performance in the epoxidation of cyclooctene.

| Entry | Complex | T / °C | Time / h | Solvent | Catalyst conc. (mol%) | Yield (%) | TOF / h ⁻¹ | Ref. |
|-------|--|--------|----------|---------------------------------|-----------------------|----------------|-----------------------|------|
| 1 | [Mo ₂ (OtBu) ₆] (1) | 25 | 0.03 | CH ₂ Cl ₂ | 0.05 | 86 | 25,000 | 24 |
| 2 | [Mo(η ⁵ -C ₅ H ₄ (CH(CH ₂) ₃)-η ¹ -CH)(CO) ₃] (2) | 25 | 0.03 | Ionic liquid | 0.05 | — ^c | 44,000 | 25 |
| 3 | [CH ₃ ReO ₃] (3) | 0 | 3 | Hexafluoroisopropanol | 0.01 | 100 | 39,000 | 26 |
| 4 | [Mo(O) ₂ (L ¹) ₂] ^a (4) | 80 | 1 | 1,2-Dichloroethane | 0.02 | 96 | 4,800 | 27 |
| 5 | [Mo(O) ₂ (Cl) ₂ (L ²)] ^a (5) | 25 | 24 | Ionic liquid | 0.1 | 99 | 8,090 | 28 |
| 6 | [Cp ^{ox} Mo(CO) ₂ (NCMe)]BF ₄ ^b (6) | 55 | 0.5 | CHCl ₃ | 0.2 | 90 | 5,421 | 29 |
| 7 | [Mo(η ⁵ -C ₅ (C ₆ H ₅) ₅)(O) ₂ Cl] (7) | 55 | 24 | — | 0.1 | 80 | 4,000 | 30 |
| 8 | [Mo(O) ₂ (L ³) ₂] ^a (8) | 55 | 4 | CHCl ₃ | 0.02 | >99 | 5,000 | 31 |
| 9 | [Mo(O) ₂ (L ⁴)(CH ₃ OH)] ^a (9) | 80 | 0.75 | 1,2-Dichloroethane | 1 | 100 | n.d. | 32 |
| 10 | (L ⁵) ₂ [W ₂ (O) ₃ (O ₂) ₄] (10) | 80 | 4 | MeCN | 0.2 | 100 | n.d. | 33 |
| 11 | (L ⁶) ₄ [γ-SiW ₁₀ O ₃₄ (H ₂ O) ₂] ^a (11) | 32 | 2 | MeCN | 0.8 | >99 | n.d. | 34 |
| 12 | [Mn ₂ L ⁷ (μ-OAc) ₃]PF ₆ ^a (12) | 25 | 0.05 | MeCN | 3 | 100 | n.d. | 35 |

^aL¹ = 2-(2'-hydroxyphenyl)oxazolinatate; L² = 5,5'-bis-methoxycarbonyl-2,2'-bipyridine; L³ = 5-(2'-hydroxyphenyl)pyrazole; L⁴ = 2[(2-hydroxy-2-phenylethylimino)methyl]phenol; L⁵ = tetrahexylammonium; L⁶ = tetrabutylammonium; L⁷ = E-1,2-bis(2,2'-bipyridyl-6-yl)ethene. ^bCp^{ox} = cyclopentadienyl ligand with pendant oxazoline group. ^cnot stated in the article.

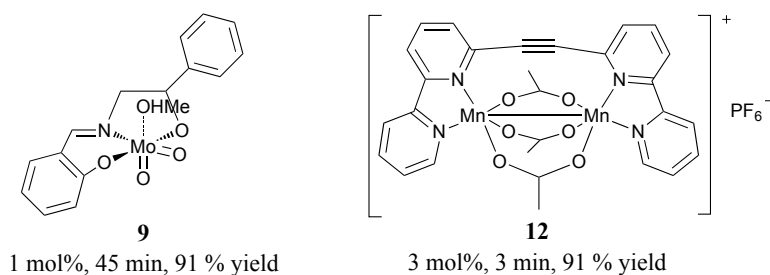


Figure 1.2 Efficient catalysts for the epoxidation of 1-octene.

Bhattacharyya *et al.* reported the successful application of an ionic diperoxo tungsten complex, $\text{PPh}_4[\text{WO}(\text{O}_2)_2(1-(2'\text{-hydroxy-phenyl})\text{ethanonoxime})]$ (**13**), in the epoxidation of 1-octene with H_2O_2 .³⁶ A very low catalyst concentration (0.05 mol%) yields 95 % 1-octene oxide within 2.25 h in acetonitrile at 40 °C. The polyoxovanadotungstate complex $[\mu\text{-}1,2\text{-H}_2\text{SiV}_2\text{W}_{10}\text{O}_{40}]^{4-}$ (**14**) is also a good catalyst for terminal olefins.³⁷ With H_2O_2 as oxidant, this system reaches a yield of 93 % (with 99 % selectivity) at a concentration of 5 mol% at room temperature.

1.3.2 Styrene

One of the catalysts succeeding in high yielding epoxidation of styrene is again MTO (**3**). It reaches quantitative substrate conversion in 3 h at 25 °C, with only 0.5 mol% catalyst applied.³⁸ A very high TOF ($> 3,000 \text{ h}^{-1}$) has been obtained with a manganese complex containing a tetradentate nitrogen base ligand (**15**).³⁹ This complex, prepared by Costas *et al.*, yields 86 % styrene oxide within 3 min with peracetic acid as oxidant. Comba and co-workers optimised the reaction conditions for iron bispidine complexes,⁴⁰ achieving with one of them (**16**) nearly quantitative yields at room temperature within 24 h (with iodosobenzene as oxidant). Good results have also been obtained with the molybdenum complex $\text{PPh}_4[\text{MoO}(\text{O}_2)_2(1-(2'\text{-hydroxyphenyl})\text{ethanonoxime})]$ (**17**)³⁶ as well as the simple iron trichloride hexahydrate (**18**).⁴¹ In presence of pyridine-2,6-dicarboxylic acid and H_2O_2 , **18** forms an efficient catalytic system that yields 91 % epoxide at a catalyst loading of 5 mol%, within 1 h at room temperature.

1.4 Terpenes

Mono- and bicyclic monoterpene hydrocarbons occur in many essential oils and their by-products, and they represent an important group of renewables which can be catalytically converted to fine chemicals. The industrially most important member of the terpene family is 1,2-limonene oxide, it finds application in the perfume industry and is widely used as building block in the manufacture of a range of important commercial products.^{42,43} α -Pinene is also utilised as starting material in the synthetic manufacture of flavours and fragrances.^{42,44}

Moreover, it is an intermediary species in the synthesis of Taxol, an anticancer drug.⁴⁵ The bicyclic terpene camphene is found in a variety of living conifers as well as in fossilized amber.⁴⁶ It is a valuable precursor for complex molecules, *e.g.* in the synthesis of a spiroring system containing a benzopyram moiety.⁴⁷ Another member of the terpene family is the terpenoid geraniol. This prochiral allylic alcohol is commonly used in perfumery, due to its own fresh, citrus flavour, and as precursor in the synthesis of a variety of other floral fragrances.⁴⁸ The following paragraphs assemble the best reaction protocols for terpene oxidation (substrates are depicted in Figure 1.3), based on substrate conversion and epoxide selectivity, from which the latter one is by far more important.

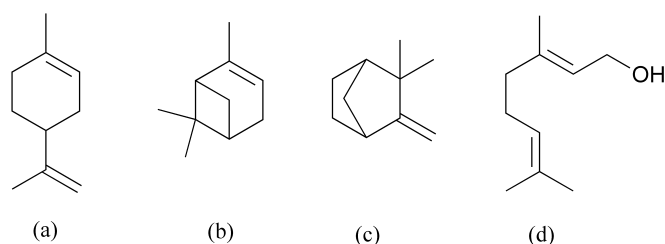


Figure 1.3 Terpene substrates covered in this chapter: (a) limonene, (b) α -pinene, (c) camphene, and (d) geraniol.

1.4.1 Limonene

Quantitative and selective conversion of limonene to 1,2-limonene oxide has only been reported in three publications, and an elaborate substrate:oxidant:catalyst ratio has proven to be crucial. Upon mixture of limonene, MTO (**3**; 5 mol%) and urea hydrogen-peroxide (UHP; 200 mol%) in chloroform, Boehlow and Spilling claimed 99 % yield of the monoepoxide after 30 minutes at 20 °C.⁴⁹ The other examples reaching these results involve molybdenum-based catalysts: Driess and co-workers applied the pre-catalyst $[\text{Mo}_2(\text{O}^t\text{Bu})_6]$ (**1**), together with TBHP as oxidant, and received > 99 % yield in 40 min.²⁴ This reaction has been carried out at room temperature, what is advantageous compared to the third catalytic system (55 °C), developed by Royo *et al.*²⁹ The complexes $[\text{Cp}^{ox}\text{Mo}(\text{CO})_2(\text{NCMe})]\text{BF}_4$ (**6**) and $[\text{Cp}^{ox}\text{Mo}(\text{C}_3\text{H}_5)(\text{CO})_2]$ (**19**) perform equally well: within 1 h, the conversion of limonene to 1,2-limonene oxide is complete (with TBHP as oxidant). A nearly quantitative conversion with very good epoxide selectivity (98 %) has been achieved as well with 1 mol% tungsten-based complex, $[(\text{C}_6\text{H}_{13})_4\text{N}]_3[\text{PO}_4\text{W}_2(\text{O})_2(\mu\text{-O}_2)_2(\text{O}_2)_{22}]$ (**20**), and H_2O_2 as oxidant at room temperature in only 30 min.⁵⁰ Manganese complexes, *e.g.* Jacobsen's catalyst⁵¹ (**21**) and $\text{Mn}(\text{OAc})_3 \cdot 2\text{H}_2\text{O}$ (**22**),⁵² also proved to be suitable catalysts for this reaction, showing excellent selectivity to 1,2-limonene oxide (100 %) with acceptable conversion (55 % and 96 %, respectively). Kühn *et al.* published a detailed investigation on the best reaction conditions employing MTO (**3**) as catalyst.⁵³ The highest selectivity towards 1,2-limonene oxide is obtained with a ratio of limonene:MTO:*t*-butylpyridine: H_2O_2 of 100:0.5:10:150, leading to

the formation of 1,2-limonene oxide with a yield of 77 % (96 % selectivity with respect to substrate conversion) after 1 h (25 °C, CH₂Cl₂ as solvent).

1.4.2 α -Pinene

For the epoxidation of α -pinene, MTO (**3**) is again the catalyst of choice, as the results show in Table 1.2. The best and straightforwardly applicable system was reported only last year by Kühn and co-workers (Table 1.2, Entry 4).⁵⁴

Table 1.2 MTO-catalysed epoxidation of α -pinene.

| Entry | Cat. conc. (mol%) | T / °C | t / h | Solvent | Oxidant | Conv. (%) | Sel. (%) | Ref. |
|-------|-------------------|--------|-------|---------------------------------|-------------------------------|-----------|----------|------|
| 1 | 0.5 | 25 | 2.5 | CH ₂ Cl ₂ | H ₂ O ₂ | 90 | 90 | 55 |
| 2 | 1 | 25 | 2 | CH ₂ Cl ₂ | H ₂ O ₂ | 70 | 50 | 56 |
| 3 | 0.3 | 10 | 5 | — | H ₂ O ₂ | >99 | 95 | 57 |
| 4 | 0.5 | 0 | 5 | CH ₃ NO ₂ | UHP | 100 | 100 | 54 |

1.4.3 Camphene

Camphene oxide can be successfully obtained through epoxidation of camphene with a variety of transition metal complexes, in contrast to α -pinene. Nevertheless, MTO (**3**) features once again among the best catalysts.⁵⁸ In the biphasic system H₂O₂/CH₂Cl₂ at 25 °C, it leads to 97 % yield of camphene oxide (with a selectivity of 98 %). Another potent catalytic system was reported by Mirkhani *et al.*⁵⁹ A Mn(salen)OAc complex (**23**) effectively catalyses the epoxidation of camphene with sodium periodate (NaIO₄), reaching 97 % yield in 10 min at 25 °C. A far less exotic oxidant, namely molecular oxygen at atmospheric pressure, needs the tris(tetrazolylenolate)iron(III) complex (**24**) to catalyse the epoxidation of camphene.⁶⁰ 1 mol% catalyst are sufficient to yield 87 % epoxide after 4 h at 20 °C. The same oxidant (O₂) is used with the cobalt-based complex **25** (Figure 1.4), leading to a good yield (72 %) of camphene oxide.⁶¹

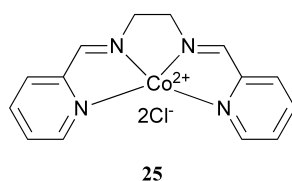
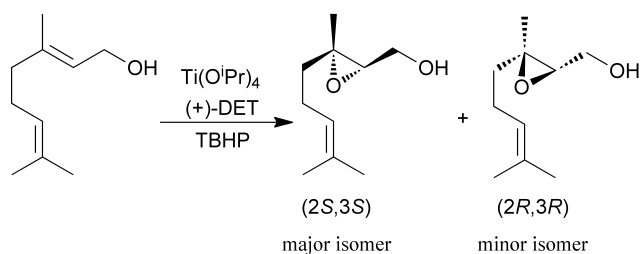


Figure 1.4 A good catalyst for camphene epoxidation with O₂ as oxidant.

1.4.4 Geraniol

The first protocol for catalytic asymmetric epoxidation was reported by Sharpless and Katsuki in 1980.⁴ The components of the catalytic system, *i.e.* (+)- or (–)-diethyl tartrate, titanium

tetraisopropoxide (**26**) and TBHP, are all commercially available at moderate cost (Scheme 1.1). This fact, as well as the simplicity of the system and the high selectivity, led to the Nobel Prize for K. B. Sharpless in 2001.⁶² Although the substrate scope of the system is limited to allylic alcohols, it is still among the best ones for the epoxidation of geraniol: Reaching a yield of 77 % (after 18 h at -20 °C), the enantiomeric excess of 95 % has not often been surpassed until now. After optimisation of this system by addition of molecular sieves and reduction of the catalyst loading to 5 mol%, Sharpless *et al.* managed to get a higher yield of 2,3-epoxygeraniol (99 %), but the *ee* slightly decreased (91 %).⁶³ The same *ee* (91 %) is obtained with [Ti(O^{*i*}Pr)₄] (**26**) in presence of L-diisopropyl tartrate (L-DIPT), however, the yield is somewhat lower (58 %).⁶⁴ The advantage of this catalytic system consists in the possibility to apply a renewable oxidant, namely tertiary furyl hydroperoxide. If the epoxidation of geraniol is catalysed by a [VO(O^{*i*}Pr)₃]/chiral bishydroxamic acid system (**27**) with aqueous TBHP as oxidant, a yield of 68 % and an *ee* of 95 % are reached, by applying only 1 mol% catalyst.⁶⁵



Scheme 1.1 Sharpless epoxidation of geraniol.

1.5 Prochiral olefins

Apart from terpenes and terpenoids, a variety of prochiral olefins are ubiquitous in fine chemical industry. The beneficial characteristics of epoxidation reactions is the ability of creating two stereogenic centres with one chemical reaction, and the epoxides are highly versatile chiral building blocks in pharmaceuticals manufacture and the production of flavour and fragrances. For this chapter, a selection of prochiral olefins has been made for presenting the state-of-the-art catalysts in homogeneous asymmetric epoxidation. They have been chosen in terms of enantioselectivity and activity, all by accepting higher catalyst loadings in favour of shorter reaction times, as with time, by-products are accumulating. Solely catalytic systems that effectively induce enantioselective products are presented herein.

1.5.1 Aryl-substituted olefins

A wide range of transition-metal based catalysts have been applied in the epoxidation of *trans*- β -methylstyrene, however, only a handful ruthenium complexes, which are summarised in Table 1.3, reach high yields combined with very good *ee*'s.

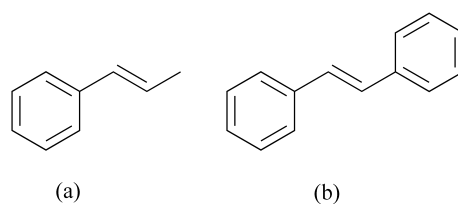


Figure 1.5 Selected aryl-substituted olefins.

As in the case of *trans*- β -methylstyrene, epoxidation of stilbene often leads to racemic mixtures (see Figure 1.5 for substrates). The above-mentioned Ru-based catalyst **31** also performs well in the epoxidation of *trans*-stilbene, giving the best yield (100 %) with encouraging 54 % *ee*.⁶⁹ Slightly higher selectivity to the S,S-epoxide shows [Ru(pydic)(pyboxip)] (**32**; 80 % yield, 63 % *ee*), although the reaction time (96 h) is significantly longer.⁷⁰ Finally, a very promising system has been developed by Beller *et al.*⁷¹ The catalyst consists of FeCl₃ · 6 H₂O (**18**), pyridine-2,6-dicarboxylic acid, and a readily accessible chiral N-arenesulfonyl-N'-benzylsubstituted ethylenediamine ligand. Stirring of the reaction mixture (H₂O₂ as oxidant) for 1 h at room temperature yields 87 % R,R-stilbene oxide with an *ee* of 42 %.

Table 1.3 State-of-the-art catalysts for *trans*- β -methylstyrene epoxidation (depicted in Figure 1.6).

| Entry | Catalyst | T / °C | t / h | Solvent | Oxidant | Yield (%) | <i>ee</i> (%) | Ref. |
|-------|----------------------|--------|-------|---------------------------------|-------------------------------|-----------|---------------|------|
| 1 | 28 (0.1 mol%) | 25 | 24 | CH ₂ Cl ₂ | PhIO | 99 | 100 | 66 |
| 2 | 29 (5 mol%) | 0 | 48 | chlorobenzene | O ₂ | 91 | 91 | 67 |
| 3 | 30 (5 mol%) | 25 | 36 | chlorobenzene | O ₂ (h ν) | 59 | 87 | 68 |
| 4 | 31 (5 mol%) | 25 | 12 | <i>t</i> -amyl alcohol | H ₂ O ₂ | 95 | 72 | 69 |

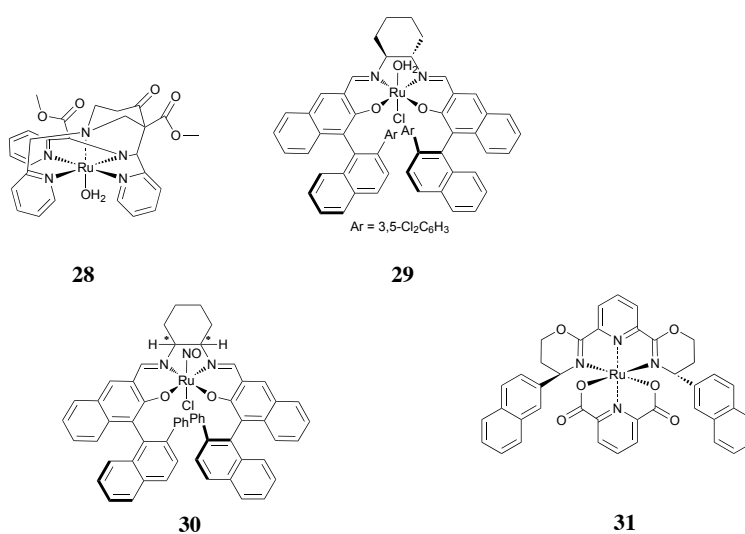
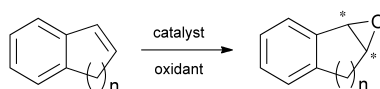


Figure 1.6 Four complexes successfully applied in *trans*- β -methylstyrene epoxidation.

1.5.2 Cyclic alkenes

For the cyclic prochiral alkenes, the class of benzene-fused cycloalkenes has been chosen (Scheme 1.2). 1,2-Dihydronaphthalene ($n = 2$) is the most often applied substrate. Various catalytic systems (Table 1.4, Entries 1, 4, 7, 9, 10) achieve high *ee*'s in combination with good yields. Three of the catalysts showing an excellent performance in the epoxidation of 1,2-dihydronaphthalene can also be successfully applied in the synthesis of indene oxide (Table 1.4, Entries 2, 5, 8). The reaction times are mostly somewhat longer, however, the selectivity is kept at a high level ($> 97\%$). The enantioselective epoxidation of benzocycloheptene is even less prone to be used as assessment for the catalyst performance. The Entries 3, 6, and 11 in Table 1.4 present the only catalysts, that were also applied in the epoxidation of this olefin.



Scheme 1.2 Epoxidation of benzene-fused cycloalkenes.

Table 1.4 Complexes successfully catalysing the epoxidation of benzene-fused cycloalkenes (depicted in Figure 1.7).

| Entry | Catalyst | Substrate | T / °C | t / h | Solvent | Oxidant | Yield (%) | <i>ee</i> (%) | Ref. |
|-------|-----------|-----------|-----------|----------|---------------------------|------------------------|--------------|------------------|------|
| 1 | 33 | $n = 2^a$ | 25 | 12 | CH_2Cl_2 | H_2O_2 | >99 | >99 | 72 |
| 2 | | $n = 1^b$ | | 24 | | ethyl acetate | 87 | 99 | |
| 3 | | $n = 3^c$ | | 24 | | | 85 | 98 | |
| 4 | 34 | $n = 2^a$ | 40 | 6 | $\text{CH}_2\text{Cl}_2/$ | H_2O_2 | 99 | 98 | 73 |
| 5 | | $n = 1^b$ | | 6 | | phosphate buffer | 98 | 98 | |
| 6 | | $n = 3^c$ | | 9 | | | 77 | 97 | |
| 7 | 35 | $n = 2^a$ | 25 | 3 | CH_2Cl_2 | H_2O_2 | 90 | 95 | 74 |
| 8 | | $n = 1^b$ | | 18 | | | 88 | 97 | |
| 9 | 36 | $n = 2^a$ | 25 | 18 | | THP ^d | 98 | 95 | 75 |
| 10 | 37 | $n = 2^a$ | -18 | 1 | $\text{CH}_2\text{Cl}_2/$ | UHP | 70 | 73 | 76 |
| 11 | | $n = 3^c$ | | 1.5 | DMF | POHP/MA ^e | 73 | 92 | |

^a1,2-Dihydronaphthalene

^bIndene

^cBenzocycloheptene

^dTrityl hydroperoxide

^eTriphenylphosphine oxide- H_2O_2 /maleic anhydride.

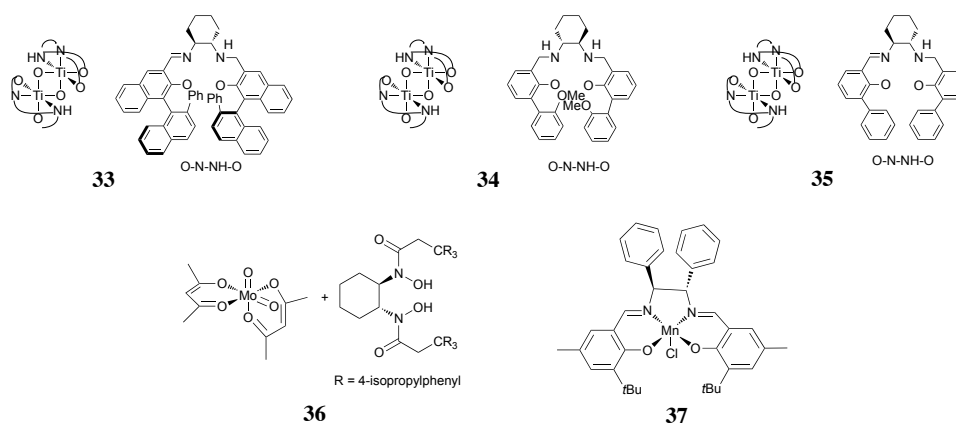
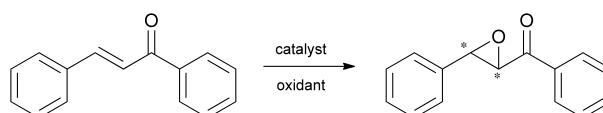


Figure 1.7 Benzene-fused cycloalkenes are epoxidised in high yields and good *ee*'s by those five complexes.

1.5.3 α,β -Unsaturated ketones

The asymmetric epoxidation of electron-deficient olefins is especially useful in the synthesis of a variety of natural products and pharmaceuticals. We have chosen chalcone as a representative example for the determination of the most potent catalysts (Scheme 1.3). Interestingly, not compounds containing the transition metals presented in the previous paragraphs give the best results, but mainly lanthanoid complexes. Shibasaki's report about Ln/BINOL catalytic systems¹⁷ marked the beginning of extensive research to find the optimum reaction conditions. Table 1.5 summarises the best catalytic systems, specifying the components present in the reaction mixture in addition to the chiral ligand BINOL. The systems are listed with their single components, as the real catalytic species is still a matter of investigation.



Scheme 1.3 Enantioselective epoxidation of the α,β -unsaturated ketone chalcone.

Table 1.5 Catalytic systems containing the chiral ligand BINOL, which efficiently catalyse the asymmetric epoxidation of chalcone.

| Entry | Metal precursor | Cat. conc. (mol%) | T / °C | Time / h | Solvent | Additive | Oxidant | Yield (%) | <i>ee</i> (%) | Ref. |
|-------|-------------------------------------|-------------------|--------|----------|-------------------|---------------------|------------------|-----------|---------------|------|
| 1 | Yb(OiPr) ₃ (38) | 5 | 25 | 1 | THF | H ₂ O | TBHP | 99 | 81 | 77 |
| 2 | La(OiPr) ₃ (39) | 5 | 25 | 0.5 | THF | PH ₃ PO | TBHP | 99 | 96 | 78 |
| 3 | La(OiPr) ₃ (39) | 5 | 25 | 0.25 | THF | PH ₃ AsO | TBHP | 98 | 96 | 79 |
| 4 | La(OiPr) ₃ (39) | 5 | 25 | 0.2 | THF | PH ₃ PO | CHP ^a | 99 | >99 | 80 |
| 5 | ZnEt ₂ (40) | 20 | 25 | 1 | Et ₂ O | — | CHP ^a | 99 | 90 | 81 |

^aCumene hydroperoxide.

1.6 Epoxidation of industrially relevant bulk olefins

1.6.1 Ethylene

Nowadays, industrial ethylene oxide production mainly employs the heterogeneous oxidation of ethylene by O₂ with a silver-based catalyst. This reaction has been developed by Shell in 1958,⁸² and still presents the method of choice. Nevertheless, there is some need for further research: First, the reaction conditions of the heterogeneous process are quite harsh, high temperatures (above 200 °C) have to be maintained, and secondly, the gas phase, a ethylene oxide/O₂ mixture, represents a security risk, as it is a potential explosive. Thirdly, it is desirable to reduce the large amount of CO₂ emitted as by-product (through combustion of ethylene and ethylene oxide). These requisites for a 'greener' method are all met by a recent publication by Subramaniam *et al.*⁸³ To the best of our knowledge, it represents the only report about the homogeneous transition-metal catalysed epoxidation of ethylene. The procedure consists of a constant-pressure batch reactor, which is charged with an alcoholic solvent (preferably methanol), the catalyst and oxidant (MTO (**3**) and H₂O₂) as well as pyridine-N-oxide as Lewis base. The reactor is pressurised with 50 bar ethylene and heated to 40 °C. With this method, ethylene oxide yields of over 50% after 9 h reaction time have been achieved.⁸³

1.6.2 Propylene

Propylene oxide is one of the major commodity chemicals used in chemical industry, and its production is mainly based on three different processes. The benchmark is the aforementioned hydrogen peroxide-propylene oxide (HPPO) process using the TS-1 catalyst. The non-catalytic chlorohydrin method (water as oxygen source) is outfashioned, as large amounts of Cl₂ are consumed and a lot of chlorinated toxic waste is produced. The hydroperoxide method, which is also known as the Halcon-ARCO process (*tert*-butyl hydroperoxide), and further developed by the Sumitomo company (cumene hydroperoxide) is also currently used.^{3,84–86} All processes require in situ production of the oxidants which is usually a quite energy-demanding process, and the direct oxidation by O₂ is prohibited, due to side reactions and combustion, respectively. Moreover, the catalytic processes suffer from a decomposition of the oxidant, particularly in the case of TS-1. Therefore, the direct oxidation of propylene to propylene oxide, in a more environmentally friendly way and with a minimal formation of by-products has been one of the most desirable goals for the chemical industry. Homogeneous catalytic epoxidation of propylene suffers from the difficulty of catalyst separation and re-use; nevertheless, the reaction can take place under milder conditions. The first report of homogeneous catalytic propylene epoxidation with high selectivity to propylene oxide dates back to 1995. An EuCl₃ catalytic system (**41**, in presence of Zn powder and acetic acid) allows the selective synthesis of propylene oxide with molecular oxygen as oxidant, however, the yields have been very low (2 %).⁸⁷ Zuwei *et al.* managed to circumvent the drawbacks of homogeneous catal-

ysis by developing a reaction-controlled phase-transfer catalysis.⁸⁸ The polyoxo-tungstate catalyst $[\pi\text{-C}_5\text{H}_5\text{NC}_{16}\text{H}_{33}]_3[\text{PO}_4(\text{WO}_3)_4]$ (**42**) forms a soluble, active species in presence of H_2O_2 . At the end of the reaction, when the oxidant is used up, the complex precipitates from the reaction mixture and can easily be reused. Moreover, by coupling the H_2O_2 production process to the 2-ethylanthraquinone/2-ethylanthrahydroquinone redox process, the catalytic epoxidation of propylene occurs without relevant by-product formation⁸⁹ and with constant yield of propylene oxide (around 85 %) over 3 cycles. Another environmentally friendly route to propylene oxide was found by Mizuno *et al.*³⁴ The silicotungstate compound (**11**) exhibits a very good selectivity (> 99 %) for the epoxide in the oxidation of propylene with H_2O_2 . After a reaction time of 8 h, a yield of 90 % propylene oxide is achieved, with a reaction temperature only slightly above room temperature (32 °C).

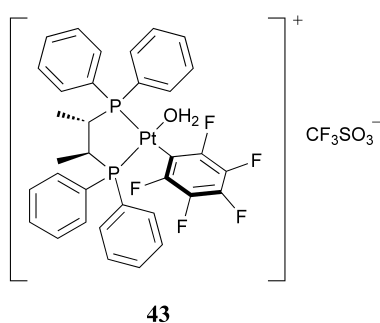


Figure 1.8 A fluorinated Pt-catalyst for propylene epoxidation.

A well-performing catalyst was recently reported by Strukul and co-workers.⁹⁰ The Pt-based fluorinated complex (**43**) (Figure 1.8) showed excellent catalytic activity with H_2O_2 as oxidant (98 % yield, 100 % epoxide selectivity). However, the need for very low reaction temperatures (-10 °C) as well as the high cost of the catalyst excludes this system from further development for an industrial bulk chemical production. In 2007, Subramaniam *et al.* presented a novel biphasic reaction for propylene oxide synthesis.⁹¹ The oxidation is catalysed by a MTO/ H_2O_2 system in methanol, and they claim propylene oxide yields exceeding 98 %. The reaction proceeds at near-ambient temperature, however, the need for high pressures of gaseous N_2 (20 bar), in order to enhance the propylene solubility in the liquid phase, presents a major drawback for industrial application.

1.7 Conclusion

Catalytic epoxidations of olefins, particularly in homogeneous phase, are among the best studied reactions in molecular (transition metal) catalysis. A broad scope of different transition metals, among which are Ti-, V-, Cr-, Mo-, W-, Mn-, Re-, Fe and Ru-catalysts, using quite a wide range of different oxidants, have been presented in the literature so far. They are usually capable to form stable epoxides in good to excellent yields without diol formation – the

most likely side reaction. Meanwhile, a good range of different olefins has been tested, from cyclic olefins (which are quite easy to epoxidise) to acyclic/terminal olefins (usually challenging for epoxidation). Also, numerous asymmetric epoxidations have been presented so far, giving good enantiomeric excesses. However, most reports are constricted to a one-time use of the catalyst, which is, presumably, in most cases destroyed upon work-up/product separation. The catalysts, which have been shown to exhibit a good activity when immobilised (ionic liquids give better results than catalysts anchored/grafted to solid supports) yet have to prove themselves to a) be efficient without activity loss for significantly more than 10, preferably for more than 10,000 runs, and b) be cheap. To the authors' opinion, these restrictions – catalyst recycling and price – are the drawbacks which homogeneous epoxidation catalysts have to overcome if they want to be competitive beyond academic interest. Particularly in the epoxidation of ethylene and propylene, remarkably little has been published, in comparison to the high number of reports on the epoxidation of easy-to-oxidise olefins (*e.g.* cyclooctene). Simple organometallic compounds, such as MTO, cover a wide range of olefin substrates. Particularly MTO seems to be one of the most potent catalysts. However, its high price (price of rhenium, but also accounting for the (somewhat) demanding synthesis) still does not render it interesting for industrial purposes, even more as it is not suitable for asymmetric catalysis.

1.8 References

1. F. Cavani, J. H. Teles, *ChemSusChem*, **2009**, 2, 508.
2. S. M. Roberts, J. Whittall, Eds., *Catalysts for fine chemical synthesis: Regio- and stereo-controlled oxidations and reductions*, Vol. 5; John Wiley Sons, Ltd: England, **2007**.
3. T. A. Nijhuis, M. Makkee, J. A. Moulijn, B. M. Weckhuysen, *Ind. Eng. Chem. Res.*, **2006**, 45, 3447.
4. T. Katsuki, K. B. Sharpless, *J. Am. Chem. Soc.*, **1980**, 102, 5974.
5. (a) K. Srinivasan, P. Michaud, J. K. Kochi, *J. Am. Chem. Soc.*, **1986**, 108, 2309. (b) W. Zhang, J. L. Loebach, S. R. Wilson, E. N. Jacobsen, *J. Am. Chem. Soc.*, **1990**, 112, 2801.
6. (a) W. A. Herrmann, R. W. Fischer, D. W. Marz, *Angew. Chem., Int. Ed.*, **1991**, 30, 1638. (b) C. C. Romão, F. E. Kühn, W. A. Herrmann, *Chem. Rev.*, **1997**, 97, 3197. (c) F. E. Kühn, A. Scherbaum, W. A. Herrmann, *J. Organomet. Chem.*, **2004**, 689, 4149.
7. K. A. Jørgensen, *Chem. Rev.*, **1989**, 89, 431.
8. B. S. Lane, K. Burgess, *Chem. Rev.*, **2003**, 103, 2457.
9. P. G. Cozzi, *Chem. Soc. Rev.*, **2004**, 33, 410.
10. T. Katsuki, *Synlett*, **2003**, 281.
11. (a) F. E. Kühn, A. M. Santos, M. Abrantes, *Chem. Rev.*, **2006**, 106, 2455. (b) F. E. Kühn, A. M. Santos, W. A. Herrmann, *Dalton Trans.*, **2005**, 2483.
12. M. K. Trost, R. G. Bergman, *Organometallics*, **1991**, 10, 1172.
13. N. Grover, F. E. Kühn, *Curr. Org. Chem.*, **2012**, 16, 16.
14. J. H. Espenson, *Chem. Commun.*, **1999**, 479.
15. J. J. Haider, R. M. Kratzer, W. A. Herrmann, J. Zhao, F. E. Kühn, *J. Organomet. Chem.*, **2004**, 689, 3735.
16. J. M. Brunel, *Chem. Rev.*, **2005**, 105, 857.
17. M. Bougauchi, S. Watanabe, T. Arai, H. Sasai, M. Shibasaki, *J. Am. Chem. Soc.*, **1997**, 119, 2329.
18. Y. Shi, *Acc. Chem. Res.*, **2004**, 37, 488.
19. O. A. Wong, Y. Shi, *Chem. Rev.*, **2008**, 108, 3958.
20. A. Russo, C. De Fusco, A. Lattanzi, *ChemCatChem*, **2012**, 4, 901.
21. A. Corma, H. Garcia, *Adv. Synth. Catal.*, **2006**, 348, 1391.
22. J. Muzart, *Adv. Synth. Catal.*, **2006**, 348, 275.

23. (a) D. Betz, P. Altmann, M. Cokoja, W. A. Herrmann, F. E. Kühn, *Coord. Chem. Rev.*, **2011**, 255, 1518. (b) M. Crucianelli, R. Saladino, F. De Angelis, *ChemSusChem*, **2010**, 3, 524.
24. S. Krackl, A. Company, S. Enthaler, M. Driess, *ChemCatChem*, **2011**, 3, 1186.
25. D. Betz, A. Raith, M. Cokoja, F. E. Kühn, *ChemSusChem*, **2010**, 3, 559.
26. P. Altmann, M. Cokoja, F. E. Kühn, *Eur. J. Inorg. Chem.*, **2012**, 3235.
27. M. Bagherzadeh, L. Tahsini, R. Latifi, L. K. Woo, *Inorg. Chim. Acta.*, **2009**, 362, 3698.
28. A. Günyar, D. Betz, M. Drees, E. Herdtweck, F. E. Kühn, *J. Mol. Catal. A: Chem.*, **2010**, 331, 117.
29. P. M. Reis, C. A. Gamelas, J. A. Brito, N. Saffon, M. Gómez, B. Royo, *Eur. J. Inorg. Chem.*, **2011**, 666.
30. M. Abrantes, A. M. Santos, J. Mink, F. E. Kühn, C. C. Romão, *Organometallics*, **2003**, 22, 2112.
31. J. A. Schachner, P. Traar, C. Sala, M. Melcher, B. N. Harum, A. F. Sax, M. Volpe, F. Belaj, N. C. Mösch-Zanetti, *Inorg. Chem.*, **2012**, 51, 7642.
32. A. Rezaeifard, I. Sheikhshoae, N. Monadi, H. Stoeckli-Evans, *Eur. J. Inorg. Chem.*, **2010**, 799.
33. I. C. M. S. Santos, F. A. A. Paz, M. M. Q. Simões, M. G. P. M. S. Neves, J. A. Cavaleiro, J. Klinowski, A. M. Cavaleiro, *Appl. Catal., A*, **2008**, 351, 166.
34. K. Kamata, K. Yonehara, Y. Sumida, K. Yamaguchi, S. Hikichi, N. Mizuno, *Science*, **2003**, 300, 964.
35. V. Madhu, B. Ekambaram, L. J. W. Shimon, Y. Diskin, G. Leitius, R. Neumann, *Dalton Trans.*, **2010**, 39, 7266.
36. N. Gharah, S. Chakraborty, A. K. Mukherjee, R. Bhattacharyya, *Inorg. Chim. Acta*, **2009**, 362, 1089.
37. Y. Nakagawa, K. Kamata, M. Kotani, K. Yamaguchi, N. Mizuno, *Angew. Chem., Int. Ed.*, **2005**, 44, 5136.
38. W. A. Herrmann, R. M. Kratzer, H. Ding, W. R. Thiel, H. Glas, *J. Organomet. Chem.*, **1998**, 555, 293.
39. L. Gomez, I. Garcia-Bosch, A. Company, X. Sala, X. Fontrodona, X. Ribas, M. Costas, *Dalton Trans.*, **2007**, 5539.
40. P. Comba, H. Wadepohl, S. Wiesner, *Eur. J. Inorg. Chem.*, **2011**, 2610.
41. B. Bitterlich, K. Schröder, M. K. Tse, M. Beller, *Eur. J. Org. Chem.*, **2008**, 4867.
42. P. Gallezot, *Catal. Today*, **2007**, 121, 76.

43. C. Sell, *The Chemistry of Fragrance: From Perfumer to Consumer*, 2nd ed.; The Royal Society of Chemistry: United Kingdom, **2006**.
44. C. Fischer, *Food Flavors: Biology and Chemistry*; The Royal Society of Chemistry: United Kingdom, **1997**.
45. P. A. Wender, T. P. Mucciario, *J. Am. Chem. Soc.*, **1992**, *114*, 5878.
46. D. H. Grayson, *Nat. Prod. Rep.*, **1998**, *15*, 439.
47. M. Majewski, G. W. Bantle, *Synth. Commun.*, **1992**, *22*, 23.
48. A. Corma, S. Iborra, A. Velty, *Chem. Rev.*, **2007**, *107*, 2411.
49. T. R. Boehlow, C. D. Spilling, *Tetrahedron Lett.*, **1996**, *37*, 2717.
50. L. Salles, J.-M. Brégeault, R. Thouvenot, *C. R. Acad. Sci. Paris, Series IIC, Chemistry*, **2000**, *3*, 183.
51. J. Cubillos, M. Vargas, J. Reyes, A. Villa, C. M. de Correa, *Chirality*, **2010**, *22*, 403.
52. K. Ravikumar, F. Barbier, J.-P. Bégué, D. Bonnet-Delpon, *Tetrahedron*, **1998**, *54*, 7457.
53. T. Michel, M. Cokoja, V. Sieber, F. E. Kühn, *J. Mol. Catal. A: Chem.*, **2012**, *358*, 159.
54. T. Michel, D. Betz, M. Cokoja, V. Sieber, F. E. Kühn, *J. Mol. Catal. A: Chem.*, **2011**, *340*, 9.
55. A. L. de Villa, D. E. D. Vos, C. C. de Montes, P. A. Jacobs, *Tetrahedron Lett.*, **1998**, *39*, 8521.
56. H. Rudler, J. R. Gregorio, B. Denise, J.-M. Brégeault, A. Deloffre, *J. Mol. Catal. A: Chem.*, **1998**, *133*, 255.
57. S. Yamazaki, *Org. Biomol. Chem.*, **2010**, *8*, 2377.
58. T. Michel, M. Cokoja, F. E. Kühn, manuscript in preparation.
59. B. Bahramian, V. Mirkhani, S. Tangestaninejad, M. Moghadam, *J. Mol. Catal. A: Chem.*, **2006**, *244*, 139.
60. R. W. Saalfrank, S. Reihls, M. Hug, *Tetrahedron Lett.*, **1993**, *34*, 6033.
61. T. Punniyamurthy, B. Bhatia, M. Reddy, G. C. Maikap, J. Iqbal, *Tetrahedron*, **1997**, *53*, 7649.
62. K. B. Sharpless, *Angew. Chem., Int. Ed.*, **2002**, *41*, 2024.
63. R. M. Hanson, K. B. Sharpless, *J. Org. Chem.*, **1986**, *51*, 1922.
64. A. Lattanzi, P. Iannece, A. Scettri, *Tetrahedron Lett.*, **2002**, *43*, 5629.
65. W. Zhang, A. Basak, Y. Kosugi, Y. Hoshino, H. Yamamoto, *Angew. Chem., Int. Ed.*, **2005**, *44*, 4389.

66. J. Benet-Buchholz, P. Comba, A. Llobet, S. Roeser, P. Vadivelu, H. Wadepohl, S. Wiesner, *Dalton Trans.*, **2009**, 5910.
67. S. Koya, Y. Nishioka, H. Mizoguchi, T. Uchida, T. Katsuki, *Angew. Chem.*, **2012**, *124*, 8368.
68. H. Tanaka, H. Nishikawa, T. Uchida, T. Katsuki, *J. Am. Chem. Soc.*, **2010**, *132*, 12034.
69. W. Mägerlein, C. Dreisbach, H. Hugl, M. K. Tse, M. Klawonn, S. Bhor, M. Beller, *Catal. Today*, **2007**, *121*, 140.
70. H. Nishiyama, Y. Motoyama, *Chem. Commun.*, **1997**, 1863.
71. F. Gelalcha, G. Anilkumar, M. Tse, A. Brückner, M. Beller, *Chem. Eur. J.*, **2008**, *14*, 7687.
72. K. Matsumoto, Y. Sawada, B. Saito, K. Sakai, T. Katsuki, *Angew. Chem., Int. Ed.*, **2005**, *44*, 4935.
73. Y. Shimada, S. Kondo, Y. Ohara, K. Matsumoto, T. Katsuki, *Synlett*, **2007**, 2445.
74. A. Berkessel, M. Brandenburg, E. Leitterstorf, J. Frey, J. Lex, M. Schäfer, *Adv. Synth. Catal.*, **2007**, *349*, 2385.
75. A. U. Barlan, A. Basak, H. Yamamoto, *Angew. Chem., Int. Ed.*, **2006**, *45*, 5849.
76. P. Pietikäinen, *J. Mol. Catal. A: Chem.*, **2001**, *165*, 73.
77. S. Watanabe, Y. Kobayashi, T. Arai, H. Sasai, M. Bougauchi, M. Shibasaki, *Tetrahedron Lett.*, **1998**, *39*, 7353.
78. K. Daikai, M. Kamaura, J. Inanaga, *Tetrahedron Lett.*, **1998**, *39*, 7321.
79. T. Nemoto, T. Ohshima, K. Yamaguchi, M. Shibasaki, *J. Am. Chem. Soc.*, **2001**, *123*, 2725.
80. K. Daikai, T. Hayano, R. Kino, H. Furuno, T. Kagawa, J. Inanaga, *Chirality*, **2003**, *15*, 83.
81. A. Minatti, K. H. Dötz, *Eur. J. Org. Chem.*, **2006**, 268.
82. P. A. Kilty, W. M. H. Sachtler, *Catal. Rev.*, **1974**, *10*, 1.
83. H.-J. Lee, M. Ghanta, D. H. Busch, B. Subramaniam, *Chem. Eng. Sci.*, **2010**, *65*, 128.
84. J. Kollar, Catalytic epoxidation of an olefinically unsaturated compound using an organic hydroperoxide as an epoxidizing agent, Halcon International, Inc., U.S. Patent 3,350,422, **1967**.
85. J. Kollar, Epoxidation process, Halcon International, Inc., U.S. Patent 3,351,635, **1967**.
86. M. N. Sheng, J. G. Zajacek, Method of Producing Epoxides, The Atlantic Richfield Company, G.B. Patent 1,136,923, **1968**.
87. I. Yamanaka, K. Nakagaki, K. J. Otsuka, *Chem. Commun.*, **1995**, 1185.

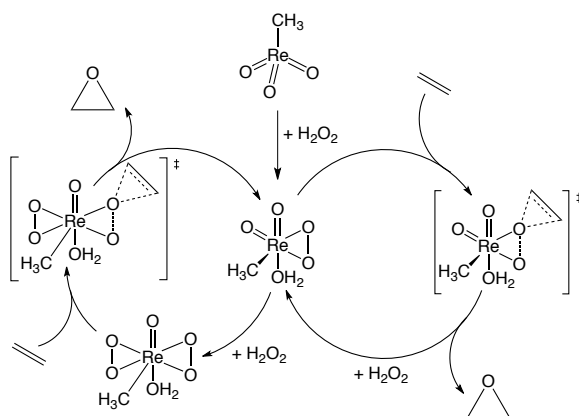
88. X. Zuwei, Z. Ning, S. Yu, L. Kunlan, *Science*, **2001**, 292, 1139.
89. Z. Ning, X. Zuwei, C. Guoying, G. Shuang, *Appl. Catal., A*, **2003**, 250, 239.
90. M. Colladon, A. Scarso, P. Sgarbossa, R. A. Michelin, G. Strukul, *J. Am. Chem. Soc.*, **2006**, 128, 14006.
91. H.-J. Lee, T.-P. Shi, D. H. Busch, D. Subramaniam, *Chem. Eng. Sci.*, **2007**, 62, 7282.

2 Objectives

This work concentrates on two transition metals that are known in epoxidation catalysis: rhenium and molybdenum. In the case of the former, only the high valent methyltrioxorhenium (MTO) will be discussed, whereas for the latter, a range of organometallic Mo(II) and Mo(VI) complexes will play an important role.

2.1 Methyltrioxorhenium

After its discovery in the late 1970s, MTO was regarded as a lab curiosity due to its restrictive synthesis.¹ Nevertheless, a better synthetic procedure was soon developed and it revealed its outstanding catalytic potential.² It is an efficient catalyst not only for olefin epoxidation,³ but for several other reactions as well, namely olefin metathesis, aldehyde olefination and even deoxygenation of epoxides.⁴ In contrary to the Mo-catalysed olefin epoxidation, the mechanism of the MTO/H₂O₂ system shown in Scheme 2.1 is widely accepted by the scientific community.⁵ Both the mono- and the bisperoxo complex are active epoxidation catalysts, with a comparable reaction rate.⁶



Scheme 2.1 The mechanism of MTO-catalysed olefin epoxidation with H₂O₂ as oxidant.

Due to the strong Lewis acidity of the metal centre, undesired side reactions such as ring opening and diol formation are usually occurring for sensitive epoxidation products.⁷ The formation of these undesired by-products can be prevented by addition of nitrogen bases, first shown by Sharpless *et al.*³ Chapter 3 presents experiments aimed at probing potential beneficial effects of chromophoric N-donor ligands in MTO adducts, as they might activate the catalytic system by providing additional energy for weakening bonds that have to be broken during the catalytic cycle.

2.2 Molybdenum complexes

Monomeric organomolybdenum carbonyl complexes of the general formula $[\eta^5-(C_5R_5)Mo(CO)_3X]$ (R = H, CH₃, CH₂Ph; X = alkyl, halide; Figure 2.1, left) are known to be pre-catalysts applicable in olefin epoxidation.⁸ A major breakthrough in terms of catalytic activity was achieved with *ansa* compounds of the general formula $[Mo(\eta^5-C_5H_4(CH(CH_2)_n)-\eta^1-CH)(CO)_3]$ (Figure 2.1, right). In both organic solvents and ionic liquids, they outperform almost all previously investigated systems.⁹

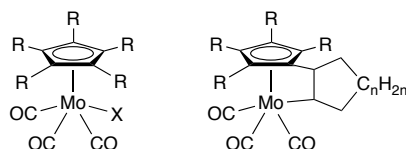


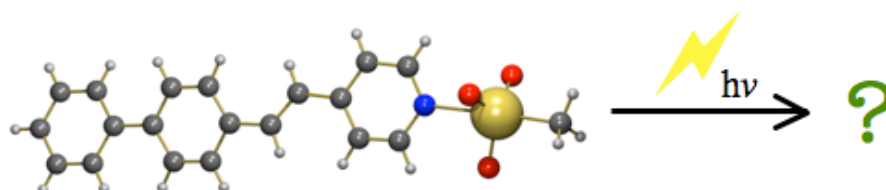
Figure 2.1 A sketch of two monomeric organomolybdenum complexes, with R = H, CH₃, CH₂Ph and X = alkyl, halide.

Besides steric influences, the electronic properties of the complex can mainly be hold responsible for the catalytic performance. The comparison of the known epoxidation pre-catalyst [CpMo(CO)₃CH₃] with its fluorinated counterpart [CpMo(CO)₃CF₃] is presented in Chapter 4. The complexes are sterically nearly identical, however, the Lewis acidity of the metal centre and hence, the catalyst activity is supposed to increase as a consequence of the electron-withdrawing CF₃ ligand. Moreover, there is an open discussion about the mechanism of the olefin epoxidation mechanism catalysed by Mo-complexes. More than three decades ago, Mimoun¹⁰ and Sharpless¹¹ proposed two mechanisms for this reaction. To date, even DFT calculations have not provided a clear answer.¹² Therefore, our research focus was set to address the elucidation of the mechanism by an experimental approach. Our investigations, based on the above-mentioned organomolybdenum carbonyl complexes and their oxidation products, *i.e.* dioxo and oxo peroxy Mo(VI) compounds, are presented in Chapter 5. The varying reactivity of [CpMo(CO)₃R]-type complexes towards the oxidant *tert*-butyl hydroperoxide is discussed in Chapter 6; therein, the complete IR and Raman spectroscopic analyses of the complexes is presented, providing the basis for force constants calculations of the molybdenum-carbonyl bonds.

2.3 References

1. R. I. Beattie, P. J. Jones, *Inorg. Chem.*, **1979**, *18*, 2318.
2. (a) W. A. Herrmann, J. G. Kuchler, J. K. Felixberger, E. Herdtweck, W. Wagner, *Angew. Chem.*, **1988**, *100*, 420; *Angew. Chem. Int. Ed. Engl.*, **1988**, *27*, 394. (b) F. E. Kühn, A. Scherbaum, W. A. Herrmann, *J. Organomet. Chem.*, **2004**, 689, 4149.
3. (a) W. A. Herrmann, R. W. Fischer, D. W. Marz, *Angew. Chem.*, **1991**, *103*, 1706; *Angew. Chem. Int. Ed. Engl.*, **1991**, *30*, 1638. (b) J. Rudolph, K. L. Reddy, J. P. Chiang, K. B. Sharpless, *J. Am. Chem. Soc.*, **1997**, *119*, 6189. (c) F. E. Kühn, A. M. Santos, W. A. Herrmann, *Dalton Trans.*, **2005**, 2483.
4. (a) W. A. Herrmann, M. Wang, *Angew. Chem.*, **1991**, *103*, 1709; *Angew. Chem. Int. Ed. Engl.*, **1991**, *30*, 1641. (b) W. A. Herrmann, W. Wagner, U. N. Flessner, U. Volkhardt, H. Komber, *Angew. Chem.*, **1991**, *103*, 1704; *Angew. Chem. Int. Ed. Engl.*, **1991**, *30*, 1636. (c) J. E. Ziegler, M. J. Zdilla, A. J. Evans, M. M. Abu-Omar, *Inorg. Chem.*, **2009**, *48*, 9998.
5. (a) W. Adam, C. M. Mitchell, *Angew. Chem.*, **1996**, *108*, 578. (b) W. Adam, C. M. Mitchell, *Angew. Chem. Int. Ed. Engl.*, **1996**, *35*, 533 (c) O. Pestovski, R. V. Eldik, P. Huston, J. H. Espenson, *J. Chem. Soc. Dalton Trans.*, **1995**, 133. (d) P. Gisdakis, W. Antonczak, S. Köstlmeier, W. A. Herrmann, N. Rösch, *Angew. Chem.*, **1998**, *110*, 2333 (e) P. Gisdakis, W. Antonczak, S. Köstlmeier, W. A. Herrmann, N. Rösch, *Angew. Chem. Int. Ed. Engl.*, **1998**, *37*, 2211. (f) P. Gisdakis, N. Rösch, *Eur. J. Org. Chem.*, **2001**, *4*, 719. (g) P. Gisdakis, I. V. Yudanov, N. Rösch, *Inorg. Chem.*, **2001**, *40*, 3755.
6. (a) A. Al-Ajlouni, J. H. Espenson, *J. Am. Chem. Soc.*, **1995**, *117*, 9243. (b) J. H. Espenson, *Chem. Commun.*, **1999**, 479. (c) W. Adam, C. R. Saha-Möller, O. Weichold, *J. Org. Chem.*, **2000**, *65*, 5001.
7. C. C. Romão, F. E. Kühn, W. A. Herrmann, *Chem. Rev.*, **1997**, *97*, 3197.
8. (a) F. E. Kühn, A. M. Santos, W. A. Herrmann, *Dalton Trans.*, **2005**, 2483. (b) F. E. Kühn, A. M. Santos, M. Abrantes, *Chem. Rev.*, **2006**, *106*, 2455. (c) N. Grover, F. E. Kühn, *Curr. Org. Chem.*, **2012**, *16*, 16.
9. (a) A. Capapé, A. Raith, F. E. Kühn, *Adv. Synth. Catal.*, **2009**, *351*, 66. (b) A. Capapé, A. Raith, E. Herdtweck, M. Cokoja, F. E. Kühn, *Adv. Synth. Catal.*, **2010**, *352*, 547. (c) D. Betz, A. Raith, M. Cokoja, F. E. Kühn, *ChemSusChem*, **2010**, *3*, 559.
10. H. Mimoun, I. Serée de Roch, L. Sajus, *Tetrahedron*, **1970**, *26*, 37.
11. K. B. Sharpless, J. M. Townsend, D. R. Williams, *J. Am. Chem. Soc.*, **1972**, *94*, 295.
12. (a) A. Comas-Vives, A. Lledós, R. Poli, *Chem. Eur. J.*, **2010**, *16*, 2147. (b) P. J. Costa, M. J. Calhorda, F. E. Kühn, *Organometallics*, **2010**, *29*, 303.

3 Chromophoric Lewis Base Adducts of Methyltrioxorhenium: Synthesis, Catalysis and Photochemistry



This chapter originated the following publication:
S. A. Hauser, V. Korinth, E. Herdtweck, M. Cokoja, W. A. Herrmann, F. E. Kühn,
Eur. J. Inorg. Chem., **2010**, 4083-4090.

3.1 Background

Much research has been dedicated to the chemistry of methyltrioxorhenium (MTO) since its discovery by Beattie and Jones¹ in the late 1970s and the improvement of the synthesis by Herrmann and co-workers² some years later. The latter group discovered the ability of MTO to act as a versatile catalyst of various organic reactions.³ MTO can be used in several catalytic processes, for instance olefin metathesis⁴ and aldehyde olefination.⁵ Most recently, MTO has been successfully applied in deoxygenation of epoxides.⁶ However, the most important and thus best studied MTO-catalysed reaction is olefin epoxidation.^{7–9} Due to the strong Lewis acidity of the metal centre, undesired side reactions such as ring opening and diol formation are usually occurring. This can be prevented by addition of bases, mostly pyridine, bipyridine or pyrazole and their derivatives, as shown by Sharpless *et al.* and other groups.^{8,10–19} The photochemistry of MTO was for the first time under examination in the early 1990s.^{20,21} MTO solutions were found to be very sensitive to UV light, the rhenium-carbon bond was reported to be photolysed after a short irradiation time, with subsequent formation of ReO_4^- and ReO_3 , at low and high concentrations, respectively.²⁰ Some years later, the studies were extended to Lewis base adducts of MTO. Interesting properties of these adducts were published,^{22,23} but no further research was conducted in this direction. This prompted us to investigate the effect of a number of novel chromophoric Lewis base adducts of MTO with respect to the complex stability under irradiation with UV light.

3.2 Results and Discussion

3.2.1 Synthesis and spectroscopic characterisation

A series of chromophoric pyridine derivatives (**1-7**, Figure 3.1) was synthesised and the coordination to MTO was examined.

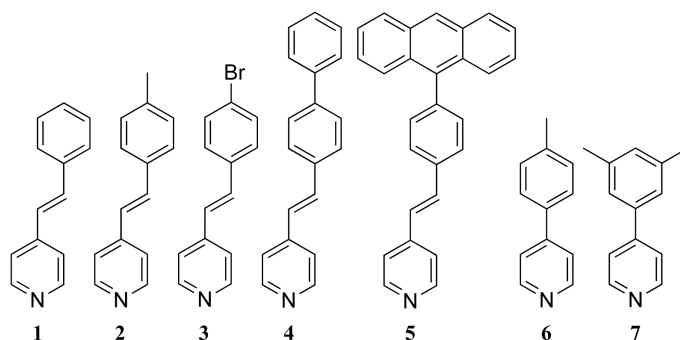
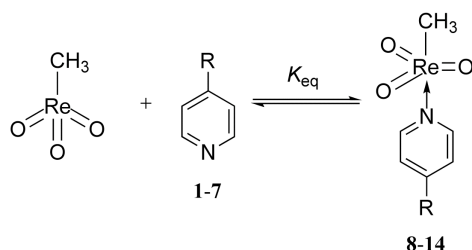


Figure 3.1 Overview of the pyridine derivatives employed as ligands for coordination to MTO.

Complexes **8-14** were formed by treatment of MTO with ligands **1-7** in a 1:1 ratio in diethyl ether at room temperature (Scheme 3.1). Subsequent cooling of the yellow solution led

to precipitation of yellow crystals, which were isolated by filtration and purified by washing with *n*-hexane. The compounds obtained are stable to air, both in the solid state and in dichloromethane solution.



Scheme 3.1 Adduct formation of MTO with pyridine derivatives in solution.

Selected ^1H and ^{13}C NMR spectroscopic data of compounds **8-14** are shown in Table 3.1. The proton signals of the MTO methyl group of the complexes are considerably shifted to higher field, indicating the strength of the Re-N bond.¹⁵ The same effect is observed in the ^{13}C NMR spectra. The vicinal protons to the nitrogen of the ligand have a different electronic environment, similar to the methyl group of the MTO, which is manifested by a high-field shift compared to the free ligand. In the IR spectra, a red-shift of Re=O bands compared to free MTO is observable. This gives rise to an enhanced electron density donated from the ligand to the Re centre, causing weakening of the Re=O bond (see Table 3.2).

Table 3.1 Selected ^1H and ^{13}C NMR spectroscopic data for complexes **8-14** in CDCl_3 .

| | $\alpha\text{-H}$ ligand, ^1H δ [ppm] | $\alpha\text{-H}$ adduct, ^1H δ [ppm] | Re-CH ₃ , ^1H δ [ppm] | Re-CH ₃ , ^{13}C δ [ppm] |
|-----------|--|--|---|--|
| MTO | — | — | 2.67 | 19.0 |
| 8 | 8.51 (1) | 8.29 | 2.03 | 24.7 |
| 9 | 8.55 (2) | 8.20 | 1.92 | 25.1 |
| 10 | 8.58 (3) | 8.26 | 1.96 | 24.0 |
| 11 | 8.59 (4) | 8.34 | 2.13 | 24.4 |
| 12 | 8.63 (5) | 8.33 | 2.00 | 24.9 |
| 13 | 8.63 (6) | 8.31 | 1.97 | 24.8 |
| 14 | 8.65 (7) | 8.32 | 1.98 | 24.4 |

Table 3.2 Characteristic IR vibrations of CH_3ReO_3 fragments (cm^{-1}) in **8-14**.

| MTO | 8 | 9 | 10 | 11 | 12 | 13 | 14 | Assignment |
|-----|----------|----------|---------------------|-----------|-----------|-----------|-----------|--------------------------|
| 998 | 934 | 936 | 931 | n.o. | n.o. | 934 | 93 | ReO_3 sym str. |
| 965 | 927 | 926 | n.o. ^[a] | 927 | 928 | 927 | n.o. | ReO_3 asym str. |

^[a] not observed.

3.2.2 X-ray crystal structure of ligand 5 and complexes 8-14

The solid-state structure of the synthesised compounds **5** and **8-14** was measured; one example is shown in Figure 3.2. Selected bond lengths are given in Table 3.3. With one exception (compound **11**), the N-base ligand coordinates *trans* to the methyl group to the rhenium centre. Complex **11**, however, exists in both *cis* and *trans* arrangements in the solid state. Together with the finding that only one peak is visible in the ^{17}O NMR spectrum, this strongly indicates that packing forces are responsible for the solid-state configuration, rather than electronic or steric ligand effects. Moreover, this conclusion is in accordance with previously reported data.²⁴

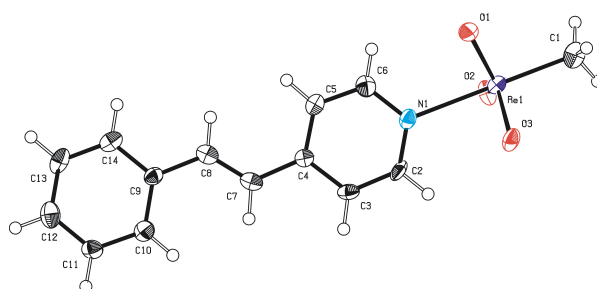


Figure 3.2 PLATON view of the solid-state structure of complex **8**. The thermal ellipsoids are shown at the 50% probability level.

Table 3.3 Selected bond lengths for complexes **8-14** (*trans* configuration) determined by single-crystal X-ray diffraction .

| | Re-N [Å] | Re-C [Å] | Re-O [Å] |
|--------------------------|----------|----------|-------------------------------|
| MTO ^[a] | — | 2.074(4) | 1.703(2) |
| 8 | 2.422(5) | 2.113(7) | 1.712(3) 1.706(6) 1.726(7) |
| 9 | 2.445(5) | 2.094(6) | 1.718(4) 1.705(4) 1.707(4) |
| 10 ^[b] | 2.439(4) | 2.099(5) | 1.717(4) 1.716(3) 1.716(3) |
| | 2.438(5) | 2.102(6) | 1.711(3) 1.716(4) 1.720(3) |
| 11 ^[b] | 2.372(3) | 2.112(4) | 1.722(3) 1.719(3) 1.713(3) |
| | 2.439(3) | 2.081(5) | 1.714(3) 1.712(3) 1.714(3) |
| 12 | 2.418(2) | 2.091(3) | 1.720(2) 1.711(2) 1.714(2) |
| 13 | 2.417(3) | 2.092(4) | 1.716(4) 1.716(3) 1.722(3) |
| 14 ^[b] | 2.408(4) | 2.102(5) | 1.713(2) 2x1.708(4) |
| | 2.392(4) | 2.101(5) | 1.706(3) 2x1.694(4) |

^[a] Values taken from ref. 25. ^[b] The values of the second, crystallographically independent molecule are printed in italics.

3.2.3 Determination of formation constants

The formation constants of the MTO-ligand adducts **8-14** were determined by means of UV/Vis spectroscopy.²⁶ Scheme 3.1 shows the equilibrium that is established in presence of MTO and a pyridine derivative. According to equation (3.1), which is derived from the Lambert-Beer law (path length: 1 cm), the absorbance of the solution (Abs) changes in function of the presence of free ligand (L), uncoordinated MTO (M) and the MTO-ligand adduct (ML).

$$Abs = \varepsilon_L \cdot [L] + \varepsilon_M \cdot [M] + \varepsilon_{ML} \cdot [ML] \quad (3.1)$$

The adduct concentration [ML] can be expressed using the formation constant (K_{eq}) by taking into account the molar balance $[M]_T = [M] + [ML]$, leading to equation (3.2).

$$Abs = \varepsilon_L \cdot [L] + \varepsilon_M \cdot [M] + \frac{\varepsilon_{ML} \cdot [M]_T \cdot K_{eq} \cdot [L]}{1 + K_{eq} \cdot [L]} \quad (3.2)$$

Above 330 nm, the absorbance of MTO is negligible, *i.e.* $\varepsilon_M \approx 0$.²⁷ If the absorbance of the free ligands at the chosen wavelength can also be ignored, *i.e.* $\varepsilon_L \approx 0$, then equation (3.3) can be used to calculate the formation constant.

$$Abs = \frac{\varepsilon_{ML} \cdot [M]_T \cdot K_{eq} \cdot [L]}{1 + K_{eq} \cdot [L]} \quad (3.3)$$

The values of the adduct formation constants (Table 3.4) are calculated by fitting of experimental absorbance data to equation (3.2) or (3.3). Figure 3.3 shows the change in the absorption spectrum upon successive addition of MTO to a ligand solution in CH_2Cl_2 .

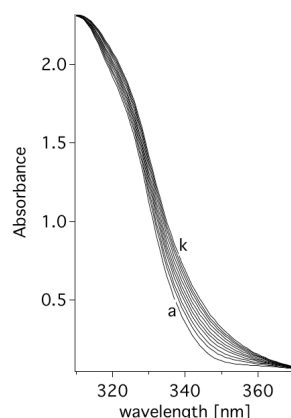


Figure 3.3 Change in the absorption in function of complex formation (**10**). (a) free ligand ($[3] = 0.1$ mM), successive addition of 1 equiv. of MTO, (k) ligand with 10 equiv. MTO.

In the case of the compound **10**, complex formation can be noticed at 350 nm. Thus, the values at this wavelength have been used for the curve fitting according to equation (3.3) (see

Figure 3.4).

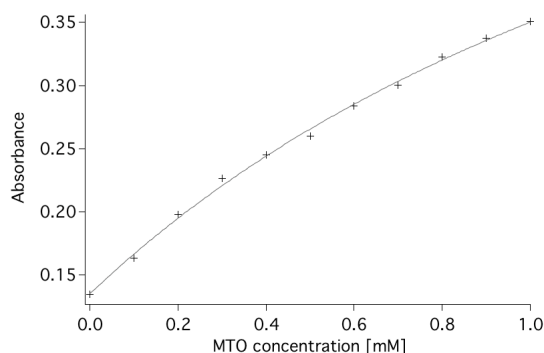


Figure 3.4 Curve fitting with equation (3.3) for determination of formation constant of complex **10**.

The values of the formation constants for complexes **8-14** are comparable to those reported in literature.^{26,28–30} Moreover, the influence of both the electronic and steric nature of the ligand can be seen. The stability of the adducts is higher when the ligand has electron-donating substituents and is less sterically crowded. The electronic effect is nicely seen when comparing the formation constant of complex **9** with that of complex **10**. The steric effect accounts for the difference in the value of the formation constant of complex **13** and complex **14**.

Table 3.4 Formation constants of compounds **8-14** in CH₂Cl₂.

| | Absorbance [nm] | Formation constant (K_{eq}) [Lmol ⁻¹] |
|-----------|-----------------|---|
| 8 | 340 | 431 ± 27 |
| 9 | 355 | 563 ± 88 |
| 10 | 350 | 386 ± 47 |
| 11 | 370 | 309 ± 36 |
| 12 | 335 | 78 ± 25 |
| 13 | 300 | 348 ± 93 |
| 14 | 300 | 286 ± 98 |

3.2.4 Application in epoxidation catalysis

The performance of ligands **2-7** was tested in the MTO-catalysed epoxidation of 1-octene with hydrogen peroxide. *Tert*-butylpyridine (*t*Bu-Pyr) was chosen as a benchmark ligand. A catalyst:ligand:oxidant:substrate ratio of 1:5:150:100 was used in all experiments, unless stated otherwise. The catalytic tests were performed at room temperature and twice with each ligand: once with exclusion of light and once in light with the goal to establish a statement about the supposed beneficial effect of chromophoric pyridine derivatives with respect to the already known advantages of simple pyridine derivatives in epoxidation catalysis with MTO.¹⁹ Further details are given in the Experimental Section. No significant diol formation or formation of other by-products could be observed.

Table 3.5 summarises the turn-over frequencies (TOF) of the different catalytic systems tested. Maximum epoxide yield is obtained after 24 h reaction time, with a substrate conversion between 50 and 80% (Figure 3.5). *t*Bu-Pyr shows no significant advantage in catalytic performance compared to the chromophoric pyridine derivatives. Moreover, it can be noted that the advantage of running the catalytic reaction under exclusion of light is negligible with either type of pyridine ligand. The yields of 1-octene epoxide with the ligand additives tested within this work are comparable to the yield achieved with MTO alone.³¹ Nevertheless, they are far from those obtained with 3-methylpyrazole or pyrazole under the same conditions.³¹

Table 3.5 Turn-over frequencies [mol(epoxide) mol(cat)⁻¹ h⁻¹] determined after 5 min.

| Ligand | TOF [h ⁻¹] | Yield [%], after 24 h with exclusion of light |
|-----------------|------------------------|---|
| 2 | 63 | 76 |
| 3 | 44 | 69 |
| 4 | 65 | 69 |
| 5 | 46 | 65 |
| 6 | 49 | 73 |
| 7 | 41 | 72 |
| <i>t</i> Bu-Pyr | 35 | 71 |

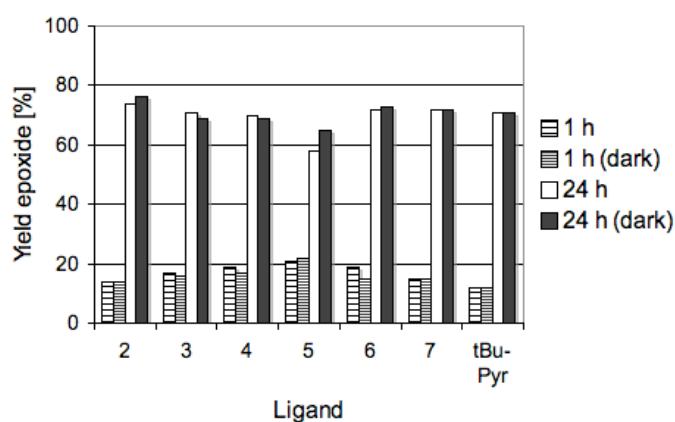


Figure 3.5 1-Octene epoxide yields with different ligands.

3.2.5 Photostability of the synthesised compounds

One aim of this work was to probe potential beneficial effect of chromophoric Lewis bases in MTO adducts. They might activate the catalytic system by providing additional energy for weakening bonds that have to be broken during the catalytic cycle. However, photoinduced homolysis of the Re-CH₃ bond in solution is the most common way of degradation of MTO.²⁰ Vogler *et al.* reported the photoassisted isomerisation of 4-styrylpyridine, where the complex remained intact, *i.e.* the MTO was not affected by UV-radiation.²³ This led to the hypothesis

that larger chromophoric systems might lead to stable MTO Lewis base adducts on the one hand, and act as photosensitisers on the other hand. The most convenient approaches to study the stability or the photo-induced degradation of the MTO adducts are ^{17}O NMR and UV/Vis spectroscopy. For the NMR studies, a 0.1 M solution of the complexes in CDCl_3 was used and treated with UV light ($\lambda = 368 \text{ nm}$). In a second experiment, a fivefold excess of ligand was added to MTO, in order to mimic the reaction conditions of the catalytic tests (*vide supra*).

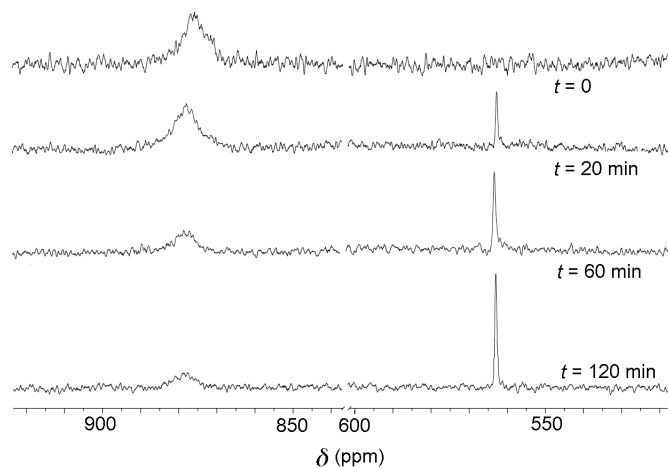


Figure 3.6 Time resolved ^{17}O NMR spectra of complex **11** before (top) and after irradiation with UV light. The signal of the MTO oxo moieties at $\delta = 879 \text{ ppm}$ is broadened due to fluxional equilibrium of complex formation, whereas the sharp peak at $\delta = 563 \text{ ppm}$ can be assigned $[\text{ReO}_4]^-$.

The chemical shift of the oxygen atoms of the freshly synthesised complexes was found to be between 865 ppm and 885 ppm which is consistent with the reported literature values.^{32,33} Upon irradiation, already after 6 min a peak at $\delta = 563 \text{ ppm}$ was detected, which could be attributed to the perrhenate anion.³² This peak became more pronounced after longer irradiation time (see Figure 3.6). There was no significant difference in stability of the MTO in the two experiments performed. Noteworthy, all complexes synthesised in this work have shown the same behaviour under irradiation with UV light. The UV/Vis spectra were recorded in CH_2Cl_2 . A 0.1 M solution of selected complexes was irradiated with UV light and several samples were taken. Figure 3.7 shows the spectral change over a time span of 2 h. Ligand absorption is very strong, it shows a maximum at 325 nm. It partially overlaps complex absorption as well as the absorbance pattern of free MTO.²⁰ Upon photolytic degradation of MTO, the ligand is protonated. Thus, its absorbance spectrum changes by a shift of the maximum to 375 nm. The above-mentioned experiments clearly show that both the MTO and the ligands are affected by prolonged irradiation with UV light. Thus, no additional stability is brought to the adducts by the use of chromophoric pyridine derivatives. Despite of the use of chromophoric pyridine derivatives as ligands on MTO, the obtained adducts are not stable to UV light. However, as described above, the catalytic epoxidation is not influenced by light.

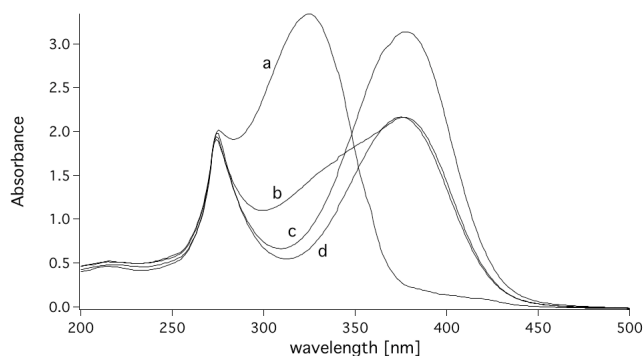


Figure 3.7 UV/Vis spectra of complex **11** in CH_2Cl_2 ($c = 0.16 \text{ mM}$). (a) Initial spectrum; (b) after 20 min exposure to UV light; (c) after 60 min; (d) after 120 min, the decrease in intensity of the peak at 377 nm can be explained by precipitation of the perrhenate and protonated ligand.

3.3 Conclusion

In this study, seven chromophoric pyridine derivatives were prepared and treated with MTO to form seven Lewis base adducts of MTO. They have been fully characterised and tested as catalysts in the epoxidation of 1-octene with H_2O_2 . With respect to the benchmark ligand *tert*-butylpyridine, the presented ligands do not show any advantages in the epoxidation of 1-octene, whether performed under exclusion of light or in daylight (see Figure 3.5). Moreover, the photochemistry of the complexes was studied by means of UV/Vis and ^{17}O NMR spectroscopy. The chromophoric ligands did not influence the adduct stability under UV irradiation. Complex decomposition occurred through the reported pathway,²⁰ as formation of the perrhenate anion was already observable after a short irradiation time with UV light (see Figure 3.6 and Figure 3.7).

3.4 Experimental Section

3.4.1 Materials and methods

All experimental work was carried out using standard Schlenk techniques under argon. Solvents were dried by standard procedures (hexane and diethyl ether over Na/benzophenone; CH_2Cl_2 over CaH_2), distilled and stored under argon over molecular sieves. High resolution NMR spectra were measured with Bruker Avance DPX-400 (^1H : 400 MHz; ^{13}C : 100.6 MHz; ^{17}O : 54.2 MHz), and JEOL NMR GX-400 (^1H : 400 MHz; ^{13}C : 100.6 MHz) spectrometers. The UV/Vis spectra were recorded on a JASCO UV/Vis V-550 spectrophotometer and the IR spectra on a Perkin-Elmer 1600 series FT-IR instrument. Microanalyses of the obtained products were performed in the Mikroanalytisches Labor of the Technical University of Munich, Garching, Germany. MTO was synthesised according to literature procedures.³⁴

3.4.2 Ligand synthesis

Ligands **1-3** were synthesised by treating a solution of 4-picoline (2.48 mmol) in THF at -60 °C with an equimolar amount of lithium diisopropylamine in THF.³⁵ The alcoholate was formed upon addition of the corresponding aldehyde, which was subsequently eliminated by refluxing in concentrated acetic acid for 18 h to form the C-C double bond. Purification was done by column chromatography on silica gel. The synthesis of ligands **4-7** was based on the Suzuki cross coupling mechanism described by Fu *et al.*³⁶ The heteroaryl boronic acid reacted with an aryl bromide in refluxing dioxane, whereas the reaction was catalysed by [Pd₂(dba)₃] (dba = dibenzylideneacetone), PCy₃ and K₃PO₄ (aq.). Subsequent purification steps included filtration, extraction of the filtrate and column chromatography. Complete analyses of the ligands can be found in Appendix A.

3.4.3 Typical procedure for the preparation of the chromophoric Lewis base adducts of MTO

An equimolar amount of MTO and ligand was dissolved in diethyl ether and the solution was stirred for 1 h before cooling the mixture in an ice bath. A yellow precipitate formed, which was filtered and washed with hexane. The solid was dried in vacuo and analysed by standard analysis methods. Complete analyses of the complexes can be found in Appendix A.

3.4.4 Single-crystal X-ray structure determination

Compound 5: C₂₇H₁₉N; $M_r = 357.43$; crystal colour and shape: colourless fragment, crystal dimensions = 0.51x0.5x0.64 mm; crystal system: monoclinic; space group: *Cc* (no. 9); $a = 14.9971(6)$, $b = 10.9497(4)$, $c = 12.4175(5)$ Å; $\beta = 114.048(2)^\circ$; $V = 1862.14(13)$ Å³; $Z = 4$; $\mu(\text{Mo-K}\alpha) = 0.073$ mm⁻¹; $\rho_{\text{calcd.}} = 1.275$ g cm⁻³; Θ range 2.38-25.34; data collected: 32910; independent data [$I_o > 2\sigma(I_o)$]/all data/ R_{int}]: 3360/3397/0.023; data/restraints/-parameters: 3397/2/329; $R1$ [$I_o > 2\sigma(I_o)$]/all data] = 0.0255/0.0258; $wR2$ [$I_o > 2\sigma(I_o)$]/all data] = 0.0709/0.0713; GOF = 1.080; $\Delta\rho_{\text{max/min}} = 0.13/-0.12$ e Å⁻³. CCDC-777693

Compound 8: C₁₄H₁₄NO₃Re; $M_r = 430.47$; crystal colour and shape: yellow fragment, crystal dimensions = 0.13x0.18x0.51 mm; crystal system: monoclinic; space group: *P2*₁ (no. 4); $a = 9.0054(2)$, $b = 7.2442(2)$, $c = 11.0721(3)$ Å; $\beta = 109.3284(11)^\circ$; $V = 681.60(3)$ Å³; $Z = 2$; $\mu(\text{Mo-K}\alpha) = 8.916$ mm⁻¹; $\rho_{\text{calcd.}} = 2.098$ g cm⁻³; Θ range 1.95-25.39; data collected: 10806; independent data [$I_o > 2\sigma(I_o)$]/all data/ R_{int}]: 2275/2281/0.059; data/restraints/-parameters: 2281/1/173; $R1$ [$I_o > 2\sigma(I_o)$]/all data] = 0.0259/0.0259; $wR2$ [$I_o > 2\sigma(I_o)$]/all data] = 0.0648/0.0648; GOF = 1.090; $\Delta\rho_{\text{max/min}} = 2.27/-2.57$ e Å⁻³. CCDC-777694

Compound 9: C₁₅H₁₆NO₃Re; $M_r = 444.49$; crystal colour and shape: yellow fragment, crystal dimensions 0.15x0.15x0.43 mm; crystal system: monoclinic; space group: *P2*₁/*c* (no.

14); $a = 9.1661(4)$, $b = 7.1741(3)$, $c = 22.3772(9)$ Å; $\beta = 97.795(2)^\circ$; $V = 1457.89(11)$ Å³; $Z = 4$; $\mu(\text{Mo-K}\alpha) = 8.341$ mm⁻¹; $\rho_{\text{calcd.}} = 2.025$ g cm⁻³; Θ range 1.84- 25.36; data collected: 29722; independent data [$I_o > 2\sigma(I_o)$]/all data/ R_{int}]: 2423/2564/0.058; data/restraints/parameters: 2564/0/183; $R1[I_o > 2\sigma(I_o)$]/all data] = 0.0289/0.0307; $wR2 [I_o > 2\sigma(I_o)$]/all data] = 0.0671/0.0680; GOF = 1.261; $\Delta\rho_{\text{max/min}} = 0.85/-1.54$ e Å⁻³. CCDC-777695

Compound 10: C₁₄H₁₃BrNO₃Re; $M_r = 509.36$; crystal colour and shape: yellow fragment, crystal dimensions 0.05x0.13x0.53 mm; crystal system: triclinic; space group: $P\bar{1}(no.2)$; $a = 5.9849(2)$, $b = 15.9131(6)$, $c = 17.0785(6)$ Å; $\alpha = 66.0608(15)$, $\beta = 85.8488(15)$, $\gamma = 86.3720(14)^\circ$; $V = 1481.68(9)$ Å³; $Z = 4$; $\mu(\text{Mo-K}\alpha) = 10.903$ mm⁻¹; $\rho_{\text{calcd.}} = 2.283$ g cm⁻³; Θ range 1.31-25.45; data collected: 18921; independent data [$I_o > 2\sigma(I_o)$]/all data/ R_{int}]: 4839/5188/0.042; data/restraints/parameters: 5188/0/363; $R1[I_o > 2\sigma(I_o)$]/all data] = 0.0264/0.0286; $wR2 [I_o > 2\sigma(I_o)$]/all data] = 0.0697/0.0721; GOF = 1.048; $\Delta\rho_{\text{max/min}} = 2.13/-1.85$ e Å⁻³. CCDC-777696

Compound 11: C₂₀H₁₈NO₃Re; $M_r = 506.56$; crystal colour and shape: yellow fragment, crystal dimensions 0.24x0.35x0.38 mm; crystal system: triclinic; space group: $P\bar{1}(no.2)$; $a = 5.7288(3)$, $b = 11.4564(6)$, $c = 27.4120(14)$ Å; $\alpha = 82.715(3)$, $\beta = 89.200(2)$, $\gamma = 77.895(2)^\circ$; $V = 1744.74(16)$ Å³; $Z = 4$; $\mu(\text{Mo-K}\alpha) = 6.983$ mm⁻¹; $\rho_{\text{calcd.}} = 1.929$ g cm⁻³; Θ range 0.75-25.37; data collected: 69973; independent data [$I_o > 2\sigma(I_o)$]/all data/ R_{int}]: 5347/6039/0.070; data/restraints/parameters: 6039/0/453; $R1[I_o > 2\sigma(I_o)$]/all data] = 0.0217/0.0279; $wR2 [I_o > 2\sigma(I_o)$]/all data] = 0.0507/0.0538; GOF = 1.068; $\Delta\rho_{\text{max/min}} = 0.87/-0.52$ e Å⁻³. CCDC-777697

Compound 12: C₂₈H₂₂NO₃Re; $M_r = 606.68$; crystal colour and shape: yellow fragment, crystal dimensions 0.15x0.18x0.36 mm; crystal system: triclinic; space group: $P\bar{1}(no.2)$; $a = 9.8694(3)$, $b = 10.9626(4)$, $c = 12.5154(7)$ Å; $\alpha = 99.490(2)$, $\beta = 105.050(2)$, $\gamma = 112.906(1)^\circ$; $V = 1149.44(9)$ Å³; $Z = 2$; $\mu(\text{Mo-K}\alpha) = 5.316$ mm⁻¹; $\rho_{\text{calcd.}} = 1.753$ g cm⁻³; Θ range 1.77-25.44; data collected: 27800; independent data [$I_o > 2\sigma(I_o)$]/all data/ R_{int}]: 3917/3955/0.039; data/restraints/parameters: 3955/0/299; $R1[I_o > 2\sigma(I_o)$]/all data] = 0.0139/0.0141; $wR2 [I_o > 2\sigma(I_o)$]/all data] = 0.0356/0.0358; GOF = 1.078; $\Delta\rho_{\text{max/min}} = 1.12/-0.44$ e Å⁻³. CCDC-777698

Compound 13: C₁₃H₁₄NO₃Re; $M_r = 418.46$; crystal colour and shape: yellow fragment, crystal dimensions 0.15x0.20x0.38 mm; crystal system: monoclinic; space group: $P2_1/c$ (no. 14); $a = 11.6924(4)$, $b = 14.3708(4)$, $c = 8.2219(3)$ Å; $\beta = 110.3695(14)^\circ$; $V = 1295.13(8)$ Å³; $Z = 4$; $\mu(\text{Mo-K}\alpha) = 9.381$ mm⁻¹; $\rho_{\text{calcd.}} = 2.146$ g cm⁻³; Θ range 1.86-25.39; data collected: 4902; independent data [$I_o > 2\sigma(I_o)$]/all data/ R_{int}]: 2196/2260/0.028; data/restraints/parameters: 2260/0/165; $R1[I_o > 2\sigma(I_o)$]/all data] = 0.0218/0.0225; $wR2 [I_o > 2\sigma(I_o)$]/all data] = 0.0556/0.0561; GOF = 1.144; $\Delta\rho_{\text{max/min}} = 1.12/-1.39$ e Å⁻³. CCDC-777699

Compound 14: C₁₄H₁₆NO₃Re; $M_r = 432.49$; crystal colour and shape: yellow needle, crystal dimensions 0.03x0.05x0.23 mm; crystal system: monoclinic; space group: $P2_1/m$ (no. 11); $a = 6.4763(9)$, $b = 11.652(2)$, $c = 18.930(3)$ Å; $\beta = 93.705(6)^\circ$; $V = 1425.5(4)$ Å³; $Z = 4$; $\mu(\text{Mo-K}\alpha) = 8.527$ mm⁻¹; $\rho_{\text{calcd.}} = 2.015$ g cm⁻³; Θ range 1.08-25.37; data collected: 35302; independent data [$I_o > 2\sigma(I_o)$]/all data/ R_{int}]: 2592/2741/0.048; data/restraints/

parameters: 2741/0/195; $R1[I_o > 2\sigma(I_o)/\text{all data}] = 0.0186/0.0200$; $wR2 [I_o > 2\sigma(I_o)/\text{all data}] = 0.0410/0.0416$; $\text{GOF} = 1.099$; $\Delta\rho_{\text{max/min}} = 1.09/-1.30 \text{ e } \text{\AA}^{-3}$. CCDC-77770

3.4.5 Formation constant measurements

An UV/Vis spectrophotometric method was used to determine the formation constants of the chromophoric Lewis base adducts of MTO. Aliquots of a 0.1 mM solution of MTO in CH_2Cl_2 were successively added to a 0.1 mM solution of the ligand in CH_2Cl_2 in a quartz cuvette (path length 1 cm, total volume 3 mL). UV/Vis spectra of the homogeneous solutions at equilibrium containing the metal complex, the ligand and the adduct were recorded in the range of 200-400 nm before and after each addition of the MTO aliquot. The values of the formation constants were calculated by fitting the equilibrium absorbance at a certain wavelength to Equation (2) or (3) according to the chosen wavelength and the free ligand absorption using the IGOR computer program.

3.4.6 Catalysis

In a typical experiment, 1-octene (0.628 mL, 4 mmol), MTO (10 mg, 0.04 mmol), ligand (0.2 mmol), 0.200 mL of mesitylene (internal standard), 0.200 mL of toluene (internal standard) and 2.45 mL of CH_2Cl_2 were added to the reaction vessel under standard conditions at room temperature. The reaction started upon addition of H_2O_2 (35% aqueous solution) (0.55 mL, 6 mmol) under vigorous stirring. The course of the reaction was monitored by quantitative GC analysis. Samples (0.2 mL) were taken at specific time intervals, treated with Na_2SO_3 to quench the excess of peroxide and to remove water, filtered and diluted with dry CH_2Cl_2 before injection into a GC column. The conversion of 1-octene and the formation of octene epoxide were calculated from calibration curves ($r^2 = 0.999$) recorded prior to the reaction course.

3.4.7 Testing the photostability of the complexes

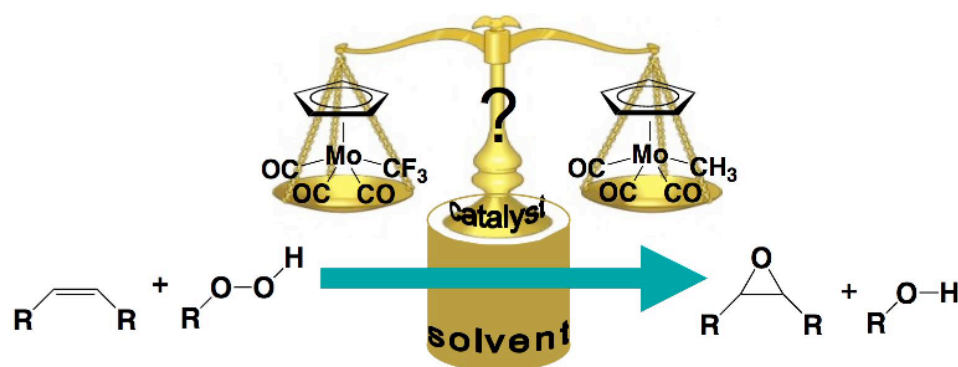
Selected ligands were treated with an equimolar amount of ^{17}O -labelled MTO (prepared by a published procedure³¹) or in a fivefold excess and the ^1H and ^{17}O NMR spectra were recorded. The adduct solutions (0.1 M in CDCl_3) were then exposed to UV light and analysed again by ^1H and ^{17}O NMR spectroscopy. For the UV/Vis analysis, a 0.1 M solution of complex **11** in CH_2Cl_2 was prepared and exposed to UV light. Samples were taken over a timespan of 2 h, diluted with CH_2Cl_2 and the UV/Vis spectra were recorded.

3.5 References

1. R. I. Beattie, P. J. Jones, *Inorg. Chem.*, **1979**, *18*, 2318.
2. W. A. Herrmann, J. G. Kuchler, J. K. Felixberger, E. Herdtweck, W. Wagner, *Angew. Chem.*, **1988**, *100*, 420; *Angew. Chem. Int. Ed. Engl.*, **1988**, *27*, 394.
3. F. E. Kühn, A. Scherbaum, W. A. Herrmann, *J. Organomet. Chem.*, **2004**, *689*, 4149.
4. W. A. Herrmann, M. Wang, *Angew. Chem.*, **1991**, *103*, 1709; *Angew. Chem. Int. Ed. Engl.*, **1991**, *30*, 1641.
5. W. A. Herrmann, W. Wagner, U. N. Flessner, U. Volkhardt, H. Komber, *Angew. Chem.*, **1991**, *103*, 1704; *Angew. Chem. Int. Ed. Engl.*, **1991**, *30*, 1636.
6. J. E. Ziegler, M. J. Zdilla, A. J. Evans, M. M. Abu-Omar, *Inorg. Chem.*, **2009**, *48*, 9998.
7. W. A. Herrmann, R. W. Fischer, D. W. Marz, *Angew. Chem.*, **1991**, *103*, 1706; *Angew. Chem. Int. Ed. Engl.*, **1991**, *30*, 1638.
8. J. Rudolph, K. L. Reddy, J. P. Chiang, K. B. Sharpless, *J. Am. Chem. Soc.*, **1997**, *119*, 6189 and references cited therein.
9. F. E. Kühn, A. M. Santos, W. A. Herrmann, *Dalton Trans.*, **2005**, 2483 and references cited therein.
10. C. Copéret, H. Adolfson, K. B. Sharpless, *Chem. Commun.*, **1997**, 1565.
11. W. A. Herrmann, H. Ding, R. M. Kratzer, F. E. Kühn, J. J. Haider, R. W. Fischer, *J. Organomet. Chem.*, **1997**, *549*, 319.
12. W. D. Wang, J. H. Espenson, *J. Am. Chem. Soc.*, **1998**, *120*, 11335.
13. W. A. Herrmann, R. M. Kratzer, H. Ding, W. R. Thiel, H. Glas, *J. Organomet. Chem.*, **1998**, *555*, 293.
14. H. Adolfsson, A. Converso, K. B. Sharpless, *Tetrahedron Lett.*, **1999**, *40*, 3991.
15. F. E. Kühn, A. M. Santos, P. W. Roesky, E. Herdtweck, W. Scherer, P. Gisdakis, I. V. Yudanov, C. Di Valentin, N. Rösch, *Chem. Eur. J.*, **1999**, *5*, 3603.
16. C. Copéret, H. Adolfson, J. P. Chiang, A. K. Yudin, *J. Org. Chem.*, **2000**, *65*, 8651.
17. P. Ferreira, W. D. Xue, É. Bencze, E. Herdtweck, F. E. Kühn, *Inorg. Chem.*, **2001**, *40*, 5834.
18. M. J. Sabater, M. E. Domine, A. Corma, *J. Catal.*, **2002**, *210*, 192.
19. P. Altmann, F. E. Kühn, *J. Organomet. Chem.*, **2009**, *694*, 4032.
20. H. Kunkely, T. Türk, C. Teixeira, C. de Meric de Bellefon, W. A. Herrmann, A. Vogler, *Organometallics*, **1991**, *10*, 2090.

21. W. A. Herrmann, F. E. Kühn, D. A. Fiedler, M. R. Mattner, M. R. Geisberger, H. Kunkely, A. Vogler, S. Steenken, *Organometallics*, **1995**, *14*, 5377.
22. H. Kunkely, A. Vogler, *J. Photochem. Photobiol. A: Chem.*, **1996**, *94*, 135.
23. H. Kunkely, A. Vogler, *J. Photochem. Photobiol. A: Chem.*, **1997**, *103*, 227.
24. M.-D. Zhou, S.-L. Zang, E. Herdtweck, F. E. Kühn, *J. Organomet. Chem.*, **2008**, *693*, 2473.
25. P. Wikrent, B. J. Drouin, S. G. Kukolich, J. C. Lilly, M. T. Ashby, W. A. Herrmann, W. Scherer, *J. Chem. Phys.*, **1977**, *107*, 2187.
26. A. M. Al-Ajlouni, A. Günyar, M.-D. Zhou, P. N. W. Baxter, F. E. Kühn, *Eur. J. Inorg. Chem.*, **2009**, 1019.
27. M. Y. Shatnawi, A. M. Al-Ajlouni, *Jordan J. Chem.*, **2009**, *4*, 119.
28. S. M. Nabavizadeh, *Inorg. Chem.*, **2003**, *42*, 4204.
29. S. M. Nabavizadeh, *Dalton Trans.*, **2005**, 1644.
30. S. M. Nabavizadeh, A. Akbari, M. Rashidi, *Eur. J. Inorg. Chem.*, **2005**, 2368.
31. S. Yamazaki, *Org. Biomol. Chem.*, **2007**, *5*, 2109.
32. W. A. Herrmann, F. E. Kühn, P. W. Roesky, *J. Organomet. Chem.*, **1995**, *485*, 243.
33. W. A. Herrmann, F. E. Kühn, M. U. Rauch, J. D. G. Correia, G. Artus, *Inorg. Chem.*, **1995**, *34*, 2914.
34. E. Tosh, H. K. M. Mitterpleininger, A. M. J. Rost, D. Veljanovski, W. A. Herrmann, F. E. Kühn, *Green Chem.*, **2007**, *12*, 1296.
35. V. Aranyos, J. Hjelm, A. Hagfeldt, H. Grennberg, *J. Chem. Soc., Dalton Trans.*, **2001**, 1319.
36. N. Kudo, M. Perseghini, G. C. Fu, *Angew. Chem. Int. Ed. Engl.*, **2006**, *45*, 1282.

4 Catalytic Olefin Epoxidation with a Fluorinated Organomolybdenum Complex



This chapter originated the following publication:

S. A. Hauser, M. Cokoja, M. Drees, F. E. Kühn, *J. Mol. Catal. A*, **2012**, 363-364, 237-244.

4.1 Background

In the last decades, organomolybdenum compounds attracted attention for their versatile use in olefin epoxidation catalysis.^{1–16} Their straightforward synthesis and easy handling promoted their application in catalytic reactions. Since the beginning of the studies of transition metal-based epoxidation catalysts, a wide range of molybdenum complexes have been synthesised and their performance has been examined in catalytic olefin epoxidation. Monomeric complexes such as $[\text{MoO}_2\text{X}_2]$ ($\text{X} = \text{CH}_3, \text{Cl}$) and their bipyridine derivatives^{17–22} as well as the carbonyl complexes $[(\eta^5\text{-C}_5\text{R}_5)\text{Mo}(\text{CO})_3\text{X}]$ ($\text{R} = \text{H}, \text{CH}_3, \text{CH}_2\text{Ph}$; $\text{X} = \text{alkyl}, \text{halide}$) and their oxidised derivatives^{2,23–26} were intensively studied in organic solvents with various substrates. Moreover, dioxo molybdenum complexes with a variety of nitrogen ligands have proven to be active and innovative epoxidation catalysts.^{27–31} However, a major breakthrough in terms of catalytic activity was achieved with ansa compounds of general formula $[\text{Mo}(\eta^5\text{-(C}_5\text{H}_4(\text{CH}(\text{CH}_2)_n))\text{-}\eta^1\text{-CH})(\text{CO})_3]$. In both organic solvents and ionic liquids, they outperform almost all previously investigated systems.^{32–34}

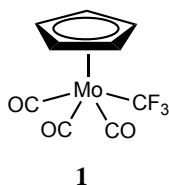


Figure 4.1 Fluorinated organomolybdenum complex $[\text{CpMo}(\text{CO})_3\text{CF}_3]$ **1**.

Besides steric influences, the electronic properties of the complex can mainly be held responsible for the catalytic performance. Therefore, it was decided to compare the known epoxidation pre-catalyst $[\text{CpMo}(\text{CO})_3\text{CH}_3]$ with its fluorinated counterpart $[\text{CpMo}(\text{CO})_3\text{CF}_3]$, originally synthesised by King and Bisnette³⁵ (Figure 4.1). The complexes are sterically nearly identical, however, the Lewis acidity of the metal centre and hence, the catalyst activity is supposed to increase as a consequence of the electron-withdrawing CF_3 ligand. On the other hand, there is little knowledge about the impact of fluorinated ligands on molecular olefin epoxidation catalysts, which certainly warrants an investigation of such compounds as catalysts. In the case of the well examined, widely applied epoxidation catalyst $[\text{CH}_3\text{ReO}_3]$ ^{36,37} it has been predicted that its fluorinated derivative $[\text{CF}_3\text{ReO}_3]$ should be stable and an even better catalyst^{37,38} than the methylated compound. However, so far the synthesis of the CF_3 derivative has not been achieved.

Additionally, the influence of different reaction media is investigated in this work. It has been shown that fluorinated solvents are beneficial in epoxidation reactions with methyltrioxorhenium^{39,40} as well as in catalyst-free epoxidations^{41–44} using H_2O_2 as oxidant. However, there is so far no report on catalytic systems utilising *tert*-butyl hydroperoxide (TBHP) as

oxidant in fluorinated solvents. Therefore, two perfluorinated solvents have been applied in the catalytic epoxidation of cyclooctene. Other reaction media currently attracting a lot of attention are ionic liquids (ILs).^{45,46} The advantages of a biphasic catalytic system, such as easy catalyst recycling and product separation, contribute to the continuous interest in developing new ILs with various characteristics, for example lower melting points or bulkier side chains.^{45,46} Immobilisation on heterogeneous carrier materials has been executed for [RReO₃]-, [X₂Mo₂O₂]- and [CpMo(CO)₃X]-systems with different success.^{2,47–49} Using 2-phase systems, however, appears to be advantageous for all these systems because of several reasons, among them the elimination of diffusion problems into the pores of mesoporous carrier materials.^{34,50–51}

4.2 Results and Discussion

4.2.1 Olefin epoxidation with a fluorinated organomolybdenum catalyst

As it is known from similar organomolybdenum complexes, *e.g.* [CpMo(CO)₃CH₃] or [CpMo(CO)₃Cl], the carbonyl complexes act as pre-catalysts, being oxidised *in situ* with TBHP, forming Mo-oxo and Mo-oxo-peroxo species that appear to be catalytically active.^{25,26} Upon treatment of [CpMo(CO)₃CF₃] with TBHP, vigorous gas evolution, which would indicate the oxidation of CO ligands to CO₂ is, however, missing. Therefore, a closer look at the oxidation of the complex was taken by means of ¹⁹F NMR spectroscopy and IR spectroscopy.

¹⁹F NMR spectroscopy

The title compound [CpMo(CO)₃CF₃] shows a single peak at 13.03 ppm in the ¹⁹F NMR spectrum (see Figure 4.2(a)). The position of the CF₃ group can be used to follow the electronic changes at the metal core and hence, to identify possible intermediates of the reaction with TBHP. Figure 4.2 shows a set of spectra of the complex with various reactants. Upon addition of the oxidant TBHP (20 equiv.), the CF₃ signal moves slightly to 12.31 ppm (Figure 4.2(b)). In comparison, addition of 20 equiv. cyclooctene (Figure 4.2(c)) induces only a very small shift of the resonance to 12.98 ppm. These shifts are most likely due to interactions of the peroxo group and the olefin, respectively, with the Mo-core. During catalytic epoxidation of cyclooctene with the oxidant TBHP (40 equiv., 25 °C), three signals become apparent (Figure 4.2(d)). Notably, the resonance at 12.43 ppm, corresponding to the starting complex **1** can be found, indicating that the complex **1** does not fully react with TBHP to the targeted oxo-peroxo species. New resonances are observed at -21.51 and -17.57 ppm. In order to shed light on the structure of the complexes giving rise to the new signals, several possible products of the reaction of **1** with TBHP were taken into account (see Scheme 4.1).

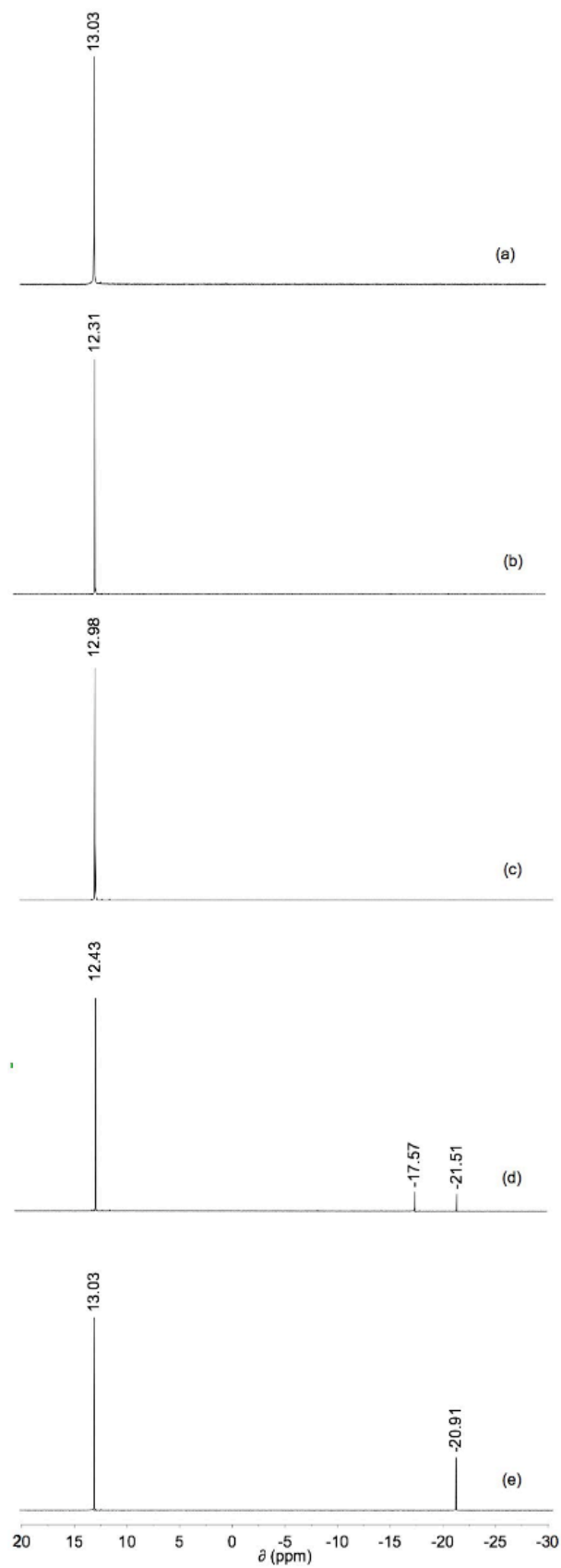
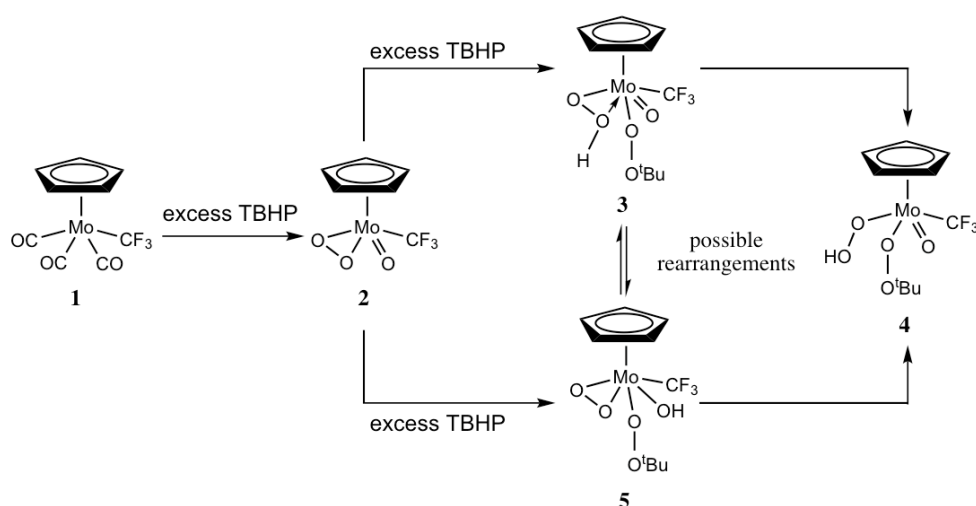


Figure 4.2 ^{19}F NMR spectra of complex $[\text{CpMo}(\text{CO})_3\text{CF}_3]$ in C_6D_6 (a) neat; (b) with 20 equiv. TBHP; (c) with 20 equiv. cyclooctene; (d) during a catalytic reaction with cyclooctene (20 equiv. per Mo) and TBHP (40 equiv., 25 °C); (e) extracted after a catalytic reaction in C_6D_6 recorded at 25 °C.

Subsequently, the ^{19}F NMR resonances of these species were calculated using density functional theory (GIAO model-B3LYP/6-31++G**) and scaled to the experimental shift of the title compound (13.03 ppm). A comparison of the experimental NMR signals in Figure 4.2(d) with the shifts of the postulated structures (Table 4.1) shows that most presumably, the signal at -21.51 ppm can be assigned to the oxidised complex $[\text{CpMo}(\eta^2\text{-O}_2)(\text{O})\text{CF}_3]$ (**2**), or to a complex bearing one η^2 -hydroperoxo- and one *tert*-butylperoxo group (Scheme 4.1, complex **3**). From a thermodynamic point of view, this Mo(VI) species should rearrange the η^2 -bound OOH to a pending linear OOH group, forming $[\text{CpMo}(\sigma\text{-O}_2\text{H})(\text{O})(\sigma\text{-O}_2^t\text{Bu})\text{CF}_3]$ (**4**), which might be the (short lived) catalytically active species and therefore its (upfield moving) shift can possibly not be seen on the NMR timescale. There is also another feasible pathway with the formation of the complex $[\text{CpMo}(\eta^2\text{-O}_2)(\text{OH})(\sigma\text{-O}_2^t\text{Bu})\text{CF}_3]$ (**5**), where the proton of the TBHP is transferred to a terminal oxo group instead of the peroxo group and could also be serving as the catalytically active species. Both intermediates have, according to our calculations, quite similar chemical shifts for the CF_3 group and can therefore not be distinguished. At the end of the reaction, after the remaining oxidant and substrate as well as the epoxide product have been removed, the resulting spectrum contains two resonances (Figure 4.2(e)). The bright yellow colour of this mixture confirms the presence of the oxo peroxo complex **2** (-20.91 ppm) besides complex **1** (13.03 ppm) as DFT-calculations predicted. Interestingly, unlike other CpMo precursors, the starting complex **1** is present even after treatment with a 40-fold excess TBHP (5.5 M in *n*-decane), indicating only partial conversion to the catalytically active species, and hence a lower catalyst concentration. This finding points to a lower reactivity of **1** towards TBHP in comparison to $[\text{CpMo}(\text{CO})_3\text{CH}_3]$.



Scheme 4.1 Oxidation of $[\text{CpMo}(\text{CO})_3\text{CF}_3]$ (**1**) with excess TBHP yields $[\text{CpMo}(\eta^2\text{-O}_2)(\text{O})\text{CF}_3]$ (**2**) and $[\text{CpMo}(\eta^2\text{-OOH})(\text{O})(\sigma\text{-O}_2^t\text{Bu})\text{CF}_3]$ (**3**), $[\text{CpMo}(\sigma\text{-O}_2\text{H})(\text{O})(\sigma\text{-O}_2^t\text{Bu})\text{CF}_3]$ (**4**) or $[\text{CpMo}(\eta^2\text{-O}_2)(\text{OH})(\sigma\text{-O}_2^t\text{Bu})\text{CF}_3]$ (**5**).

Table 4.1 Comparison of experimental and calculated ^{19}F NMR shifts of different CpMo- CF_3 species (experimental values recorded in C_6D_6 ; standard deviation of calculated shifts: ± 3 ppm).

| Complex | Calc. ^{19}F NMR shift [ppm] | Exp. ^{19}F NMR shift [ppm] |
|---|---------------------------------------|--------------------------------------|
| [CpMo(CO) $_3$ CF $_3$] (1) | +13.03 ^a | +13.03 ^a |
| [CpMo(O) $_2$ CF $_3$] | -20.3 | Not observed |
| [CpMo(η^2 -O $_2$)(O)CF $_3$] (2) | -23.4 | -21.51; -20.91 |
| [CpMo(O)(OH)(σ -O $_2^t$ Bu)CF $_3$] | -33.7 | Not observed |
| [CpMo(η^2 -OOH)(O)(σ -O $_2^t$ Bu)CF $_3$] (3) | -19.9 | (-17.57) |
| [CpMo(σ -OOH)(O)(σ -O $_2^t$ Bu)CF $_3$] (4) | -27.6 | Not observed |
| [CpMo(η^2 -O $_2$)(OH)(σ -O $_2^t$ Bu)CF $_3$] (5) | -20.3 | (-17.57) |

^aUsed as scaling point for the calculated chemical shifts.

IR spectroscopy

While ^{19}F NMR spectroscopy allows using the CF_3 group as a probe for monitoring the reaction of **1** with TBHP and tracing possible products, IR spectroscopy is a convenient tool for studying carbonyl ligands. The complex [CpMo(CO) $_3$ CF $_3$] displays two bands in the carbonyl region, namely at 2045 and 1935 cm^{-1} (Figure 4.3(a)). Upon addition of cyclooctene, these two bands immediately shift to higher wavenumbers (2051 and 1968 cm^{-1} , Figure 4.3(b)). This slight shift is induced by solvent effects. The presence of TBHP in decane also induces a solvent effect, as can be deduced by the IR spectrum of the mixture (Figure 4.3(c)). However, the bands are less significantly shifted to 2050 and 1966 cm^{-1} .

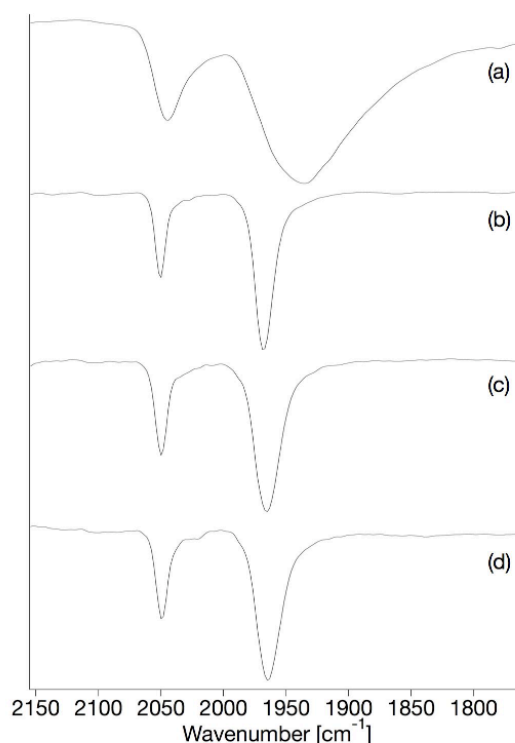


Figure 4.3 IR spectra of (a) solid [CpMo(CO) $_3$ CF $_3$], (b) after addition of cyclooctene only, (c) after addition of TBHP only, and (d) after addition of both cyclooctene and TBHP.

During a catalytic reaction, the two carbonyl bands are found at 2049 and 1965 cm^{-1} (Figure 4.3(d)). They do not shift any more significantly, but decrease in intensity over time, giving rise to a comparatively slow oxidation of the carbonyl compound **1**.

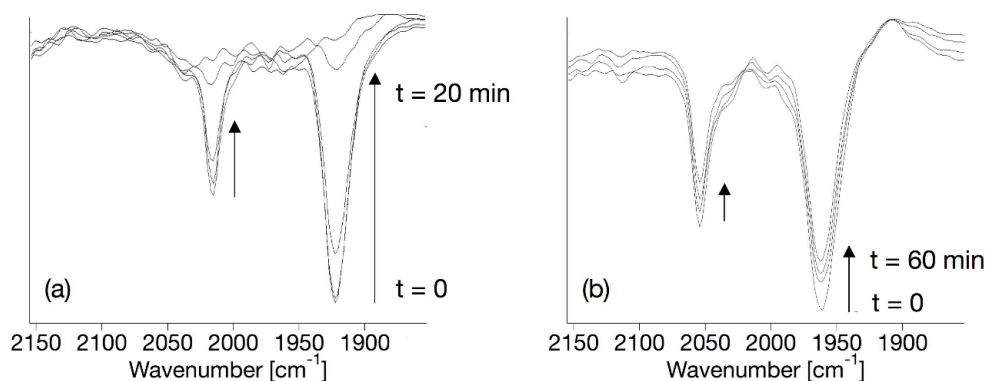


Figure 4.4 Changes in the CO vibration intensities over time of (a) $[\text{CpMo}(\text{CO})_3\text{CH}_3]$ and (b) $[\text{CpMo}(\text{CO})_3\text{CF}_3]$ upon addition of 100 equiv. TBHP.

The slow oxidation of the compound **1** can be nicely visualised (Figure 4.4). Addition of 100 equiv. TBHP to the carbonyl complex leads to oxidative decarbonylation. The methylated complex is completely oxidised after 20 minutes reaction time, which can be seen by the absence of the carbonyl bands. The intensity of the carbonyl bands of complex $[\text{CpMo}(\text{CO})_3\text{CF}_3]$, however, only decreases to a minor degree, even after 1 hour. Unfortunately, due to the present excess of TBHP, the formation of Mo=O or Mo–O bands cannot be followed *in situ* by this technique.

4.2.2 Catalytic investigations

Comparison of the catalytic activity of $[\text{CpMo}(\text{CO})_3\text{CF}_3]$ with $[\text{CpMo}(\text{CO})_3\text{CH}_3]$

The comparison of the two monomeric complexes, $[\text{CpMo}(\text{CO})_3\text{CH}_3]$ and compound **1**, in the catalytic epoxidation of cyclooctene in benzene reveals the superiority of $[\text{CpMo}(\text{CO})_3\text{CH}_3]$ (see Figure 4.5). At a concentration of 0.5 mol%, it surpasses the turnover frequency of **1** by one order of magnitude (see Table 4.2). The lower catalytic activity of **1** vs. $[\text{CpMo}(\text{CO})_3\text{CH}_3]$ is contra intuitive since the Mo centre in **1** is supposed to be more Lewis acidic and hence more active as catalyst. It is the question, whether **1** is principally a less active catalyst in the series of $[\text{CpMo}(\text{CO})_3\text{X}]$ complexes, or if the formation of the catalytically active species from **1** is inhibited or incomplete, leading to a lower concentration of the actual catalyst than expected when assuming complete conversion of the carbonyl precursor to the active species. Such a lower catalyst concentration is evidenced by the reaction of **1** with TBHP, monitored by ^{19}F NMR and IR experiments (*vide supra*), showing that even in the presence of an excess of TBHP, compound **1** can still be detected. To circumvent the problem of lower catalyst concentration, a control experiment was performed. 0.50 mol% of **1** was completely oxidised *in*

situ with an excess TBHP, before addition of cyclooctene and oxidant (2 equiv. TBHP per olefin). The herewith collected kinetic data revealed the absence of an induction period and therefore a higher TOF (660 h^{-1}) of the fluorinated compound, however, the yield of epoxide after 4 hours (76%) was identical to the experiment without pre-treatment of **1**. Since TBHP obviously is not the optimal oxidant for **1**, we chose to study the influence of solvents on the reactivity of TBHP versus compound **1**, in order to answer the question if the low catalytic activity of **1** is intrinsical, as seen in Figure 4.5 and Table 4.2.

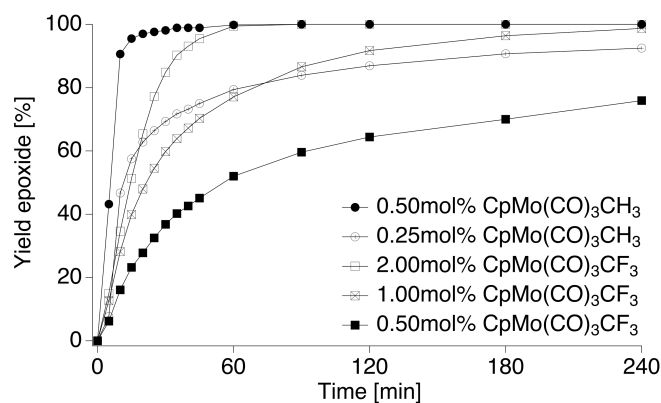


Figure 4.5 Kinetic data of the catalytic epoxidation of cyclooctene at 25 °C, using TBHP (2 equiv. per olefin, 5.5 M in *n*-decane) as oxidant in C_6D_6 .

Table 4.2 Activities of the applied pre-catalysts expressed in terms of turn-over frequencies (TOF, determined at the steepest slope of the kinetic curve).

| Complex | Concentration [mol%] | TOF [h^{-1}] | Yield after 4 h [%] |
|---|----------------------|-------------------------|---------------------|
| $[\text{CpMo}(\text{CO})_3\text{CH}_3]$ | 0.50 | 1139 | 100 |
| $[\text{CpMo}(\text{CO})_3\text{CH}_3]$ | 0.25 | 1874 | 93 |
| 1 | 2.00 | 118 | 100 |
| 1 | 1.00 | 186 | 100 |
| 1 | 0.50 | 240 | 76 |

Fluorinated solvents

Despite the moderate activity in comparison to $[\text{CpMo}(\text{CO})_3\text{CH}_3]$, compound **1** was applied in catalytic epoxidation reactions using different solvents. Therefore, perfluorinated solvents, such as hexafluorobenzene (HFB) and hexafluoroisopropanol (HFI) were tested. Aliphatic solvents such as tetradecafluorohexane were not used due to the low solubility of **1** in these solvents.

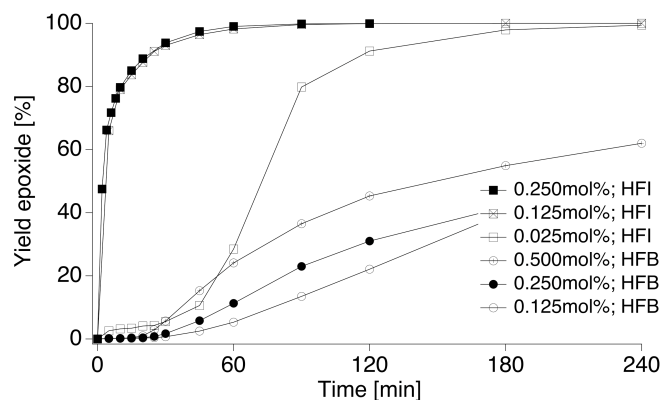
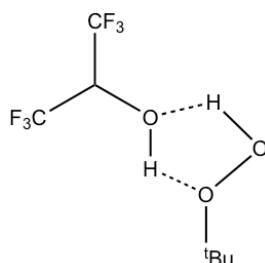


Figure 4.6 Kinetic data of the influence of the catalyst concentration and different solvents (hexafluoroisopropanol (HFI) and hexafluorobenzene (HFB)) on the epoxidation of cyclooctene (ratio cyclooctene : TBHP = 1 : 1.2, 25 °C).

Figure 4.6 shows the kinetic data collected using the solvents mentioned above. It is clearly visible that HFI positively influences the catalytic activity of $[\text{CpMo}(\text{CO})_3\text{CF}_3]$. At the same concentration, the TOF of $[\text{CpMo}(\text{CO})_3\text{CF}_3]$ in HFI is almost two orders of magnitude larger than in HFB (see Table 4.3). It is reported that fluorinated alcohols activate hydrogen peroxide via hydrogen bonding,^{39–44,52,53} hence, it is reasonable to assume that an organic peroxide can be activated in the same way, rendering the oxidation of **1** faster and more efficient than in aliphatic or aromatic solvents. Consequently, upon addition of an excess of THBP (20 equiv.) to a solution of **1** in HFI, gas evolution is observed and in the IR spectrum of the product, the carbonyl bands are no longer visible.

Thus, we examined whether HFI can activate TBHP to allow oxygen atom transfer to an olefin without a metal catalyst involved. Indeed, after 4 h reaction time of TBHP and cyclooctene in HFI as solvent, a conversion of 10% olefin (100% epoxide selectivity) is reached. The strong H-bond donor ability of HFI increases the nucleophilicity of the α -oxygen atom of the peroxide and thus facilitates the oxygen-oxygen bond cleavage (Scheme 4.2). This enhanced reactivity also influences the oxidation of $[\text{CpMo}(\text{CO})_3\text{CF}_3]$, as the induction period due to the slow formation of the active species is only visible at a very low catalyst concentration.



Scheme 4.2 Proposed activation of TBHP with HFI.

The comparison of the pre-catalysts $[\text{CpMo}(\text{CO})_3\text{CF}_3]$ and $[\text{CpMo}(\text{CO})_3\text{CH}_3]$ at a concen-

Table 4.3 Activity of $[\text{CpMo}(\text{CO})_3\text{CF}_3]$ (**1**) in dependence of the solvent (ratio cyclooctene : TBHP = 1 : 1.2, 25 °C).

| Solvent | Catalyst conc. [mol%] | TOF [h ⁻¹] |
|-----------------------|-----------------------|------------------------|
| Hexafluoroisopropanol | 0.250 | 5702 |
| Hexafluoroisopropanol | 0.125 | 6339 |
| Hexafluoroisopropanol | 0.025 | 4110 |
| Hexafluorobenzene | 0.500 | 77 |
| Hexafluorobenzene | 0.250 | 94 |
| Hexafluorobenzene | 0.125 | 143 |

tration of 0.125 mol% in epoxidation of cyclooctene at room temperature revealed the strong dependence of catalyst and solvent system (Figure 4.7). While in the highly nucleophilic solvent HFI $[\text{CpMo}(\text{CO})_3\text{CF}_3]$ is far more active than $[\text{CpMo}(\text{CO})_3\text{CH}_3]$, the latter complex shows a better performance than $[\text{CpMo}(\text{CO})_3\text{CF}_3]$ in HFB, where no activation of the peroxide by the solvent takes place (Table 4.4). Indeed, this indicates that the catalytically active species of the fluorinated compound surpasses the activity of the corresponding active species of the CH_3 -system. Thus, the performance of $[\text{CpMo}(\text{CO})_3\text{CF}_3]$ is limited by its difficult oxidation, *i.e.* the slow formation of the catalyst. The reaction carried out in isopropanol only yielded a minor epoxide formation. In this system, the catalyst appears to be deactivated through solvent coordination to the molybdenum core, which blocks the coordination site of the oxidant. In case of HFI, no similar coordination takes place due to its very different electronic properties.

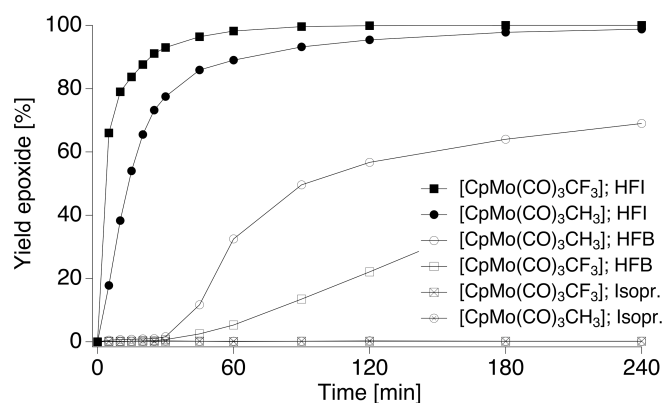


Figure 4.7 Kinetic data of the catalytic epoxidation of cyclooctene (TBHP as oxidant) in various solvents with different complexes (0.125 mol% concentration) at room temperature.

Furthermore, the epoxidation of other olefins was carried out to test the catalytic activity of the compound $[\text{CpMo}(\text{CO})_3\text{CF}_3]$. Cyclooctene is known as being very easily epoxidised (with 100% selectivity to the epoxide), in contrast to 1-octene or styrene. This also proved true in the case of the title compound (Figure 4.8). A moderate yield with low selectivity (24% epoxide) was achieved for styrene, whereas the epoxidation of 1-octene remained at a low level, but with 99% selectivity to the epoxide, within a reaction time of 4h.

Table 4.4 Activities of the pre-catalysts in dependence of the solvent (0.125 mol% complex, ratio cyclooctene : TBHP = 1 : 1.2, 25 °C).

| Complex | Solvent | TOF [h ⁻¹] |
|--|-----------------------|------------------------|
| 1 | Hexafluoroisopropanol | 6339 |
| [CpMo(CO) ₃ CH ₃] | Hexafluoroisopropanol | 1969 |
| 1 | Hexafluorobenzene | 143 |
| [CpMo(CO) ₃ CH ₃] | Hexafluorobenzene | 677 |
| 1 | Isopropanol | 14 |
| [CpMo(CO) ₃ CH ₃] | Isopropanol | 15 |

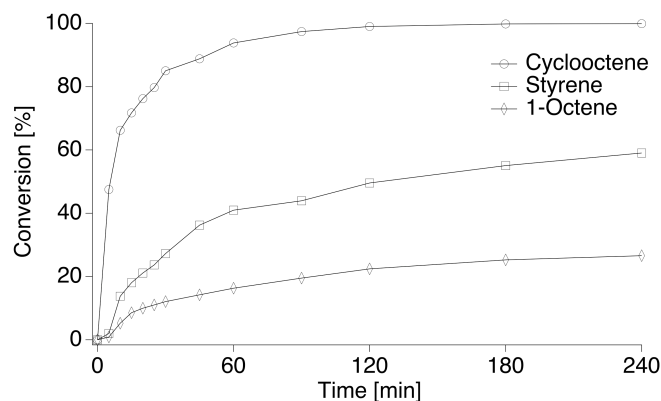


Figure 4.8 Kinetic data of the catalytic epoxidation different olefins (0.5 mol% catalyst, 200 equiv. olefin, 400 equiv. TBHP, 25 °C, hexafluoroisopropanol).

As mentioned above, oxidation of complex **1** prior to the catalytic application in an epoxidation reaction leads to the disappearance of the induction period often observed with tricarbonyl pre-catalysts. Therefore, we isolated the oxo peroxy complexes **2** and [CpMo(O₂)(O)CH₃]. The comparison of their catalytic activity in the epoxidation of cyclooctene (see Figure 4.9) proves the assumption mentioned above that the fluorinated complex **2** is more active (TOF of 2049 h⁻¹) than its non-fluorinated analogue (TOF of 1265 h⁻¹).

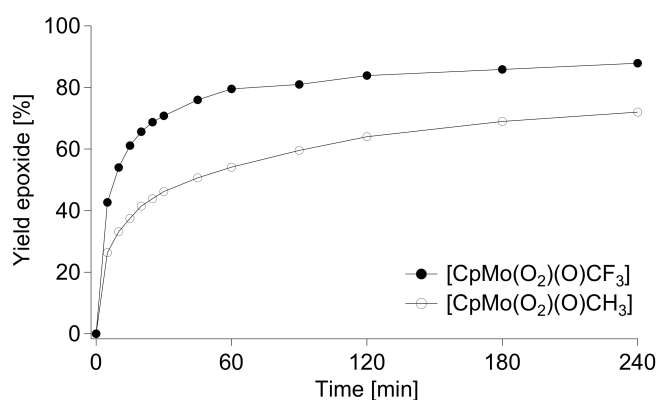


Figure 4.9 Kinetic data of the performance of the oxidised complexes in the epoxidation of cyclooctene in C₆D₆ (0.25 mol% catalyst, 400 equiv. cyclooctene, 480 equiv. TBHP, 25 °C).

4.2.3 Catalysis in ionic liquids

The complex $[\text{CpMo}(\text{CO})_3\text{CF}_3]$ was also applied in 2-phase catalytic epoxidation reactions. Although the reaction carried out in $[\text{bmim}][\text{NTf}_2]$ (bmim = 1-butyl-3-methyl-imidazolium; NTf_2 = bis(trifluoromethanesulfonimide)) is substantially slower (Figure 4.10), the numerous advantages of using ILs as reaction media make it worth accepting longer reaction times (93% yield after 24 h). The almost negligible loss in activity from one catalysis cycle to another proves the stability and reusability of the complex (see Figure 4.11). This characteristic stands in contrast to a previously reported Mo-based epoxidation catalyst,³⁴ which performed very well in 2-phase catalytic epoxidation reactions but showed an important loss of activity from the second cycle onwards. It is possible that the higher stability of the fluorinated complex is due to the increased Lewis acidity of the Mo-core.

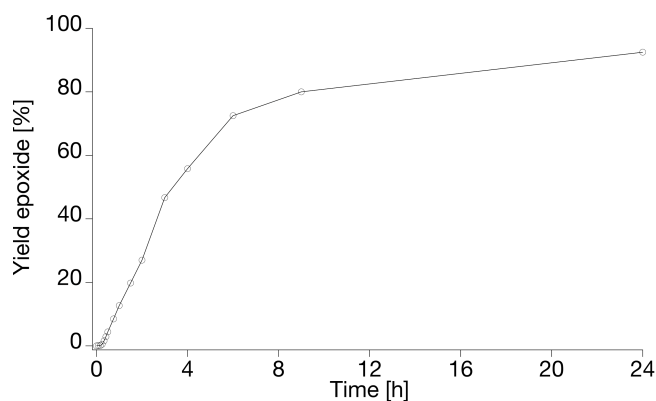


Figure 4.10 Epoxidation of cyclooctene catalysed by $[\text{CpMo}(\text{CO})_3\text{CF}_3]$ in $[\text{bmim}][\text{NTf}_2]$ (1 mol% catalyst, 100 equiv. cyclooctene, 200 equiv. TBHP, 25 °C).

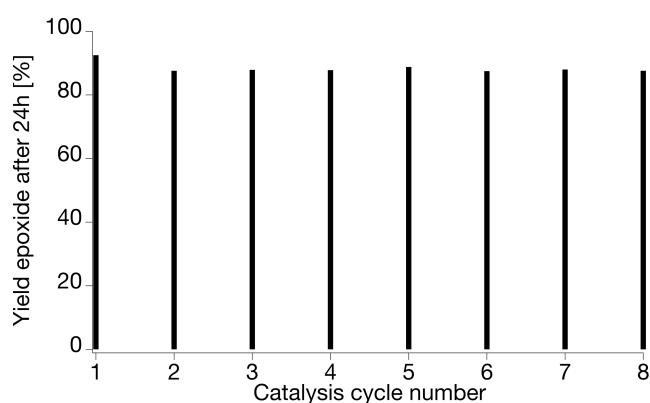


Figure 4.11 Recycling of $[\text{CpMo}(\text{CO})_3\text{CF}_3]$ in $[\text{bmim}][\text{NTf}_2]$.

4.3 Conclusion

The fluorinated organomolybdenum complex $[\text{CpMo}(\text{CO})_3\text{CF}_3]$ acts as a pre-catalyst of the epoxidation of olefins, as its non-fluorinated counterpart $[\text{CpMo}(\text{CO})_3\text{CH}_3]$ does. The fluorinated complex allows mechanistic ^{19}F -NMR studies, indicating the nature of the catalytically active Mo-species, which was an unresolved subject of debates for a very long time.^{4,19,26,54–55} With benzene as the solvent, the performance of $[\text{CpMo}(\text{CO})_3\text{CF}_3]$ in the catalytic epoxidation of cyclooctene stays behind the performances of known complexes like $[\text{CpMo}(\text{CO})_3\text{CH}_3]$ or $[\text{CpMo}(\text{CO})_3\text{Cl}]$ in homogeneous epoxidation of cyclooctene.^{1–3,24–26} However, in a reaction medium that activates the oxidant, such as hexafluoroisopropanol, the activity of the fluorinated catalyst outperforms $[\text{CpMo}(\text{CO})_3\text{CH}_3]$. With hexafluoroisopropanol as a solvent, a TOF of $> 6300 \text{ h}^{-1}$ was achieved in the epoxidation of cyclooctene. Taking into account that the catalytic reactions were all performed at room temperature, this represents the highest TOF for pre-catalysts of general formula $[\text{CpMo}(\text{CO})_3\text{X}]$ ($\text{X} = \text{alkyl, halide}$). So far, only the ansa compounds $[\text{Mo}(\eta^5\text{-C}_5\text{H}_4(\text{CH}(\text{CH}_2)_n)\text{-}\eta^1\text{-CH})(\text{CO})_3]$ show better performances in catalytic epoxidation of cyclooctene at room temperature.³⁴ Moreover, it is possible to epoxidise substrates such as styrene and 1-octene, at least in moderate to good yields after 4 h at room temperature, applying only 0.5 mol% catalyst.

The advantage of $[\text{CpMo}(\text{CO})_3\text{CF}_3]$ in epoxidation catalysis is the high stability of the oxidised species. The epoxidation of cyclooctene with 1 mol% catalyst in the ionic liquid $[\text{bmim}][\text{NTf}_2]$ is almost quantitative after 24 h. Accordingly, the activity of the catalyst is lower than of previously reported ones.^{32–34} However, the yield stays at a similar level for at least 8 catalysis cycles, which proves the recyclability of the catalyst.

4.4 Experimental Section

4.4.1 Materials and methods

All experimental synthetic work was carried out using standard Schlenk techniques under argon. Catalytic reactions were performed under normal laboratory atmosphere. Solvents were dried by standard procedures and stored under argon over molecular sieves. Commercially available chemicals are used as received, unless stated otherwise. Strongly toxic substances (TBHP, hexafluoroisopropanol) were handled with necessary safety precautions. High-resolution NMR spectra were measured with a Bruker Avance DPX-400 (^1H : 400.0 MHz; ^{13}C : 100.6 MHz; ^{19}F : 376.5 MHz; ^{95}Mo : 26.1 MHz) spectrometer, the signals were referenced to the solvent residual signal (C_6D_6 ; ^1H : 7.16 ppm; ^{13}C : 128.06 ppm) or external standards in a capillary (^{19}F : C_6F_6 at -164.9 ppm; ^{95}Mo : $\text{Mo}(\text{CO})_6$ in C_6D_6 at -1856 ppm). The IR spectra were recorded on a Varian ATR-FTIR instrument.

4.4.2 Synthesis of the complexes

The organomolybdenum complexes [CpMo(CO)₃CH₃], [CpMo(CO)₃CF₃] and [CpMo(O₂)(O)CH₃] were synthesised according to literature procedures.^{56,35,26} The spectral data were in agreement to the reported values.^{56,35,26} The oxidised complex [CpMo(O₂)(O)CF₃] was prepared following a slightly changed literature procedure.²⁶ The tricarbonyl precursor [CpMo(CO)₃CF₃] was treated with 20 equiv. TBHP at room temperature in dichloromethane. After 24 h, excess oxidant was quenched with MnO₂, the solution was filtrated and the solvent evaporated. The yellow solid was washed with hexane and dried in vacuo.

[CpMo(CO)₃CH₃]: ¹H NMR (400.0 MHz, C₆D₆, 25 °C): δ = 4.42 (s, 5H, Cp), 0.39 (s, 3H, CH₃) ppm. ¹³C NMR (100.6 MHz, C₆D₆, 25 °C): δ = 240.5 (1C, CO), 227.4 (2C, CO), 92.4 (5C, Cp), -22.2 (1C, CH₃) ppm. ⁹⁵Mo NMR (26.1 MHz, C₆D₆, 25 °C): δ = -1736 ppm. IR: $\tilde{\nu}(\text{CO}) = 2003.4$ (s), 1891.8 (vs), 1876.0 (vs) cm⁻¹.

[CpMo(CO)₃CF₃]: ¹H NMR (400.0 MHz, C₆D₆, 25 °C): δ = 4.55 (s, 5H, Cp) ppm. ¹³C NMR (100.6 MHz, C₆D₆, 25 °C): δ = 237.4 (1C, CO), 227.5 (1C, CO), 227.4 (1C, CO), 151.2 (1C, q, $J_{(C,F)} = 367.1$ Hz, CF₃), 93.1 (5C, Cp) ppm. ¹⁹F NMR (376.5 MHz, C₆D₆, 25 °C): δ = 13.03 (s, 3F, CF₃) ppm. ⁹⁵Mo NMR (26.1 MHz, C₆D₆, 25 °C): δ = -1458 ppm. IR: $\tilde{\nu}(\text{CO}) = 2044.8$ (m), 1960.9 (s), 1937.4 (s) cm⁻¹.

[CpMo(O₂)(O)CH₃]: ¹H NMR (400.0 MHz, C₆D₆, 25 °C): δ = 5.20 (s, 5H, Cp), 1.95 (s, 3H, CH₃) ppm. ¹³C NMR (100.6 MHz, C₆D₆, 25 °C): δ = 109.3 (5C, Cp), 24.8 (1C, CH₃) ppm. ⁹⁵Mo NMR (26.1 MHz, C₆D₆, 25 °C): δ = -609 ppm. IR: $\tilde{\nu} = 3103.1$ (m), 1363.4 (m), 1191.8 (m), 1051.8 (m), 1022.1 (m), 972.0 (s), 950.7 (vs), 910.2 (s), 877.5 (vs), 850.5 (s), 833.1 (m), 671.1 (w, b), 601.7 (m), 567.0 (vs) cm⁻¹.

[CpMo(O₂)(O)CF₃]: Yield 36%. ¹H NMR (400.0 MHz, C₆D₆, 25 °C): δ = 5.30 (s, 5H, Cp) ppm. ¹³C NMR (100.6 MHz, C₆D₆, 25 °C): δ = 148.0 (1C, q, $J_{(C,F)} = 370.2$ Hz, CF₃), 112.5 (5C, Cp) ppm. ¹⁹F NMR (376.5 MHz, C₆D₆, 25 °C): δ = -20.91 (s, 3F, CF₃) ppm. ⁹⁵Mo NMR (26.1 MHz, C₆D₆, 25 °C): δ = -709 ppm. IR: $\tilde{\nu} = 3113.3$ (m), 1458.9 (m), 1420.5 (w), 1363.4 (m), 1191.8 (m), 1094.4 (vs, with shoulders at 1079.9 and 1064.5), 1027.9 (m), 972.0 (m), 952.7 (vs), 908.3 (m), 890.0 (vs), 850.5 (m), 835.0 (m), 713.5 (m), 570.8 (s), 525.3 (vs) cm⁻¹. Elemental analysis: C₆H₅F₃MoO₃ (278.06 g mol⁻¹); calc. C, 25.92; H, 1.81%; found C, 26.18; H, 1.99%.

4.4.3 Kinetic studies

In all catalytic reactions, TBHP (5.5M in decane, over 4Å molecular sieves) was used as oxidant and cyclooctene as substrate. The reactions were done at room temperature and initiated by addition of the oxidant. The kinetic data was collected by using ¹H NMR and GC methods. (a) The reactions monitored by ¹H NMR were carried out in C₆D₆ in a total volume of 0.4-0.8 mL. The relative amounts of catalyst, substrate and oxidant were chosen with respect to the requirements of the kinetic analysis.

(b) The quantitative GC analysis was performed by taking samples of the reaction mixture at specific time intervals and treating them with MnO_2 to quench excess peroxide. After filtration, the samples were diluted with an isopropanol solution containing the standards p-xylene and indane (4 mg/L). The conversion of cyclooctene and the formation of cyclooctene epoxide were calculated from calibration curves ($r^2 = 0.999$) recorded prior to the reaction course.

4.4.4 Computational details

^{19}F NMR chemical shifts have been calculated with the help of density functional theory for possible intermediates after TBHP addition to the starting complex $[\text{CpMo}(\text{CO})_3\text{CF}_3]$. All calculations have been performed with the theory package Gaussian03⁵⁷. Designated intermediates were first optimised with the density functional theory functional B3LYP^{58–60} with the double-zeta basis set 6-31G*⁶¹ (Mo: Stuttgart97-ECP⁶²) and checked via frequency calculation if they have no negative vibration mode. Secondly, a GIAO^{63–65} (gauge-independent atomic orbital) single point calculation has been carried for each intermediate with B3LYP 6-311++G**⁶⁶ (Mo: Stuttgart97-ECP). Unscaled isotropic shielding values of all calculations were scaled to the starting complex $[\text{CpMo}(\text{CO})_3\text{CF}_3]$ as the experimentally observed chemical shift of 13.03 ppm.

4.5 References

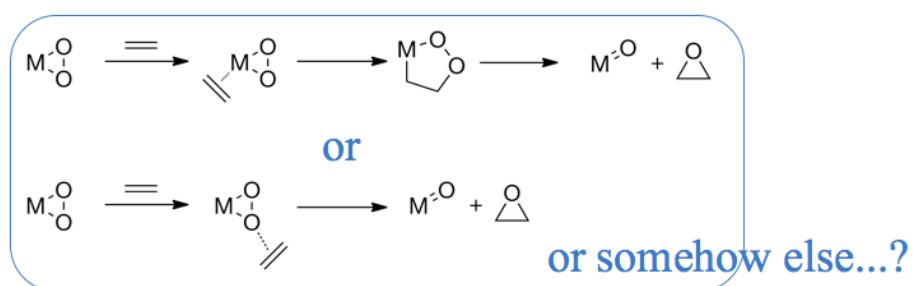
1. F. E. Kühn, A. M. Santos, W. A. Herrmann, *Dalton Trans.*, **2005**, 2483.
2. F. E. Kühn, A. M. Santos, M. Abrantes, *Chem. Rev.*, **2006**, *106*, 2455.
3. N. Grover, F. E. Kühn, *Curr. Org. Chem.*, **2012**, *16*, 16.
4. M. B. Trost, R. G. Bergman, *Organometallics*, **1991**, *10*, 1172.
5. I. S. Gonçalves, A. M. Santos, C. C. Romão, A. D. Lopes, J. E. Rodríguez-Borges, M. Pillinger, P. Ferreira, J. Rocha, F. E. Kühn, *J. Organomet. Chem.*, **2001**, *636*, 1.
6. R. Poli, *Chem. Eur. J.*, **2004**, *10*, 332.
7. F. E. Kühn, J. Zhao, M. Abrantes, W. Sun, C. A. M. Afonso, L. C. Branco, I. S. Gonçalves, M. Pillinger, C. C. Romão, *Tetrahedron Lett.*, **2005**, *46*, 47.
8. A. A. Valente, J. D. Seixas, I. S. Gonçalves, M. Abrantes, M. Pillinger, C. C. Romão, *Catal. Lett.*, **2005**, *101*, 127.
9. A. M. Martins, C. C. Romão, M. Abrantes, M. C. Azevedo, J. Cui, A. R. Dias, M. T. Duarte, M. A. Lemos, T. Lourenço, R. Poli, *Organometallics*, **2005**, *24*, 2582.
10. M. Abrantes, F. A. Almeida Paz, A. A. Valente, C. C. L. Pereira, S. Gago, A. E. Rodrigues, J. Klinowski, M. Pillinger, I. S. Gonçalves, *J. Organomet. Chem.*, **2009**, *694*, 1826.
11. P. Neves, C. C. L. Pereira, F. A. Almeida Paz, S. Gago, M. Pillinger, C. M. Silva, A. A. Valente, C. C. Romão, I. S. Gonçalves, *J. Organomet. Chem.*, **2010**, *695*, 2311.
12. C. Dinoi, M. Ciclosi, E. Manoury, L. Maron, L. Perrin, R. Poli, *Chem. Eur. J.*, **2010**, *16*, 9572.
13. M. Abrantes, P. Neves, M. M. Antunes, S. Gago, F. A. Almeida Paz, A. E. Rodrigues, M. Pillinger, I. S. Gonçalves, C. M. Silva, A. A. Valente, *J. Mol. Catal. A: Chem.*, **2010**, *320*, 19.
14. P. M. Reis, C. A. Gamelas, J. A. Brito, N. Saffon, M. Gómez, B. Royo, *Eur. J. Inorg. Chem.*, **2011**, 666.
15. M. Abrantes, S. M. Bruno, C. Tome, M. Pillinger, I. S. Gonçalves, A. A. Valente, *Catal. Comm.*, **2011**, *15*, 64.
16. J. Pisk, D. Agustin, V. Vrdoljak, R. Poli, *Adv. Synth. Catal.*, **2011**, *353*, 2910.
17. F. E. Kühn, A. M. Santos, A. D. Lopes, I. S. Gonçalves, E. Herdtweck, C. C. Romão, *J. Mol. Catal. A: Chem.*, **2000**, *164*, 25.
18. F. E. Kühn, A. D. Lopes, A. M. Santos, E. Herdtweck, J. J. Haider, C. C. Romão, A. G. Santos, *J. Mol. Catal. A: Chem.*, **2000**, *151*, 147.

19. F. E. Kühn, M. Groarke, E. Bencze, E. Herdtweck, A. Prazeres, A. M. Santos, M. J. Calhorda, C. C. Romão, I. S. Gonçalves, A. D. Lopes, M. Pillinger, *Chem. Eur. J.*, **2002**, *8*, 2370.
20. A. A. Valente, Z. Petrovski, L. C. Branco, C. A. M. Afonso, M. Pillinger, A. D. Lopes, C. C. Romão, C. D. Nunes, I. S. Gonçalves, *J. Mol. Catal. A: Chem.*, **2004**, *218*, 5.
21. A. Al-Ajlouni, A. A. Valente, C. D. Nunes, M. Pillinger, A. M. Santos, J. Zhao, C. C. Romão, I. S. Gonçalves, F. E. Kühn, *Eur. J. Inorg. Chem.*, **2004**, 1716.
22. A. Günyar, F. E. Kühn, *J. Mol. Catal. A: Chem.*, **2010**, *319*, 108.
23. M. Abrantes, A. M. Santos, J. Mink, F. E. Kühn, C. C. Romão, *Organometallics*, **2003**, *22*, 2112.
24. J. Zhao, A. M. Santos, E. Herdtweck, F. E. Kühn, *J. Mol. Catal. A: Chem.*, **2004**, *222*, 265.
25. C. Freund, M. Abrantes, F. E. Kühn, *J. Organomet. Chem.*, **2006**, *691*, 3718.
26. A. M. Al-Ajlouni, D. Veljanovski, A. Capapé, J. Zhao, E. Herdtweck, M. J. Calhorda, F. E. Kühn, *Organometallics*, **2009**, *28*, 639.
27. A. A. Valente, J. Moreira, A. D. Lopes, M. Pillinger, C. D. Nunes, C. C. Romão, F. E. Kühn, I. S. Gonçalves, *New J. Chem.*, **2004**, *28*, 308.
28. S. M. Bruno, C. C. L. Pereira, M. S. Balula, M. Nolasco, A. A. Valente, A. Hazell, M. Pillinger, P. Ribeiro-Claro, I. S. Gonçalves, *J. Mol. Catal. A: Chem.*, **2007**, *261*, 79.
29. A. C. Coelho, M. Nolasco, S. S. Balula, M. M. Antunes, C. C. L. Pereira, F. A. A. Paz, A. A. Valente, M. Pillinger, P. Ribeiro-Claro, J. Klinowski, I. S. Gonçalves, *Inorg. Chem.*, **2011**, *50*, 525.
30. F. Madeira, S. Barroso, S. Namorado, P. M. Reis, B. Royo, A. M. Martins, *Inorg. Chim. Acta*, **2012**, *383*, 152.
31. S. S. Balula, S. M. Bruno, A. C. Gomes, A. A. Valente, M. Pillinger, I. S. Gonçalves, D. J. Macquarrie, J. H. Clark, *Inorg. Chim. Acta*, **2012**, *387*, 234.
32. A. Capapé, A. Raith, F. E. Kühn, *Adv. Synth. Catal.*, **2009**, *351*, 66.
33. A. Capapé, A. Raith, E. Herdtweck, M. Cokoja, F. E. Kühn, *Adv. Synth. Catal.*, **2010**, *352*, 547.
34. D. Betz, A. Raith, M. Cokoja, F. E. Kühn, *ChemSusChem*, **2010**, *3*, 559.
35. R. B. King, M. B. Bisnette, *J. Organomet. Chem.*, **1964**, *2*, 15.
36. C. C. Romão, F. E. Kühn, W. A. Herrmann, *Chem. Rev.*, **1997**, *97*, 3197.
37. F. E. Kühn, A. Scherbaum, W. A. Herrmann, *J. Organomet. Chem.*, **2004**, *689*, 4149.
38. R. Wiest, T. Leininger, G. H. Jeung, M. Bénard, *J. Phys. Chem.*, **1992**, *96*, 10800.
39. J. Iskra, D. Bonnet-Delpon, J.-P. Bégué, *Tetrahedron Lett.*, **2002**, *43*, 1001.

40. M. C. A. van Vielt, I. W. C. E. Arends, R. A. Sheldon, *Chem. Commun.*, **1999**, 821.
41. A. Berkessel, J. A. Adrio, *Adv. Synth. Catal.*, **2004**, 346, 275.
42. M. C. A. van Vielt, I. W. C. E. Arends, R. A. Sheldon, *Synlett*, **2001**, 2, 248.
43. M. C. A. van Vielt, I. W. C. E. Arends, R. A. Sheldon, *Synlett*, **2001**, 8, 1305.
44. J.-P. Bégué, D. Bonnet-Delpon, B. Crousse, *Synlett*, **2004**, 1, 18.
45. T. Welton, *Chem. Rev.*, **1999**, 99, 2071.
46. B. Kirchner, Topics in Current Chemistry, Vol. 290, Springer, Berlin Heidelberg, **2010**.
47. P. Ferreira, I. S. Gonçalves, F. E. Kühn, A. D. Lopes, M. A. Martins, A. Pina, J. Rocha, C. C. Romão, A. M. Santos, T. M. Santos, A. A. Valente, *Eur. J. Inorg. Chem.*, **2000**, 2263.
48. A. Sakthivel, J. Zhao, M. Hanzlik, A. S. T. Chiang, W. A. Herrmann, F. E. Kühn, *Adv. Synth. Catal.*, **2005**, 347, 473.
49. C. D. Nunes, M. Pillinger, A. A. Valente, I. S. Gonçalves, J. Rocha, P. Ferreira, F. E. Kühn, *Eur. J. Inorg. Chem.*, **2002**, 1100.
50. K. R. Jain, F. E. Kühn, *J. Organomet. Chem.*, **2007**, 692, 5532.
51. D. Betz, W. A. Herrmann, F. E. Kühn, *J. Organomet. Chem.*, **2009**, 694, 3320.
52. A. Berkessel, J. A. Adrio, D. Hüttenhain, J. M. Neudörfl, *J. Am. Chem. Soc.*, **2006**, 128, 8421.
53. A. Berkessel, J. A. Adrio, *J. Am. Chem. Soc.*, **2006**, 128, 13412.
54. A. Comas-Vives, A. Lledós, R. Poli, *Chem. Eur. J.*, **2010**, 16, 2147.
55. P. J. Costa, M. J. Calhorda, F. E. Kühn, *Organometallics*, **2010**, 29, 303.
56. R. B. King, Organometallic Syntheses (Vol. 1), Academic Press, New York, **1965**, pp. 145.
57. M. J. Frisch et al., Gaussian 03 Rev. E.01, **2004**, Gaussian Inc., Wallingford, CT.
58. S. H. Vosko, L. Wilk, M. Nusair, *Can. J. Phys.*, **1980**, 58, 1200.
59. C. Lee, W. Yang, R. G. Parr, *Phys. Rev. B*, **1988**, 37, 785.
60. A. D. Becke, *J. Chem. Phys.*, **1993**, 98, 5648.
61. W. J. Hehre, R. Ditchfield, J. A. Pople, *J. Chem. Phys.*, **1972**, 56, 2257.
62. D. Andrae, U. Haeussermann, M. Dolg, H. Stoll, H. Preuss, *Theor. Chim. Acta*, **1990**, 77, 123.
63. R. Ditchfield, *Mol. Phys.*, **1974**, 27, 789.
64. K. Wolinski, J. F. Hilton, P. Pulay, *J. Am. Chem. Soc.*, **1990**, 112, 8251.

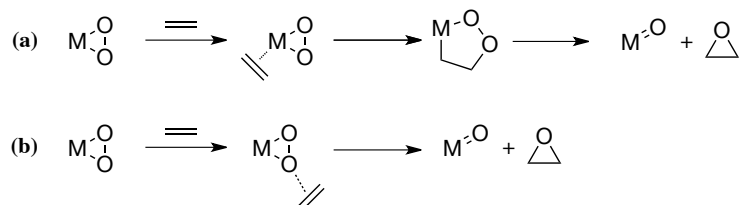
65. J. R. Cheeseman, G. W. Trucks, T. A. Keith, M. J. Frisch, *J. Chem. Phys.*, **1996**, *104*, 5497.
66. R. Krishnan, J.S. Binkley, R. Seeger, J. A. Pople, *J. Chem. Phys.*, **1980**, *72*, 650.

5 The Quest of the Mechanism of Olefin Epoxidation Catalysed by Monomeric Organomolybdenum Complexes



5.1 Background

Monomeric cyclopentadienyl molybdenum oxides belong to the first synthesised high oxidation state organometallics. However, when Cousins and Green published the first molybdenum(VI) cyclopentadienyl dioxo complex, $[\eta^5\text{-}(\text{C}_5(\text{CH}_3)_5)\text{Mo}(\text{O})_2\text{Cl}]$ (**1**), about 50 years ago,¹ they did not foresee the importance of such organomolybdenum compounds in catalysis. The breakthrough for the interest in high oxidation state organometallics and its broad catalytic applicability was founded on the discoveries of related organorhenium complexes by Beattie and Jones and by Herrmann *et al.*²⁻⁴ In the last decades, organomolybdenum compounds attracted attention for their versatile use in olefin epoxidation catalysis.⁵ The straightforward synthesis and easy handling of tricarbonyl organomolybdenum derivatives especially promoted their application in catalytic reactions. Due to the industrial importance of enantiopure epoxide synthesis, several attempts have been undertaken to develop them into valuable catalysts for asymmetric epoxidation reactions,^{6,7} however, so far with different success regarding enantiomeric excess and epoxide yield. A major drawback to ameliorate these results is the ignorance of the stereochemistry of the transition state. It is of great importance to have an idea on which way the oxygen transfer from the peroxide to the olefin occurs, in order to introduce chiral or sterically crowding groups at the right place, where they influence the chirality of the epoxide.



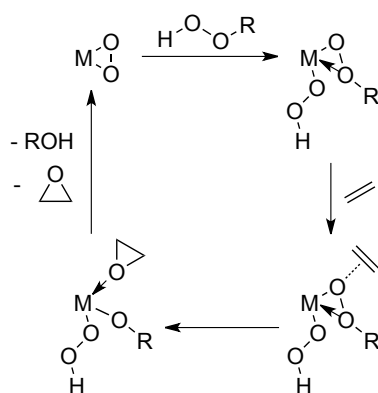
Scheme 5.1 The simplified representation (M = Mo, not involved ligands at the metal centre are omitted for clarity) of the two possible pathways of the oxygen transfer from the peroxide to the olefin proposed by (a) Mimoun *et al.*⁸ and (b) Sharpless *et al.*⁹

More than three decades ago, Mimoun *et al.*⁸ proposed a mechanism for the stoichiometric Mo-catalysed olefin epoxidation, where the reaction proceeds via a five-membered metallacycle (Scheme 5.1(a)). This led to the assumption that the peroxo compound could be the intermediate in oxygen transfer. Shortly after, Sharpless *et al.*⁹ published a mechanistic proposal for the Mo-catalysed olefin epoxidation, where the olefin attacks directly at a peroxo-oxygen atom (Scheme 5.1(b)).

While the mechanism of the stoichiometric reaction was presented in a number of publications,⁸⁻¹² the mechanism of the catalytic reaction has still been subject of controversial discussions. In 1977, Sharpless *et al.* proved the intermediacy of an intact alkyl peroxo complex as active species. They showed that the ¹⁸O-labelled terminal oxo groups of the metal complex

were not transferred to the olefin while using unlabelled *tert*-butyl hydroperoxide (TBHP) as oxidant.¹³ In the early 1990s, Trost and Bergman stated the catalytic activity in olefin epoxidation of $[\eta^5\text{-}(\text{C}_5(\text{CH}_3)_5)\text{Mo}(\text{O})_2\text{Cl}]$ (**1**). However, they found that the corresponding oxo peroxy complex $[\eta^5\text{-}(\text{C}_5(\text{CH}_3)_5)\text{Mo}(\text{O}_2)(\text{O})\text{Cl}]$ (**2**) was catalytically inactive.¹⁴ In absence of olefin, **1** reacted with *tert*-butyl hydroperoxide (TBHP) to **2** which can therefore be identified as a unwanted side-product in the catalytic reaction.

Some years later, Thiel proposed a mechanism specifically for olefin epoxidation with TBHP, outlined in Scheme 5.2.^{15–17} It is similar to the pathway proposed by Sharpless, as the olefin attacks exogenously at an electrophilic oxygen atom without coordination to the metal centre, however, oxygen transfer occurs from the coordinated *tert*-butyl peroxy ligand instead of a coordinated peroxy ligand.



Scheme 5.2 Thiel's proposal for Mo-catalysed olefin epoxidation with TBHP.

Subsequent studies with cyclopentadienyl containing Mo-complexes showed, however, that oxo peroxy Mo-complexes can act as epoxidation catalysts, as reported by Kühn *et al.*¹⁸ They proved the catalytic activity of $[\eta^5\text{-}(\text{C}_5\text{H}_5)\text{Mo}(\text{O}_2)(\text{O})\text{CH}_3]$ (**3**) and proposed a catalytic cycle (see Scheme 5.3(a)). The oxo peroxy complex seems to be formed from the dioxo complex $[\eta^5\text{-}(\text{C}_5\text{H}_5)\text{Mo}(\text{O})_2\text{CH}_3]$ (**4**) in presence of a large excess of oxidant, and contributes as well to the epoxidation of the olefin, however, with a slower rate constant than **4**.

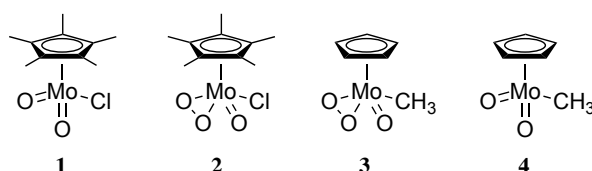
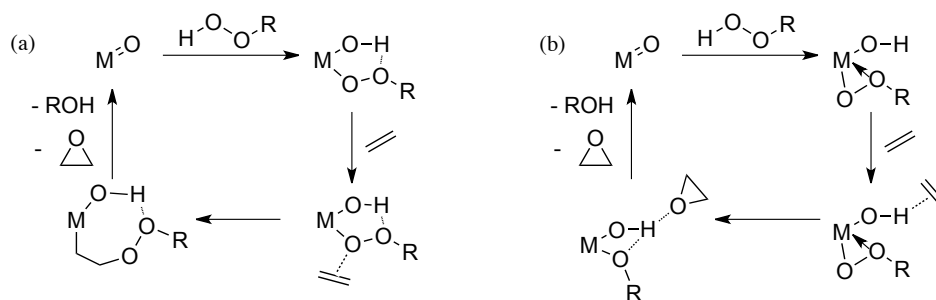


Figure 5.1 Monomeric organomolybdenum complexes in piano-stool configuration that have been applied in catalytic olefin epoxidation. Complexes **1**, **3** and **4** are active catalysts, whilst complex **2** showed no catalytic activity under the chosen reaction conditions.

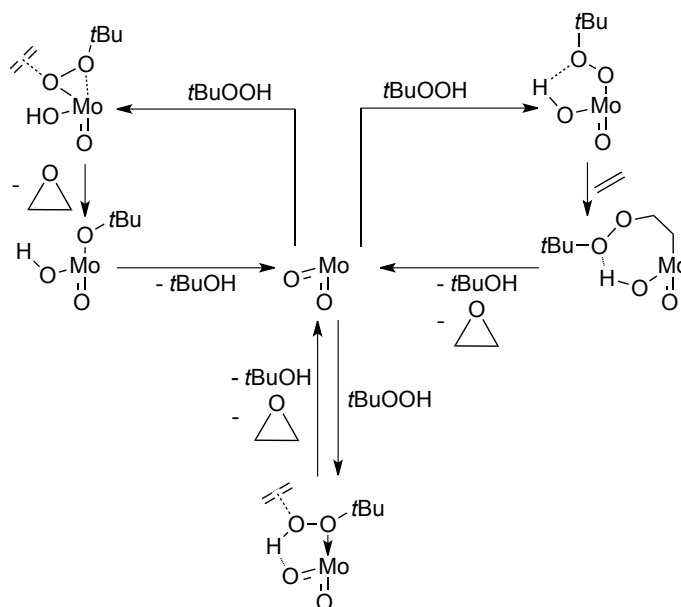
These experimental evidences are, from a mechanistic point of view, not easily consolidated. Does the reason of the catalytic inactivity of **2** lie in the presence of the electron-

withdrawing chloro ligand or the sterically encumbering Cp*? Very recently, two independent computational studies affronted this question (Scheme 5.3).^{19,20}



Scheme 5.3 Intermediates in the mechanistic pathway proposed by (a) Calhorda *et al.*²⁰ and (b) Poli *et al.*¹⁹

On the one hand, Calhorda *et al.* studied the $[\eta^5\text{-}(\text{C}_5\text{H}_5)\text{Mo}(\text{O})_2\text{CH}_3]$ -system, and proposed a Mimoun-like pathway where a seven-membered metallacycle is formed after the olefin attack at the α -oxygen of the peroxy ligand.²⁰ Poli *et al.*, on the other hand, found a variant of the Sharpless pathway to be energetically most favourable for the $[\eta^5\text{-}(\text{C}_5(\text{CH}_3)_5)\text{Mo}(\text{O})_2\text{Cl}]$ -system.¹⁹ They also calculated a possible pathway for the epoxidation of ethylene catalysed by $[\eta^5\text{-}(\text{C}_5(\text{CH}_3)_5)\text{Mo}(\text{O}_2)(\text{O})\text{Cl}]$ and found higher activation barriers in the transition states. A possible explanation is the higher electron density on the Mo-atom, decreasing less the energy of the O–O σ^* orbital of the ROO^- ligand. Another influence may have the greater steric crowding of the Cp* ligand.



Scheme 5.4 The three pathways compared based on DFT calculations by Poli *et al.* for olefin epoxidation by a $[\text{MoO}_2\text{L}]$ system (L = ONO-type tridentate Schiff base ligand). The ligands are omitted for clarity, as well as the olefin is simplified to ethylene.²¹

Lately, another computational study²¹ attempted to elucidate the oxygen transfer process

in the case of $[\text{MoO}_2\text{L}(\text{D})]$, with L = ONO-type tridentate Schiff base ligand and D a donor molecule (Scheme 5.4). Three different mechanisms were compared and the energies of all of their transition states were in a reasonable range, *i.e.* no one could be excluded or preferred uniquely.

5.2 Experimental approach

A series of organomolybdenum compounds was synthesised and characterised by means of NMR and IR spectroscopy. They were then applied as (pre-)catalysts of the epoxidation of cyclooctene with *tert*-butyl hydroperoxide as oxidant for the determination of the catalytically active species and for the assessment of kinetic data. Second, several experiments were carried out to shed light on the mechanism of the catalytic olefin epoxidation: The determination of the rate constants in the catalysed epoxidation of cyclooctene allows an insight in the structure of the possible active species, and ^{13}C NMR spectroscopy was used for observing the substrate environment during a catalytic cycle. The investigations performed with complex $[\text{CpMo}(\text{CO})_3\text{CF}_3]$ (**5**) have already been presented in the previous chapter.

5.3 Results and Discussion

5.3.1 Activity of the catalyst precursors – $[\text{Cp}'\text{Mo}(\text{CO})_3\text{R}]$

There exist many reports on the catalytic activity of carbonyl organomolybdenum complexes in olefin epoxidation.^{18,22–28} They act as pre-catalysts, as oxidative decarbonylation takes place in presence of an oxidant. Although the catalytically active species needs to be formed in the beginning of the reaction, it has been shown that the use of the carbonyl derivatives has to be preferred to the application of the oxidised species, due to their higher stability and the easier handling.^{24,25}

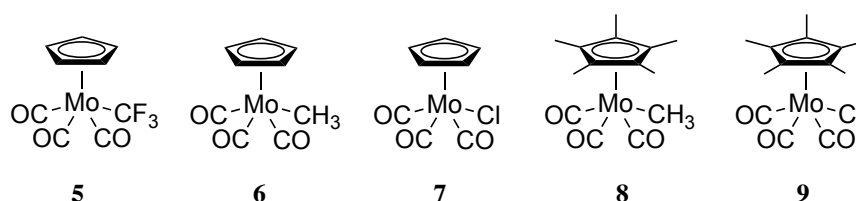


Figure 5.2 A set of monomeric carbonyl organomolybdenum complexes that are known olefin epoxidation pre-catalysts.

The complexes shown in Figure 5.2 have all been synthesised and their NMR spectroscopic characterisation is summarised in Table 5.1. Furthermore, they have been applied in the epoxidation of cyclooctene with TBHP at room temperature. In the beginning of the reaction, the pre-catalyst is decarbonylated (*in situ*) by the oxidant (TBHP). The rate of conversion

Table 5.1 Characteristic spectroscopic data of complexes **5-9** (NMR spectra recorded in C₆D₆, at 25 °C).

| Complex | ¹ H NMR shift [ppm] | ¹³ C NMR shift [ppm] | ⁹⁵ Mo NMR shift [ppm] |
|----------|---------------------------------------|--|----------------------------------|
| 5 | 4.55 (Cp) | 237.4; 227.5; 227.4 (CO) 151.2 (CF ₃) 93.1 (C ₅ H ₅) | -1458 |
| 6 | 4.42 (Cp) 0.39 (CH ₃) | 240.5; 227.4 (CO) 92.4 (C ₅ H ₅) -22.2 (CH ₃) | -1736 |
| 7 | 4.58 (Cp) | 243.1; 225.1 (CO) 95.5 (C ₅ H ₅) | -887 |
| 8 | 1.48 (Cp*) 0.28 (CH ₃) | 243.4; 229.8 (CO) 104.0 (C ₅ (CH ₃) ₅) 10.1 (C ₅ (CH ₃) ₅) -11.5 (CH ₃) | -1596 |
| 9 | 1.44 (Cp*) | 247.4; 228.2 (CO) 108.6 (C ₅ (CH ₃) ₅) 10.4 (C ₅ (CH ₃) ₅) | -819 |

to the oxidised species depends on the concentration of the oxidant as well as the ligand R coordinated to the Mo-centre. Moreover, as the decarbonylation is an exothermic process, the initial epoxidation reaction is accelerated, which induces in general higher turnover frequencies. Figure 5.3 shows the kinetic data of the epoxidation of cyclooctene with TBHP at room temperature with 0.25 mol% [Cp'Mo(CO)₃R]. The performance of the pre-catalysts is varying with respect to both cyclopentadienyl moiety and ligand R. While the complexes containing a chloro ligand are fast oxidised to the Mo(VI)-species which is catalytically active, [CpMo(CO)₃CF₃] shows a very long induction time at the chosen concentration. This is due to the fact that the decarbonylation of this complex is very slow, thus the concentration of the catalytically active species stays at a low level in the beginning of the reaction. In order to determine the turn-over frequency (TOF) and turn-over number (TON) of the catalyst precursors, *i.e.* to assess the catalytic characteristics of the complexes under the present reaction conditions, a range of experiments using different catalyst concentration all by keeping the other variables constant has been executed. Table 5.2 summarises the results, and leads to the conclusion that a Cp moiety is more favourable than Cp* (probably because of sterics) and that the positive influence on the catalytic activity of the complex decreases from Cl > CH₃ > CF₃. This is more difficult to explain, as the shielding of the [CpMo(CO)₃]⁺ core increases in the order Cl < CF₃ < CH₃. A possible explanation of this is the formation of different oxidation products upon decarbonylation, as it was shown that for R = Cl, only the dioxo derivative is formed in presence of TBHP at room temperature, and for R = CH₃, formation of [CpMo(O₂)(O)CH₃] is predominant with a large excess of oxidant. The remarkable gap to the activity of the fluorinated complex **5** can be explained by its slow oxidation, and the resulting low concentration of the catalytically active species (see Chapter 4 for more details).

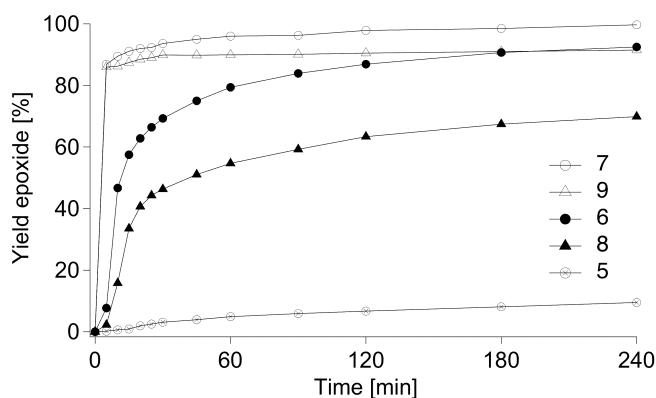


Figure 5.3 Kinetic data of the performance of various tricarbonyl organomolybdenum derivatives in the epoxidation of cyclooctene in C_6D_6 (ratio pre-catalyst : cyclooctene : TBHP = 0.0025 : 1 : 1.2, 25 °C).

Table 5.2 Highest activities of the applied pre-catalysts expressed in terms of turn-over frequencies (TOF, determined at the steepest slope of the kinetic curve) and turnover number (TON, determined with the conversion achieved after 4h).

| Complex | Concentration [mol%] | TOF [h^{-1}] | TON [-] |
|---------|----------------------|------------------|---------|
| 5 | 0.500 | 240 | 152 |
| 6 | 0.250 | 1874 | 370 |
| 7 | 0.063 | 7932 | 1472 |
| 8 | 0.500 | 857 | 146 |
| 9 | 0.125 | 5852 | 584 |

5.3.2 Catalytic activity of the chloro derivatives

Oxidation of $[Cp'Mo(CO)_3Cl]$ with excess TBHP at room temperature yields $[Cp'Mo(O)_2Cl]$.²³ Further conversion to the oxo peroxy derivative, however, was observed in catalytic reactions with higher temperatures and prolonged reaction times, in presence of a large excess oxidant.¹⁴ It was reported that complex **1** is degraded to complex **2** during a catalytic reaction, thus poisoning the catalyst **1** as it does not show any activity under the applied reaction conditions.^{14,29}

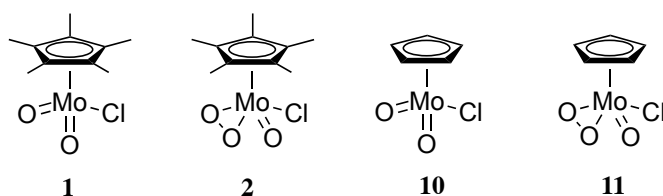


Figure 5.4 Isolated organomolybdenum complexes bearing a chloro-moiety as well as oxo and/or peroxy ligands.

As the dioxo complexes **1** and **10** were known to be active epoxidation catalysts, it was questionable if complex **11** would be active as well. Therefore, the complexes were isolated

(see Table 5.3 for characterisation) and applied in the epoxidation of cyclooctene with TBHP at room temperature.

Table 5.3 Characteristic spectroscopic data of complexes **1-2** and **10-11** (NMR spectra recorded in C_6D_6).

| Complex | 1H NMR shift [ppm] | ^{13}C NMR shift [ppm] | ^{95}Mo NMR shift [ppm] |
|-----------|-----------------------|---|---------------------------|
| 1 | 1.62 (Cp*) | 125.2 ($C_5(CH_3)_5$) | -402 |
| 2 | 1.53 (Cp*) | 11.1 ($C_5(CH_3)_5$) 126.0 ($C_5(CH_3)_5$) 11.0 ($C_5(CH_3)_5$) | -411 |
| 10 | 5.40 (Cp) | 115.4 (C_5H_5) | -453 |
| 11 | 5.38 (Cp) | 115.4 (C_5H_5) | -558 |

As in the case of the tricarbonyl catalyst precursors, the Cp-complexes exhibit a higher activity than the Cp*-derivatives (see Figure 5.5). As expected, complex **2** shows no catalytic activity at room temperature. This is in agreement with literature reports^{14,29} and DFT calculations¹⁹ that state a higher energy state of the oxygen transfer step for $[Cp^*Mo(O_2)(O)Cl]$ (45.1 kcal mol⁻¹) than for $[Cp^*Mo(O)_2Cl]$ (25.9 kcal mol⁻¹) with H_3COOH as an oxidant.

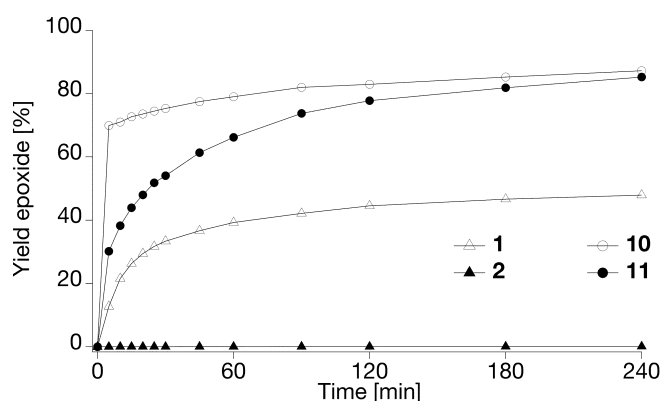


Figure 5.5 Kinetic data of the performance of the four chloro organomolybdenum derivatives in the epoxidation of cyclooctene in C_6D_6 (ratio catalyst : cyclooctene : TBHP = 0.0025 : 1 : 1.2, 25 °C).

Comparison of the TOF of the Mo(VI)-derivatives with their respective Mo(II)-precursors (Tables 5.2 and 5.4) leads to the conclusion that the pre-catalysts show a substantially higher activity. It is supposed that the exothermicity observed in the beginning of those reactions induces this enhancing effect in the initial period.

5.3.3 Comparison of $[Cp^*Mo(O_2)(O)R]$ -type complexes

As mentioned in the introduction, there is a surprising difference in reactivity between the oxo peroxy complexes **2** and **3**. The isolation of other oxo peroxy complexes (shown in Figure 5.6)

Table 5.4 Highest activities of the applied catalysts expressed in terms of turn-over frequencies (TOF, determined at the steepest slope of the kinetic curve) and turnover number (TON, determined with the conversion achieved after 4h).

| Complex | Concentration [mol%] | TOF [h ⁻¹] | TON [-] |
|-----------|----------------------|------------------------|---------|
| 1 | 0.125 | 1225 | 383 |
| 2 | 0.250 | – | – |
| 10 | 0.125 | 4214 | 617 |
| 11 | 0.125 | 2219 | 559 |

and their application in the epoxidation of cyclooctene should therefore serve to elucidate this fact.

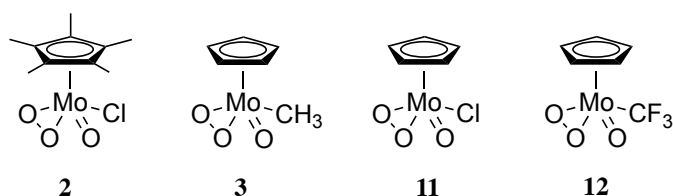


Figure 5.6 Isolated oxo peroxo organomolybdenum complexes.

Complexes **2**, **3**, **11** and **12** were thoroughly spectroscopically characterised. Table 5.5 summarises the resonances observed in ¹H, ¹³C, and ⁹⁵Mo NMR spectra. Latter reveals a trend (with exceptions) to the catalytic activity in olefin epoxidation: the stronger the shielding of the Mo-core (the more negative the resonance), the better is the performance of the complex in epoxidation catalysis (see also Table 5.7). In the case of complex **2**, the steric bulk of the Cp* ligand influences the catalytic activity enormously, as it shows no activity.

Table 5.5 Characteristic spectroscopic data of complexes **2-3** and **11-12** (NMR spectra recorded in C₆D₆).

| Complex | ¹ H NMR shift [ppm] | ¹³ C NMR shift [ppm] | ⁹⁵ Mo NMR shift [ppm] |
|-----------|--------------------------------|---|----------------------------------|
| 2 | 1.53 (Cp*) | 126.0 (C ₅ (CH ₃) ₅) | -411 |
| 3 | 5.23 (Cp) | 11.0 (C ₅ (CH ₃) ₅) | -609 |
| | 1.95 (CH ₃) | 109.3 (C ₅ H ₅) | |
| 11 | 5.38 (Cp) | 24.8 (CH ₃) | -558 |
| | 5.30 (Cp) | 115.4 (C ₅ H ₅) | |
| 12 | | 112.5 (C ₅ H ₅) | -709 |
| | | 148.0 (CF ₃) | |

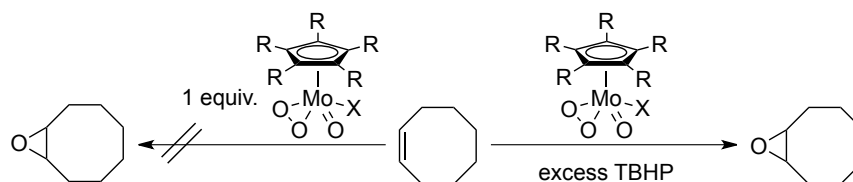
In the FT-IR spectra of the compounds, the symmetric/asymmetric Mo(η²-O₂) stretching frequencies are located at 585/567 cm⁻¹ for complex **2**, at 575/561 cm⁻¹ for complex **3**, at 560/518 cm⁻¹ for complex **11** and at 571/525 cm⁻¹ for complex **12**. The weak IR and Raman features between 850 and 870 cm⁻¹ were referred to the O-O stretching of the peroxo group. The ring tilt mode can be assigned to the IR bands around 355 cm⁻¹.

Table 5.6 Selected FT-IR and Raman frequencies (cm^{-1}) of compounds **2**, **3**, **11** and **12**.

| 2 | | 3 | | 11 | | 12 | | Assignment |
|----------|--------------|----------|-------|-----------|--------|-----------|--------------|---|
| IR | Raman | IR | Raman | IR | Raman | IR | Raman | |
| 927vs | ^a | 951vs | 949vs | 936vs | 933s | 953vs | ^a | $\nu(\text{Mo}=\text{O})$ |
| 878vs | | 878vs | 872s | 882vs | 878m | 890vs | | $\nu(\text{CC})$ and $\nu(\text{C}-\text{CH}_3)$ of Cp* |
| | | | | | | | | $\gamma(\text{CH})$ of Cp |
| 858vvw | | 850vw | | 862vw | 861w | 870vw | | $\nu(\text{O}-\text{O})$ |
| 585s | | 575s | 576m | 560s | 559m | 571s | | $\nu_s(\text{Mo}(\eta^2-\text{O}_2))$ |
| 567vs | | 561vs | 559s | 518s,b | 518w,b | 525vs | | $\nu_a(\text{Mo}(\eta^2-\text{O}_2))$ |
| 349vs | | 368m | 368s | 352s | 351s | 376vs | | $\nu(\text{MoCp})$ |
| 295m | | | | 308m,b | 309m | 302w | | O=MoCp deformation |
| 255w | | 256s | 258vs | 265w | 264s | 243vs | | O=Mo($\eta^2-\text{O}_2$) deformation |
| 228m | | 219s | 218m | 228w | 218m | 204m | | O=Mo($\eta^2-\text{O}_2$) deformation |

^a not determined

A first catalytic experiment was made by reacting the complexes stoichiometrically with cyclooctene. While the bisperoxo complex $[(\text{CH}_3)_3\text{Re}(\text{O}_2)_2\text{O} \cdot \text{H}_2\text{O}]$ formed of MTO with 2 equivalents H_2O_2 is an active oxygen transfer agent when isolated and reacted stoichiometrically with an olefin,³⁰ the monoperoxo complex $[(\text{CH}_3)_3\text{Re}(\text{O}_2)\text{O}_2]$ does not induce the formation of epoxides from olefins in absence of H_2O_2 . The same accounts for the Mo(VI)-complexes presented herein (Scheme 5.5). No epoxide formation is observed, even at 55 °C, in absence of excess TBHP.



Scheme 5.5 Oxo peroxo organomolybdenum compounds with R = H and X = Cl; CH_3 ; CF_3 catalytically epoxidise olefins in presence of excess TBHP, applied in a stoichiometric amount, however, they do not transfer an oxygen atom to an olefin in absence of an oxidant.

Table 5.7 Highest activities of the applied catalysts expressed in terms of turn-over frequencies (TOF, determined at the steepest slope of the kinetic curve) and turnover number (TON, determined with the conversion achieved after 4h).

| Complex | Concentration [mol%] | TOF [h^{-1}] | TON [-] |
|-----------|----------------------|-------------------------|---------|
| 2 | 0.250 | – | – |
| 3 | 0.250 | 1268 | 288 |
| 11 | 0.125 | 2219 | 559 |
| 12 | 0.125 | 2371 | 581 |

The kinetics of the catalytic reaction with excess TBHP is shown in Figure 5.7. As in the case of the catalytic precursors $[\text{Cp}'\text{Mo}(\text{CO})_3\text{R}]$, the cyclopentadienyl-containing complexes

perform better, whereof $[\text{CpMo}(\text{O}_2)(\text{O})\text{CF}_3]$ displays the highest activity in terms of TOF (see Table 5.7).

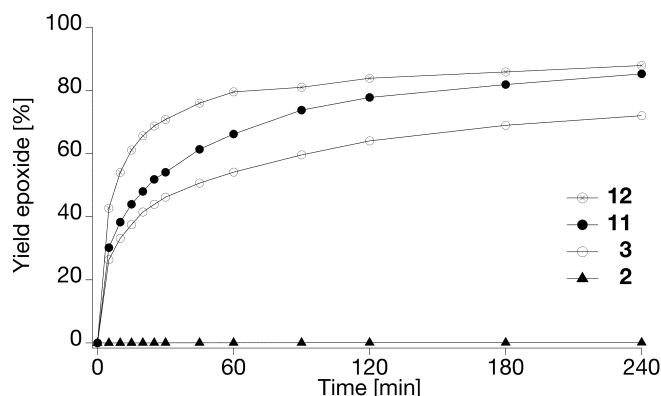
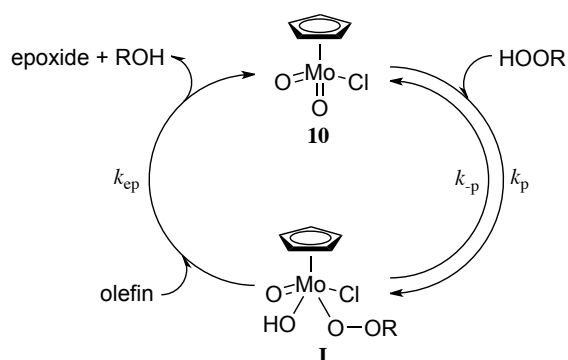


Figure 5.7 Kinetic data of the performance of the four oxo peroxy organomolybdenum derivatives in the epoxidation of cyclooctene in C_6D_6 (ratio catalyst : cyclooctene : TBHP = 0.0025 : 1 : 1.2, 25 °C).

5.3.4 Mechanistic studies with $[\text{CpMo}(\text{O})_2\text{Cl}]$

Mechanistic studies with complex **3** have proven the presence of a σ -bound peroxy-group as intermediate in the catalytic cycle.¹⁸ This is in accordance to results reported by Thiel *et al.*, who proposed a concerted oxygen transfer from a pendant peroxy group on a peroxy Mo(VI)-complex to the olefin in the epoxidation reaction with TBHP as the oxidant.^{15–17} We therefore performed the same experiments with complex **10** in order to support the mechanistic similarity of the different Mo(VI)-complexes presented herein.



Scheme 5.6 Proposed general epoxidation mechanism.

Based on published results,¹⁸ one can assume a mechanism as presented in Scheme 5.6. During a catalytic reaction, complex **10** is in equilibrium with the reactive intermediate **I**, and the rate of olefin epoxidation can be defined as follows:

$$\text{rate} = -\frac{d[\text{olefin}]}{dt} = k_{ep} \cdot [\text{olefin}] \cdot [\mathbf{I}] \quad (5.1)$$

Taking into account the total mass balance $[\text{Mo}]_{total} = [\mathbf{10}] + [\mathbf{I}]$, equation (5.1) stipulates a linear increase of the epoxidation rate with increasing catalyst concentration. The kinetics of the epoxidation was thus examined by series of experiments with constant olefin and TBHP concentration, but varying catalyst concentration (Figure 5.8). The initial rate was determined based on the conversion of the olefin to the epoxide after 90 seconds reaction time, and the value of rate constant k_{ep} was calculated ($14.013 \pm 1.144 \text{ M}^{-1}\text{s}^{-1}$).

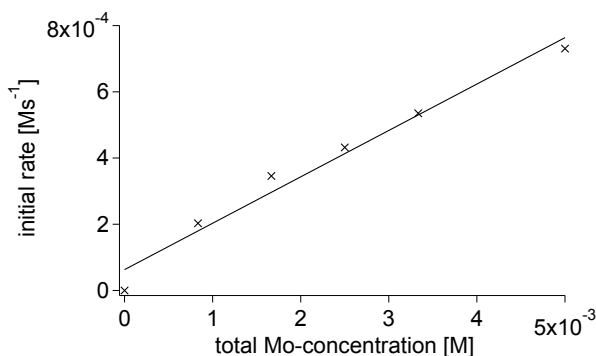


Figure 5.8 Linear dependence of the oxidation initial rate of cyclooctene (0.01 M) on $[\text{Mo}]_{total}$ according to equation (5.1). The reactions were carried out at 25 °C in CDCl_3 with $[\text{TBHP}] = 1 \text{ M}$.

The rate equation (5.1) can then be re-written by means of a steady-state approximation, *i.e.* the concentration of the intermediate \mathbf{I} does not change over time, so that it becomes:

$$\text{rate} = -\frac{d[\text{olefin}]}{dt} = \frac{k_{ep} \cdot k_p \cdot [\text{olefin}] \cdot [\text{TBHP}] \cdot [\text{Mo}]_{total}}{k_{-p} + k_p \cdot [\text{TBHP}] + k_{ep} \cdot [\text{olefin}]} \quad (5.2)$$

A second series of experiments was performed by varying the concentration of TBHP (Figure 5.9). Fitting of the kinetic data points to equation (5.2) allowed again extraction of the rate constant $k_{ep} = 9.227 \pm 0.086 \text{ M}^{-1}\text{s}^{-1}$, which is close to the one estimated above.

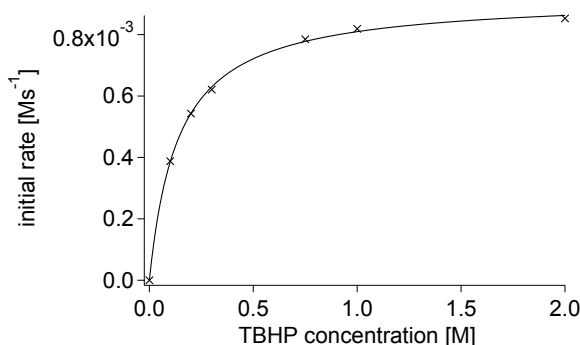


Figure 5.9 Variation of the oxidation initial rate of cyclooctene (0.1 M) catalysed by 10 (0.001 M) against the concentration of TBHP in CDCl_3 at 25 °C. The curve fitting was done by using equation (5.2) with $k_p = 6.612 \pm 0.005 \text{ M}^{-1}\text{s}^{-1}$; $k_{-p} = 0.005 \text{ s}^{-1}$; $k_{ep} = 9.227 \pm 0.086 \text{ M}^{-1}\text{s}^{-1}$.

5.3.5 Mechanistic investigations by means of ^{13}C NMR spectroscopy

In order to rule out the pathway proceeding via a Mimoun-type mechanism, a study based on α,β - ^{13}C -labelled styrene and complex **5** was carried out. The rate of epoxidation of this particular olefin is known to be slow at room temperature in presence of Mo-based catalysts (see Chapter 4). In order to assure monitoring of the reaction by continuously recording short ^{13}C -NMR spectra (526 scans), the reaction temperature was set to 10 °C. The catalyst : substrate ratio was chosen 1 : 2, with an excess (100 equiv. with respect to catalyst) TBHP as oxidant present. If the oxygen transfer occurs via a Mimoun-type mechanism, complexes of the type of **13** or **14** (shown in Figure 5.10) would be formed and give rise to distinct signals in the ^{13}C NMR spectra.

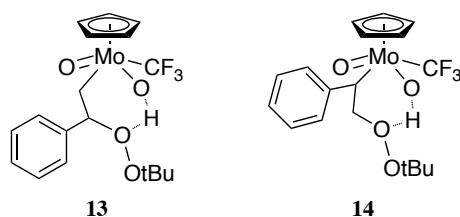


Figure 5.10 Two possible reaction intermediates in the epoxidation of styrene if the reaction proceeds via a Mimoun-type pathway.

Table 5.8 Comparison of calculated and experimental ^{13}C NMR shifts of possible reaction intermediates/products (experimental values recorded in C_6D_6).

| | Calc. ^{13}C NMR shift [ppm] | Exp. ^{13}C NMR shift [ppm] |
|---------------|---------------------------------------|--------------------------------------|
| Styrene | 146.91; 116.47 | 137.36; 113.56 |
| Styrene oxide | 57.17; 56.81 | 52.76; 51.29 |
| Styrene diol | 77.52; 73.16 | 75.34; 68.57 |
| 13 | 17.79; 23.99 | – ^a |
| 14 | 33.51; 0.58 | – |

^a not observed

Table 5.8 summarises the calculated signals possibly observable during the catalysed epoxidation of styrene (the values correspond to the labelled α - and β -carbon atom, respectively). The corresponding signals that were observed experimentally are listed on the right hand side. Figure 5.11 shows the recorded spectra, and it is important to note that the substrate (top) contains some impurities at 29.17 and 15.91 ppm, probably due to ethylbenzene. Addition of the pre-catalyst shows no effect on the ^{13}C NMR spectrum (Figure 5.11, middle), whereas addition of the oxidant leads to several new peaks (Figure 5.11, bottom): on the one hand, signals from TBHP and decane (marked with asterisks) are visible. On the other hand, traces of styrene oxide and styrene diol are observable. The major oxidation product, however, has signals at 87.19 and 65.87 ppm. Although it is not unambiguously identified, it is supposed to be polymerised styrene oxide.

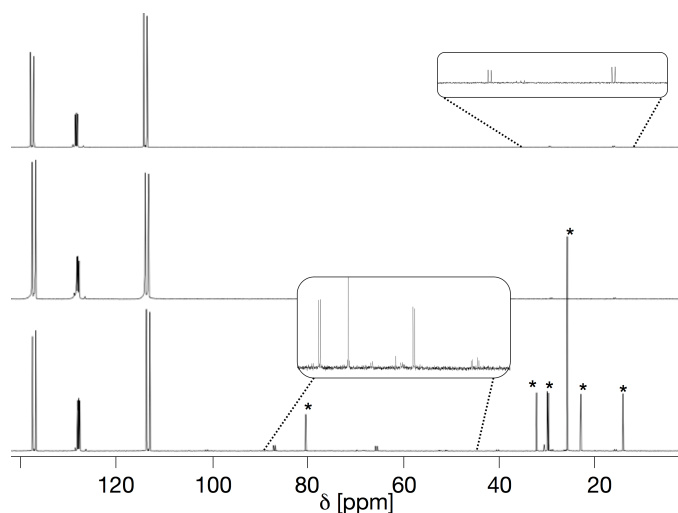


Figure 5.11 ^{13}C NMR spectra of α,β - ^{13}C -labelled styrene in C_6D_6 (top); the same solution after addition of complex **5** (middle); and 30 min after the subsequent addition of TBHP (bottom). Signals marked with an asterisk belong to the decane solution of TBHP.

This experiment corroborates a reaction pathway that does not involve substrate coordination to the molybdenum centre. Thus, a Sharpless-type exogenous oxygen-transfer is happening, in line with the mechanism proposed by Thiel.^{15–17}

5.4 Conclusion

Herein, the kinetics of cyclooctene epoxidation with various molybdenum-based (pre-)catalysts are presented. Cp^* -containing complexes generally show poorer performances than complexes with Cp ligands, possibly due to sterical hindrance. A simple correlation of the ^{95}Mo NMR shift (*i. e.* the electronic shielding of the Mo-core) and the catalytic activity cannot be drawn. Both for the pre-catalysts and the oxo peroxo derivatives, no unambiguous trend is observable, indicating the important influence of the ligand R. On the one hand, there are remarkable differences in the ease of decarbonylation of the tricarbonyl complexes, where the chloro derivative is almost instantaneously oxidised and the fluorinated complex not completely even after one hour, a fact that affects their catalytic performance. On the other hand, investigations of the Mo(VI)-complexes show the impact of the sterical crowding of the ligand R on the catalytic performance. Although the shielding of the molybdenum core increases in the order $\text{Cl} < \text{CH}_3 < \text{CF}_3$, the TOF obtained in the epoxidation of cyclooctene at room temperature with the oxo peroxo complexes decreases in the order $\text{CF}_3 > \text{Cl} > \text{CH}_3$, thus indicating a negative influence of the methyl group.

^{13}C NMR experiments indicate the absence of substrate coordination to the metal core, thus, a mechanistic pathway that proceeds via a Mimoun-type mechanism is ruled out. This is also supported by the mechanistic studies with $[\text{CpMo}(\text{O})_2\text{Cl}]$, where the determination of the rate constants suggests an oxygen-transfer via a σ -bound alkylperoxo group.

5.5 Experimental Section

5.5.1 Materials and methods

All experimental synthetic work was carried out using standard Schlenk techniques under argon. Catalytic reactions were performed under normal laboratory atmosphere. High-resolution NMR spectra were measured with a Bruker Avance DPX-400 (^1H : 400.0 MHz; ^{13}C : 100.6 MHz; ^{19}F : 376.5 MHz; ^{95}Mo : 26.1 MHz) spectrometer, the signals were referenced to the solvent residual signal (^1H ; ^{13}C) or an external standard (^{95}Mo : $\text{Mo}(\text{CO})_6$ in C_6D_6 at -1856 ppm). Mid-IR spectra were recorded on a Varian ATR-FTIR instrument. Far-IR spectra ($700\text{-}40\text{ cm}^{-1}$, 128 scans, resolution 4 cm^{-1}) were recorded with a dedicated Bio-Rad FTS-40 spectrometer equipped with wire-mesh beam splitter, polyethylene-windowed deuterated triglycine sulfate (DTGS) detector, and high-pressure mercury lamp as source. Raman spectra ($50\text{-}4000\text{ cm}^{-1}$, 256 scans, resolution 4 cm^{-1}) were excited with a Spectra-Physics Nd-YAG-laser (1,024 nm) and recorded by means of a dedicated Bio-Rad FT-Raman spectrometer equipped with a liquid N_2 -cooled Ge detector. The laser power at sample position was about 100-200 mW.

5.5.2 Synthesis of the complexes

The organomolybdenum complexes $[\text{Cp}'\text{Mo}(\text{CO})_3\text{R}]$,^{31–34} $[\text{Cp}'\text{Mo}(\text{O})_2\text{R}]$ ²³ and $[\text{Cp}'\text{Mo}(\text{O})_2(\text{O})\text{R}]$ ^{18,29} were synthesised according to literature procedures or adaptations of these procedures. The spectral data listed throughout the text are in agreement with the reported values.

5.5.3 Catalysis studies

In all catalytic reactions, TBHP (5.5M in decane, over 4Å molecular sieves) was used as oxidant and cyclooctene as substrate, unless stated otherwise. The reactions were done at room temperature and initiated by addition of the oxidant. The kinetic data was collected by using ^1H NMR and GC.

(a) The reactions monitored by ^1H NMR were carried out in C_6D_6 in a total volume of 0.4-0.8 mL. The relative amounts of catalyst, substrate and oxidant were chosen with respect to the requirements of the kinetic analysis.

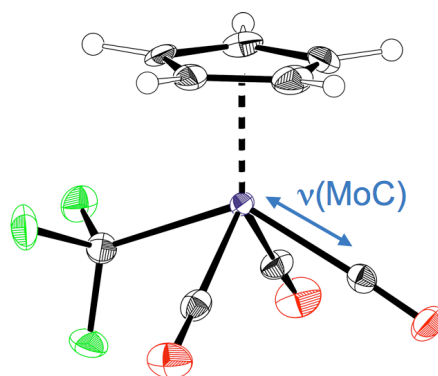
(b) The quantitative GC analysis was performed by taking samples of the reaction mixture at specific time intervals and treating them with MnO_2 to quench excess peroxide. After filtration, the samples were diluted with an isopropanol solution containing the standards p-xylene and indane (4 mg/L). The conversion of cyclooctene and the formation of cyclooctene epoxide were calculated from calibration curves ($r^2 = 0.999$) recorded prior to the reaction course.

5.6 References

1. M. Cousins, M. L. H. Green, *J. Chem. Soc.*, **1963**, 889.
2. R. I. Beattie, P. J. Jones, *Inorg. Chem.*, **1979**, *18*, 2318.
3. W. A. Herrmann, J. G. Kuchler, J. K. Felixberger, E. Herdtweck, W. Wagner, *Angew. Chem.*, **1988**, *100*, 420.
4. W. A. Herrmann, J. G. Kuchler, J. K. Felixberger, E. Herdtweck, W. Wagner, *Angew. Chem. Int. Ed. Engl.*, **1988**, *27*, 394.
5. N. Grover, F. E. Kühn, *Curr. Org. Chem.*, **2012**, *16*, 16.
6. M. Abrantes, A. Sakthivel, C. C. Romão, F. E. Kühn, *J. Organomet. Chem.*, **2006**, *691*, 3137.
7. M. Abrantes, F. A. Almeida Paz, A. A. Valente, C. C. L. Pereira, S. Gago, A. E. Rodrigues, J. Klinowski, M. Pillinger, I. S. Gonçalves, *J. Organomet. Chem.*, **2009**, *694*, 1826.
8. H. Mimoun, I. Sere de Roch, L. Sajus, *Tetrahedron*, **1970**, *26*, 37.
9. K. B. Sharpless, J. M. Townsend, D. R. Williams, *J. Am. Chem. Soc.*, **1972**, *94*, 295.
10. P. Chaumette, H. Mimoun, L. Saussine, J. Fischer, A. Mitschler, *J. Organomet. Chem.*, **1983**, *250*, 291.
11. R. A. Sheldon, *Rec. Trav. Chim. Pays-Bas*, **1973**, *92*, 253.
12. R. A. Sheldon, *Rec. Trav. Chim. Pays-Bas*, **1973**, *92*, 367.
13. A. O. Chong, K. B. Sharpless, *J. Org. Chem.*, **1977**, *42*, 1587.
14. M. B. Trost, R. G. Bergman, *Organometallics*, **1991**, *10*, 1172.
15. W. R. Thiel, T. Priermeier, *Angew. Chem. Int. Ed. Engl.*, **1995**, *34*, 1737.
16. W. R. Thiel, *J. Mol. Cat. A: Chem.*, **1997**, *117*, 449.
17. W. R. Thiel, J. Eppinger, *Chem. Eur. J.*, **2006**, *3*, 696.
18. A. M. Al-Ajlouni, D. Veljanovski, A. Capapé, E. Herdtweck, J. Zhao, M. J. Calhorda, F. E. Kühn, *Organometallics*, **2009**, *28*, 639.
19. A. Comas-Vives, A. Lledós, R. Poli, *Chem. Eur. J.*, **2010**, *16*, 2147.
20. P. J. Costa, M. J. Calhorda, F. E. Kühn, *Organometallics*, **2010**, *29*, 303.
21. J. Morlot, N. Uyttebroeck, D. Agustin, R. Poli, *ChemCatChem*, **2012**, doi: 10.1002/cctc.201200068.
22. F. E. Kühn, A. M. Santos, M. Abrantes, *Chem. Rev. 2006*, *106*, 2455.

23. M. Abrantes, A. M. Santos, J. Mink, F. E. Kühn, C. C. Romão, *Organometallics*, **2003**, 22, 2112.
24. J. Zhao, A. M. Santos, E. Herdtweck, F. E. Kühn, *J. Mol. Catal. A: Chem.*, **2004**, 222, 265.
25. C. Freund, M. Abrantes, F. E. Kühn, *J. Organomet. Chem.*, **2006**, 691, 3718.
26. A. Capapé, A. Raith, F. E. Kühn, *Adv. Synth. Catal.*, **2009**, 351, 66.
27. A. Capapé, A. Raith, E. Herdtweck, M. Cokoja, F. E. Kühn, *Adv. Synth. Catal.*, **2010**, 352, 547.
28. D. Betz, A. Raith, M. Cokoja, F. E. Kühn, *ChemSusChem*, **2010**, 3, 559.
29. D. Chakraborty, M. Bhattacharjee, R. Krätzner, R. Siefken, H. W. Roesky, I. Usón, H.-G. Schmidt, *Organometallics*, **1999**, 18, 106.
30. W. A. Herrmann, R. W. Fischer, W. Scherer, M. U. Rauch, *Angew. Chem. Int. Ed. Engl.*, **1993**, 32, 1157.
31. R. B. King, M. B. Bisnette, *J. Organomet. Chem.*, **1964**, 2, 15.
32. R. B. King, *Organometallic Syntheses (Vol. 1)*, Academic Press, New York, **1965**, pp. 145-147.
33. F. Abugideiri, R. Poli, *Synthetic Methods of Organometallic and Inorganic Chemistry (Vol. 8)*, W. A. Herrmann, Ed., Georg Thieme, Stuttgart, **1997**, pp. 103-104.
34. R. B. King, M. B. Bisnette, *J. Organomet. Chem.*, **1967**, 8, 287.

6 The $[\eta^5\text{-(C}_5\text{H}_5)\text{Mo(CO)}_3\text{R}]$ Compound Class: Similarities and Differences



6.1 Background

Since the unravelling of the uniquely wide catalytic applicability of methyltrioxorhenium, CH_3ReO_3 , it has been argued that its perfluorinated derivative, CF_3ReO_3 might be an even more potent catalyst for a variety of reactions.¹ Despite theoretical predictions concerning the stability of this compound,² it could not be synthesised until today. Furthermore, most other derivatives of CH_3ReO_3 are either unstable or catalytically largely inactive.^{1,3} Nevertheless, the idea of deriving a class of highly active, tailor made molecular catalysts, based on a simple concept is tempting. In contrast to its rhenium congeners, compounds of formula $[\eta^5\text{-(C}_5\text{H}_5\text{)Mo(O}_2\text{)(O)R}]$ are on average more stable and the variation of the group R is more easily achieved.⁴ Some of these compounds are active catalysts for oxidation reactions, matching even CH_3ReO_3 in activity.⁵ The most important drawback in comparison to CH_3ReO_3 , however, is that they do not activate hydrogen peroxide but alkyl hydroperoxides. The latter, although of widespread use both in academia and industry are considered as less environmentally friendly oxidants than hydrogen peroxide since they do not produce water but alcohols as by-products of the oxidation reaction. Nevertheless, the $[\eta^5\text{-(C}_5\text{H}_5\text{)Mo(O}_2\text{)(O)R}]$ derivatives as well as their tricarbonyl precursors may be an interesting case study on whether CF_3 derivatives might be indeed 'better' catalysts than their methyl analogues and whether it might be worthwhile to apply such compounds as catalysts in oxidation reactions.

6.2 Results and Discussion

As a first step, the elucidation of the bonding properties of the tricarbonyl complexes by means of IR and Raman spectrometric measurements is attempted. Both the CO stretching frequencies and the molybdenum-carbon stretching frequencies (of the carbonyl ligand) allow a judgement of the bonding properties in the complexes and make the calculations of the force constants of these bonds possible. The assignment of the frequencies of the title complexes has been partly done before.⁶⁻⁹ A complete overview of the most studied cyclopentadienyl molybdenum tricarbonyl complexes, however, has never been presented. The objective of this investigation is to analyse the force field data, obtained by normal coordinate analysis (NCA) from experiments, and to discuss the frequency assignments and regularities in molecular parameters (bond lengths, force constants) as a function of the ligand R involved. Furthermore, the resolution of the single crystal structure of the fluorinated complex provides an insight in the structural differences, although they were expected to be rather small. As the methyl derivative,¹⁰ it crystallises as racemic twin.

Going from the tricarbonyl pre-catalysts to their oxidised derivatives, another crystal structure is presented. Analogous to $[\text{CpMo(O}_2\text{)(O)CH}_3]$,¹¹ the thermodynamic oxidation product of the fluorinated complex is the oxo peroxy derivative $[\text{CpMo(O}_2\text{)(O)CF}_3]$. The comparison

of the crystal structures of those two complexes reveals interesting insights into the structural features, and a possible explanation of the enhanced performance of the fluorinated Mo(VI)-derivative is given.

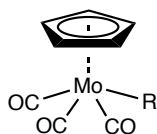


Figure 6.1 Sketch of the investigated molecular organomolybdenum complexes with R = CF₃ (1), CH₃ (2), Cl (3).

6.2.1 Vibrational spectra

Force Field Study

Normal coordinate calculations by means of Wilson's **GF** matrix method were performed to obtain force constants by optimising the vibrational frequencies using a symmetrised valence force field. The PC-based program package developed by Mink and Mink was used for the calculations.¹²

Normal coordinate calculation of the title complexes is not trivial and, therefore, is not carried out routinely (see comments in ref. 13). In order to carry out a 'complete' normal coordinate analysis, we have introduced as point masses the Cp ring, CH₃, CD₃ and CF₃ groups using 'spectroscopic masses' as 77.1,¹³ 16.5, 19.5 and 79¹⁴ atomic mass units for Cp, CH₃, CD₃ and CF₃, respectively.

The molecules belong to C_s point group and the irreducible representation for the simplified structure is 13 A' + 8 A". If we consider the molecules as having planar symmetry (C_s), then all the 21 fundamentals should appear both in the IR and Raman spectra as well. This is in good agreement with our experimental observations (see Table 6.1). Geometrical parameters were taken from Table 6.5, but we use a uniform CO bond length of 1.14 Å.

The starting force fields were adopted from literature: Ref. 6 for CO stretching and ref. 13 for other stretchings and skeletal coordinates. The calculated results were refined to the experimental frequencies of the complexes. Tables 6.2, 6.3 and 6.4 outline the results (calculated fundamental frequencies, potential energy distributions, complete and selected force constants). Due to the strong solid state effect obtained in both in IR and Raman spectra the fundamental frequencies were obtained as averaged frequencies of multiple (generally 2-3 well defined bands or shoulders) features of a certain mode. These fundamental frequencies are listed in Tables 6.2 and 6.4.

The calculated frequencies are found to be in very good agreement with the experimental observations (Table 6.2). The small isotope shifts of CD₃ group are nicely reproduced by the calculation. The Potential Energy Distribution (PED) indicates that the CO stretchings are rather localised modes with small (about 10%) contribution of MoC stretchings. In contrast,

the MoC stretching modes (ν_5 , ν_7 and ν_{16}) are more complex vibrations, exhibiting strong interactions with the MoCO linear bending coordinates.

Comparison of the vibrational spectra and force constants of $[\eta^5\text{-}(\text{C}_5\text{H}_5)\text{Mo}(\text{CO})_3\text{R}]$ complexes

The three title complexes have been chosen for comparison, as all of them are known pre-catalysts for the epoxidation of olefins with TBHP as oxidant.^{10,11,15–17} There are several reports about the infrared spectra of $[\text{CpMo}(\text{CO})_3\text{R}]$ -type complexes,^{6–9} however, to the best of our knowledge, Table 6.1 presents for the first time a comprehensive overview of the IR and Raman frequencies of the above-mentioned complexes, together with the complete assignment of the corresponding vibrational modes in accordance with several reports.^{18–21} Only a simplified force constant calculation (discussing only CO stretching vibrations and force constants) of the four complexes has been published so far.⁶

Whilst the fundamental frequencies of the cyclopentadienyl ligand practically do not depend on the ligand R bound to the metal centre, the CO stretching and Mo-ligand vibrations significantly changes with the R group (see Table 6.1).

For better comparison, we have summarised the characteristic stretching modes of the complexes in Table 6.4. The averaged CO stretching frequencies ($\nu_1 + \nu_2 + \nu_{14}$) are decreasing in the following order $1983 > 1978 \gg 1945 \text{ cm}^{-1}$ for complexes **1**, **3** and **2**, respectively. It is suggested that the coordination of the CO group is very similar in complexes **1** and **3** but different for the CH_3 (**2**) derivative, where the CO group is more strongly bound. Exactly this trend is reflected in the averaged MoC stretching frequencies as well: $485 \gg 462 > 455 \text{ cm}^{-1}$ for complexes **2**, **1** and **3**, respectively. Of course the higher MoC stretching frequency leads to a higher MoC stretching force constant, 3.11 Ncm^{-1} in case of complex **2**, while smaller values of 2.86 and 2.94 Ncm^{-1} were obtained for complexes **1** and **3**, respectively.

By changing R from CH_3 to CF_3 or Cl, the above discussed differences can be explained with the lower electron density on the metal core, inducing a weaker metal-ligand interaction, but strengthening the C=O bond. Comparison of the complex containing a chloro ligand (**3**) reveals important similarities to the bonding in the CF_3 -derivative. In this case, structural properties such as steric crowding seem to be responsible for the different reactivity.

The coordination of the cyclopentadienyl ligand is slightly weaker in the CH_3 -derivative; the force constant is 3.11 Ncm^{-1} referring to the lower stretching frequency, 335 cm^{-1} (Table 6.4). It is reasonable that the CF_3 and Cl ligands change the electron density on the metal and the Mo-Cp interaction becomes stronger.

It is interesting to note that the differences between the stretching force constants $K_1(\text{CO})$ and $K_2(\text{CO})$ are bigger for the complexes **1** and **3** (about 1.5 Ncm^{-1} , Table 6.4), whereas it is only about 0.5 Ncm^{-1} for complex **2**. The CF_3 and Cl ligands possibly exhibit a stronger 'trans influence' to the CO group in the opposite position by weakening its bonding.

Table 6.1 IR and Raman frequencies assigned to the spectroscopic modes of vibration.

| [CpMo(CO) ₃ CF ₃] 1 | | [CpMo(CO) ₃ CH ₃] 2 | | [CpMo(CO) ₃ CD ₃] 2a | | [CpMo(CO) ₃ Cl] 3 | | Assignment |
|--|---------|--|----------|---|----------|--|---------|---|
| IR | Raman | IR | Raman | IR | Raman | IR | Raman | |
| 3126m | 3130m | 3113m | 3123m | 3113m | 3123m | 3132m | 3127m | $\nu_s(\text{CH})$, Cp |
| | 3108w | | 3100w | | 3102w | 3118m | 3111w | $\nu_a(\text{CH})$, Cp |
| | | 2981m | 2982m | 2233m | 2236m | 3103m | | $\nu_a(\text{CH})$, Cp |
| | | 2902m | 2905m | 2116m | 2114m | | | $\nu_a(\text{CH}_3/\text{CD}_3)$ |
| | | 2020w,sh | 2019m | 2018w,sh | 2018m | | | $\nu_s(\text{CH}_3/\text{CD}_3)$ |
| 2060w,sh | 2056m | | | | | | | $\nu_s(\text{C}\equiv\text{O})$ |
| 2048s | 2042s | 2006s | 2003s | 2004s | 2002s | 2040vs | 2041vs | $\nu_s(\text{C}\equiv\text{O})$ |
| 1980w,sh | 1977s | | | 1948w,sh | 1945w,sh | | 1974w | $\nu_a(\text{C}\equiv\text{O})$ |
| 1963s | 1962vs | 1920m,sh | 1921s,sh | 1920m,sh | 1920s,sh | 1969vs | 1960s | $\nu_a(\text{C}\equiv\text{O})$ |
| | | | | | | | 1949vs | $\nu_a(\text{C}\equiv\text{O})$ |
| 1934vs | 1932s | 1903vs | 1900vs | 1901vs | 1889vs | 1932vs | 1930m | $\nu_a(\text{C}\equiv\text{O})$ |
| 1916m,sh | | | | | | 1924s,sh | | $\nu_a(\text{C}\equiv\text{O})$ |
| 1430m | 1427m | 1423m | 1425m | 1423m | 1421m,b | 1421m | 1422vw | $\nu_a(\text{CC})$, Cp |
| | | 1423m | 1420m | 1062m | 1061m | | | $\delta_a(\text{CH}_3/\text{CD}_3)$ |
| | 1356w | 1354w | 1352w | 1353w | 1352w | 1354w | 1355vw | $\nu_a(\text{CC})$, Cp |
| | | 1161m | 1161m | 883m | 881s | | | $\delta_s(\text{CH}_3/\text{CD}_3)$ |
| 1113vw | 1109s | 1109vw | 1107s | 1109vw | 1107s | 1110vw | 1109s | $\nu_s(\text{CC})$, Cp |
| | 1069m | 1060m | 1061m | 1062m | 1061m | 1064m | 1061m | $\beta(\text{CH})$, Cp |
| 1050s | 1057m | | | | | | | $\nu_a(\text{CF}_3)$ |
| 1043s | | | | | | | | $\nu_a(\text{CF}_3)$ |
| 1012s | | 1011m | 1011vw | 1012m | 1009vw | 1014m | | $\beta(\text{CH})$, Cp |
| 1004s | 1005vw | | | | 1003vw | 1005m | 1007vw | $\beta(\text{CH})$, Cp |
| 982s | 978vw | | | | | | | $\nu_s(\text{CF}_3)$ |
| 831m | 827m | 825s | 822vw | 822s | 821vw | 822s | 816vw | $\gamma(\text{CH})$, Cp |
| 695m | 692m | | | | | | | $\delta_s(\text{CF}_3)$ |
| | | 613w | 608vw | 488vs | | | | $\rho(\text{CH}_3/\text{CD}_3)$ |
| | | | | 475s | 475s | | | $\rho(\text{CH}_3/\text{CD}_3)$ |
| 613w | | 613w | 608vw | 614w,sh | | 601w | ~600vw | $\delta_s(\text{MoCO})$ |
| 573s | 571w | 587s | 584vw | 597s | 596w | 561s | 560vw | $\delta_s(\text{MoCO})$ |
| 546vs | 544w | 562vs | 562m | 561vs | 563vw | 524s | ~520vw | $\beta_a(\text{MoCO})$ |
| | | 755w | 758vw | 548s,sh | 549vw | | | $\rho(\text{CH}_3/\text{CD}_3)$ |
| 525w | 521w | | | | | | | $\delta_a(\text{CF}_3)$ |
| 512w | | | | | | | | $\delta_a(\text{CF}_3)$ |
| 479s | 477w | 502w,sh | | 498m,sh | 498w,sh | 471s | 464w | $\nu_s(\text{MoC})$ |
| 479s | 477w | 489vs | 482m | 488vs | 490w,sh | 471s | 464w | $\gamma_a(\text{MoCO})$ |
| 455ms | 458ms | 465w,sh | | 463w,sh | 476ms | | | $\beta_a(\text{MoCO})$ |
| | | | | | | 432w | 428vw | $\beta_a(\text{MoCO})$ |
| 430vs | 432m | 451s | 453m | 448s | 451s | 432w | 428vw | $\nu_a(\text{MoC})$ |
| 404m | 402m | 437m | 438vs | 429ms | 429s | 415m | 420vw | $\gamma(\text{MoCO})$, |
| | | 405w | 408ms | 392m | 391m | | | $\nu(\text{MoC})$, CH_3/CD_3 |
| | | | | | | | 383w,sh | $\nu_a(\text{MoCp})$, tilt |
| 366w | 361w,sh | 355w | 355s | 353m | 352vs | | 371m | $\nu_a(\text{MoCp})$, tilt |
| | | 336w | 334vs | 334w | 333vs | 361s ^a | 350w,sh | $\nu_s(\text{MoCp})$ |
| 352vw | 350vs | | | | | 337vw ^a | 338ms | $\nu_s(\text{MoCp})$ |
| | | | | | | 281vs ^a | 278w | $\nu(\text{MoCl})$ |

continued on next page

Table 6.1 continued

| [CpMo(CO) ₃ CF ₃] | | [CpMo(CO) ₃ CH ₃] | | [CpMo(CO) ₃ CD ₃] | | [CpMo(CO) ₃ Cl] | | Assignment |
|--|--------|--|--------|--|---------|----------------------------|-------|---------------------------------|
| 1 | | 2 | | 2a | | 3 | | |
| IR | Raman | IR | Raman | IR | Raman | IR | Raman | |
| 251s | 249s | | | | | | | $\nu(\text{MoC}), \text{CF}_3$ |
| 234m | 233m | | | | | | | $\rho(\text{CF}_3)$ |
| | | | 173s | 125vw,sh | 160s | | | $\tau(\text{CH}_3/\text{CD}_3)$ |
| | | | 160m | | 148m | | | $\tau(\text{CH}_3/\text{CD}_3)$ |
| 137w | 137w,m | 130w,sh | 133w | | 130w,sh | | | $\delta(\text{CpMoR})$ |
| 119w | 119w | 107w | | 104w | | | | $\delta_s(\text{CMoC})$ |
| 106vw | | | | | | | | $\delta_s(\text{CMoC})$ |
| | | | 90w,sh | | 90w,sh | | | $\delta_a(\text{CMoC})$ |
| 60vw | | 60vw | | | | | | $\delta(\text{CMoCp})$ |

^a Far-infrared data taken from reference 20

^b Notation of fundamental modes: ν – stretching; δ – bending or deformation; ρ – rocking; β – in plane, γ – out of plane deformation; τ – torsion; subscript 's' symmetric, subscript 'a' anti-symmetric.

Table 6.3 Calculated force constants for [CpMo(CO)₃CH₃] and [CpMo(CO)₃CD₃].

| Force constants | Groups involved and descriptions | Numerical values of force constants | Units |
|-------------------------|--|-------------------------------------|-------|
| K ₁ (C'O) | C'O opposite to CH ₃ /CD ₃ | 13.969 | a |
| K ₂ (CO) | CO close to CH ₃ /CD ₃ | 14.396 | a |
| F _s (CO,CO) | Interaction between CO, CO groups | 0.555 | a |
| F _l (C'O,CO) | Interaction between C'O, CO groups | 0.278 | a |
| K(MoC) | Mo-CO | 3.108 | a |
| F(MoC,MoC) | Mo-CO | 0.011 | a |
| K(Mo-Me) | Mo-CH ₃ , Mo-CD ₃ | 1.527 | a |
| K(Mo-Cp) | Mo-Cp | 3.110 | a |
| H(MoCO) | MoCO linear bending (in plane) | 0.865 | b |
| h(MoCO,MoCO) | MoCO, MoCO interaction | 0.008 | b |
| H'(MoCO) | MoCO linear bending (out of plane) | 0.534 | b |
| h'(MoCO,MoCO) | MoCO, MoCO interaction | 0 | b |
| H(CMoMe) | skeletal bending | (0.55) ^c | b |
| H(CMoC) | skeletal bending | (0.62) | b |
| H(CMoCp) | skeletal bending | (0.48) | b |
| H(CpMoMe) | skeletal bending | (0.50) | b |
| F(MoMe,MoC') | stretch-stretch interaction | (0.10) | a |
| F(MoMe,MoC) | stretch-stretch interaction | (0.05) | a |

Remarks:

Units of force constants are: a, 10² Nm⁻¹; b, 10⁻¹⁸ Nmrad⁻²;

^c The constrained values are listed in brackets.

Table 6.2 Experimental and calculated fundamental frequencies for [CpMo(CO)₃CH₃] and [CpMo(CO)₃CD₃].

| | [CpMo(CO) ₃ CH ₃] | | [CpMo(CO) ₃ CD ₃] | | Potential Energy Distribution ^d (%) | Description of mode |
|-------------------|--|--------|--|--------|--|-----------------------------------|
| | Exper. ^a | Calcd. | Exper. | Calcd. | | |
| A ₁ ' | 2012 | 2010 | 2010 | 2004 | 83 ν_s CO + 10 ν_s MoC | CO sym. stretching |
| 2 | 1903 | 1890 | 1900 | 1890 | 81 ν_a CO + 11 ν_a MoC | CO asym. stretching |
| 3 | 598 | 592 | 602 | 592 | 55 β_s MoCO + 25 β_a MoCO ^c + 8 δ_s CMoC | MoCO bending |
| 4 | 562 | 562 | 562 | 562 | 61 β_a MoCO + 21 β_s MoCO + ν_s MoC | MoCO bending |
| 5 | 502 | 503 | 498 | 503 | 47 ν_s MoC + 14 γ_a MoCO + 13 ν_a MoC | MoC stretching |
| 6 | 485 | 484 | 489 | 484 | 48 γ_a MoCO + 15 ν_s MoC + 10 ν MoCp | MoCO bending |
| 7 | 452 | 450 | 450 | 447 | 53 ν_a MoC + 22 γ_a MoCO + 12 ν MoCp | MoC stretching |
| 8 | 406 | 408 | 392 | 388 | 70 ν Mo-Me + 17 ν_a MoC + 9 ν_s MoC | Mo-Me stretching |
| 9 | 335 | 335 | 333 | 333 | 83 ν MoCp + 10 ν_s MoC + 5 ν Mo-Me | Mo-Cp stretching |
| 10 | 131 ^b | 145 | 130 | 139 | 61 δ_s CpMoMe + 13 δ CMoCp + 10 β MoCO | CpMoMe deformation |
| 11 | 107 | 110 | 104 | 108 | 43 δ_s MoC ₃ + 32 δ CMoCp | MoC ₃ sym. deformation |
| 12 | 90 | 99 | 90 | 99 | 41 δ_a CMoC + 32 δ_a CMoCp + 16 δ CpMoMe | CMoC deformation |
| 13 | 60 | 66 | 60 | 66 | 57 δ CMoCp + 26 δ CpMoMe | CMoCp deformation |
| A ₁₄ ' | 1920 | 1911 | 1907 | 1900 | 92 ν_a CO + 8 ν_a MoC | CO asym. stretching |
| 15 | 562 | 560 | 562 | 560 | 87 β_a MoCO + 6 δ_a CMoCp | MoCO deformation |
| 16 | 502 | 508 | 498 | 508 | 72 ν_a MoC + 11 γ_a MoCO + 6 ν_a CO | MoC stretching |
| 17 | 465 | 463 | 470 | 463 | 61 γ_a MoCO + 19 δ_a CMoC + 9 δ_s MoCO | MoCO deformation |
| 18 | 438 | 432 | 429 | 432 | 85 γ_a MoCO + 5 ν_a CO + 4 δ_a CMoC | MoCO deformation |
| 19 | 130 | 144 | 130 | 136 | δ_a CMoMe + 43 δ_a CMoC | CMoMe deformation |
| 20 | - | 120 | 120 | 120 | 91 δ CMoCp + 5 β_a MoCO | CMoCp deformation |
| 21 | 107 | 104 | 90 | 104 | 76 δ_a CMoC + 21 γ_a MoCO | CMoC deformation |

^a Averaged IR and Raman frequencies were used as fundamentals when the wavenumbers were slightly different or split due to the solid state effects.

^b Experimental frequencies below 150 cm⁻¹ were assigned on the basis of normal coordinate calculations.

^c The β (MoCO) are the linear bendings of Mo-C-O groups in the plane of CMoCp, the notation of γ (MoCO) requests the linear bendings perpendicular to the plane of CMoCp.

^d Potential Energy Distributions (PED) were taken from the result of [CpMo(CO)₃CH₃] calculations.

If we consider that the MoC stretching force constant value, 3.11 Ncm^{-1} refers to the averaged bond distance of 1.991 \AA for complex **2**, and that the averaged bond distance for complex **1**, 2.006 \AA , corresponds to a value of 2.86 Ncm^{-1} of the force constant, then the MoC bond length of complex **3** can be estimated around 2.001 \AA by a linear approximation of the bond force constant versus the inverse of the square of the bond length, *i.e.* within the error range of the averaged experimental bond distance (see Table 6.5).

Values of Cotton-Kraihanzel CO stretching force constants, K_1 and K_2 ²¹ have been estimated from the CO stretching frequencies.⁶ The two force constants for $[\text{CpMo}(\text{CO})_3\text{CH}_3]$ were 15.49 and 16.45 Ncm^{-1} , which are about 10% higher than our result from the full calculation. For the other two complexes the extent of force constant overestimation varies between 7 and 12%. Therefore, it can be concluded that the C.-K. method strongly overestimates the CO stretching force constants for this type of tricarbonyl complexes.

Table 6.4 Comparison of characteristic stretching frequencies (cm^{-1}) and bond stretching force constants (Ncm^{-1}) of the tricarbonyl complexes.

| Frequencies | $[\text{CpMo}(\text{CO})_3\text{CF}_3]$ 1 | $[\text{CpMo}(\text{CO})_3\text{CH}_3]$ 2 | $[\text{CpMo}(\text{CO})_3\text{Cl}]$ 3 | Description |
|---------------------------------------|---|---|---|-------------------|
| ν_1, A' | 2052 ^a | 2112 | 2041 | CO sym. stretch |
| ν_{14}, A'' | 1971 | 1920 | 1963 | CO asym. stretch |
| ν_2, A' | 1927 | 1903 | 1929 | CO asym. stretch |
| ν_5, A' | 478 | 502 | 468 | MoC sym. stretch |
| ν_{16}, A'' | 478 | 502 | 468 | MoC asym. stretch |
| ν_7, A' | 431 | 452 | 430 | MoC asym. stretch |
| ν_8, A' | 250 | 406 | 280 | MoR stretch |
| ν_9, A' | 351 | 335 | 355 | MoCp stretch |
| Forces constants | | | | |
| $K_1(\text{CO})^b$ | 14.01 | 13.97 | 14.05 | |
| $K_2(\text{CO})$ | 15.38 | 14.40 | 15.30 | |
| $F_s(\text{CO}, \text{CO})^c$ | 0.59 | 0.56 | 0.62 | |
| $F_l(\text{C}'\text{O}, \text{CO})^d$ | 0.29 | 0.28 | 0.31 | |
| $K(\text{MoC})$ | 2.86 | 3.11 | 2.94 | |
| $K(\text{Mo-R})$ | 1.88 | 1.53 | 1.28 | |
| $K(\text{Mo-Cp})$ | 3.18 | 3.11 | 3.16 | |

^a All fundamental vibrational frequencies are averaged values of experimental data listed in Table 6.1. For numbering of frequencies see Table 6.2;

^b Carbonyl ligand opposite to R group;

^c Stretch-stretch interaction between two CO groups in 'short' distance;

^d Stretch-stretch interaction between two CO groups in 'long' distance.

6.2.2 Molecular structures

Comparison of the crystal structures of the complexes of type $[\eta^5\text{-}(\text{C}_5\text{H}_5)\text{Mo}(\text{CO})_3\text{R}]$

The crystal structure of the fluorinated molybdenum tricarbonyl derivative was unveiled from single-crystal X-ray diffraction studies (Figure 6.2). As its non-fluorinated methyl analogue, it crystallises as racemic twin.

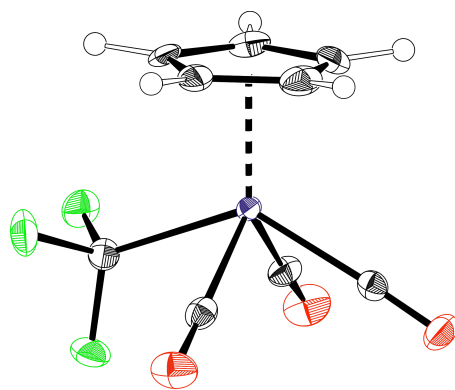


Figure 6.2 Ortep drawing of the solid-state structure of $[\text{CpMo}(\text{CO})_3\text{CF}_3]$. The thermal ellipsoids are shown at the 50% probability level.

The comparison of the bond lengths in the three title compounds (listed in Table 6.5) reveals interesting features. The atom numbering has been re-done for the Cl and CH_3 derivatives according to Figure 6.3, in order to provide a consistent basis.

It can be noted that the length of the molybdenum-carbon bonds (of the carbonyl ligands, C1-C3) are longest for complex **1**. The Mo-C2 bond, being opposite to the R group, shows a *,trans effect'*, however, no clear trend can be defined: it is elongated by 0.012 Å compared to the *cis*-carbonyls in complex **1**, whilst in complex **3**, this bond is shorter than the adjacent ones. Further, the carbon-oxygen bonds show varying lengths, again with some *,trans effect'*: a considerable elongation is apparent in complex **3**, and in complex **1**, it is shortened. In complex **2**, however, no similar tendency can be observed. The study of the Mo-C-O bond angles shows only small differences between the three complexes, with complex **3** having the most bent carbonyls (*i.e.* the angles deviate the most from 180°). Comparison of complex **1** to complex **2** reveals that in the latter, the angles between the carbonyls and the methyl group are smaller than the angles between the carbonyl ligands, whereas in complex **1**, all angles between the three carbonyls and the CF_3 group are nearly constant.

Table 6.5 Comparison of selected bond lengths (Å) and angles (degrees) of the tricarbonyl complexes (the atom annotation is done as shown in Figure 6.3).

| | [CpMo(CO) ₃ CF ₃] 1 | [CpMo(CO) ₃ CH ₃] ¹⁰ 2 | [CpMo(CO) ₃ Cl] ²² 3 |
|--------------------|--|--|--|
| <i>Bond length</i> | | | |
| Mo-C1 | 2.003(3) | 1.984(4) | 2.014(2) |
| Mo-C2 | 2.015(3) | 1.997(4) | 1.980(2) |
| Mo-C3 | 2.001(3) | 1.993(4) | 2.008(2) |
| Mo-R | 2.234(3) | 2.326(3) | 2.503(6) |
| C1-O1 | 1.145(4) | 1.144(4) | 1.138(3) |
| C2-O2 | 1.137(3) | 1.139(5) | 1.145(3) |
| C3-O3 | 1.143(3) | 1.131(4) | 1.136(3) |
| <i>Bond angle</i> | | | |
| C1-Mo-C2 | 76.80(11) | 78.09(17) | 78.15(10) |
| C2-Mo-C3 | 76.11(11) | 78.87(15) | 75.80(10) |
| R-Mo-C1 | 76.45(10) | 72.39(13) | 78.15(7) |
| R-Mo-C3 | 75.99(10) | 72.41(17) | 77.86(7) |
| Mo-C1-O1 | 176.9(2) | 178.9(4) | 176.8(2) |
| Mo-C2-O2 | 177.6(2) | 178.9(4) | 177.9(2) |
| Mo-C3-O3 | 178.4(2) | 177.0(3) | 177.9(2) |

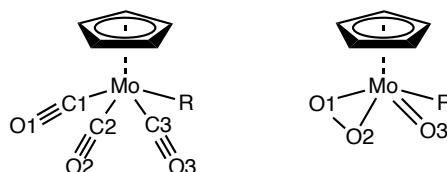


Figure 6.3 Drawings of the tricarbonyl (left) and oxo peroxo (right) complexes (R = CF₃, CH₃, Cl) with the atom numbering used in Tables 6.5 and 6.6.

Comparison of the crystal structures of [CpMo(O₂)(O)CF₃] and [CpMo(O₂)(O)CH₃]

By treatment of the tricarbonyl complexes with excess TBHP, the carbonyl ligands are displaced by, in case of R = CH₃, CF₃, an oxo and a η²-peroxo group. The solid state structure of [CpMo(O₂)(O)CH₃] being known for some time,¹¹ it has now been possible to isolate and crystallise its fluorinated counterpart (see Figure 6.4). Therefore, we attempted to draw some explanations from the comparison of the bond lengths and angles of the two complexes, summarised in Table 6.6. In fact, catalysis experiments performed with cyclooctene as substrate and TBHP as oxidant at room temperature revealed the higher activity of the fluorinated oxo peroxo complex (see Chapter 4).

It is noteworthy that the Mo-oxo bond is shorter in the fluorinated complex than in the methyl-containing derivative, and that the inverse situation exists for the two bonds through which the peroxo group is connected to the molybdenum centre. Apparently, the enhanced Lewis acidity of the Mo-core of the CF₃ derivative causes a elongation of the Mo-peroxo bonds, that can thus be broken more easily to form the catalytically active species in presence of excess oxidant. Furthermore, the bond angles between the oxygen atoms are substantially larger in

[CpMo(O₂)(O)CF₃], probably facilitating the coordination of the organic peroxide and consequently enabling a better catalytic performance.

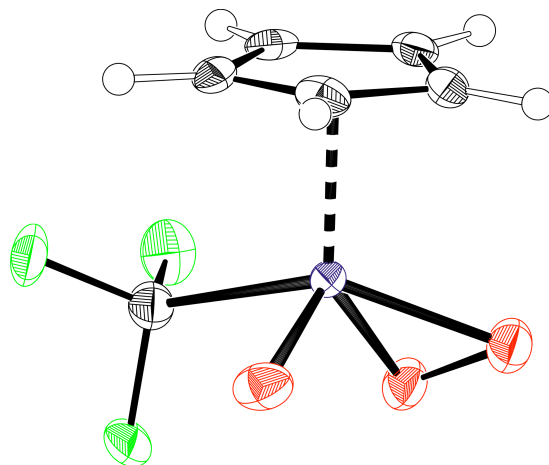


Figure 6.4 Ortep drawing of the solid-state structure of [CpMo(O₂)(O)CF₃]. The thermal ellipsoids are shown at the 50% probability level.

Table 6.6 Comparison of selected bond lengths (Å) and angles (degrees) of two oxo peroxy derivatives (the atom annotation is done as shown in Figure 6.3).

| | [CpMo(O ₂)(O)CF ₃] | [CpMo(O ₂)(O)CH ₃] ^{II} |
|--------------------|--|--|
| <i>Bond length</i> | | |
| Mo-O1 | 1.922(2) | 1.840(9) |
| Mo-O2 | 1.933(2) | 1.857(7) |
| Mo-O3 | 1.689(2) | 1.728(6) |
| O1-O2 | 1.440(3) | 1.271(14) |
| Mo-R | 2.197(3) | 2.168(7) |
| <i>Bond angle</i> | | |
| O1-Mo-O2 | 43.88(9) | 40.2(4) |
| O2-Mo-O3 | 108.15(10) | 104.9(4) |
| R-Mo-O1 | 76.86(10) | 80.2(4) |
| R-Mo-O3 | 93.85(12) | 97.4(3) |

6.3 Conclusion

Although the slow reactivity of [CpMo(CO)₃CF₃] with TBHP has not been fully explained, this study allowed the complete assignment of the frequencies of the title complexes. The determination of the force fields, obtained by NCA from the experimental spectra was successfully carried out and permitted a profound discussion of the frequency assignments and regularities in molecular parameters (bond lengths, force constants) as a function of the ligand R involved. Additionally, the resolution of the single crystal structure of the fluorinated tricarbonyl complex provided an insight in the structural differences compared to the other studied complexes, and suggested small sterical factors that influence the different reactivity.

The same counts for the oxidised complexes $[\text{CpMo}(\text{O}_2)(\text{O})\text{CF}_3]$ and $[\text{CpMo}(\text{O}_2)(\text{O})\text{CH}_3]$: the better performance in olefin epoxidation of the former, fluorinated complex is, on the one hand, due to the enhanced Lewis acidity of the metal centre, and, on the other hand, due to the slight differences in geometry. Comparison of the crystal structures indicates an elongation of the Mo-O bonds of the peroxo ligand in $[\text{CpMo}(\text{O}_2)(\text{O})\text{CF}_3]$, thus facilitating the breaking of one of the two bonds to form the catalytically active species in presence of excess oxidant.

6.4 Experimental Section

The tricarbonyl complexes $[\text{CpMo}(\text{CO})_3\text{R}]$ were synthesised according to published procedures ($\text{R} = \text{CF}_3$,⁷ CH_3/CD_3 ,²³ Cl^{24}).

Mid-IR ($350\text{-}4000\text{ cm}^{-1}$, 32 scans, resolution 4 cm^{-1}) absorption spectra were recorded in an N_2 purged atmosphere using dynamically aligned Varian Scimitar-2000, and Varian IR-670 spectrometers. Far-IR spectra ($700\text{-}40\text{ cm}^{-1}$, 128 scans, resolution 4 cm^{-1}) were recorded with a dedicated Bio-Rad FTS-40 spectrometer equipped with wire-mesh beam splitter, polyethylene-windowed deuterated triglycine sulfate (DTGS) detector, and high-pressure mercury lamp as source.

IR spectra were recorded with a Golden Gate or GladiATR micro attenuated total reflectance (ATR) accessory equipped with a diamond ATR element. Some of the far-IR spectra were obtained also with a GladiATR attachment or in transmittance mode in polyethylene pellet. Raman spectra ($50\text{-}4000\text{ cm}^{-1}$, 256 scans, resolution 4 cm^{-1}) were excited with a Spectra-Physics Nd-YAG-laser (1,024 nm) and recorded by means of a dedicated Bio-Rad FT-Raman spectrometer equipped with a liquid N_2 -cooled Ge detector. The laser power at sample position was about 100-200 mW.

Single crystals of $[\text{CpMo}(\text{CO})_3\text{CF}_3]$ suitable for XRD-analysis were obtained by slow sublimation in vacuum (10^{-3} mbar) at $60\text{ }^\circ\text{C}$; single crystals of $[\text{CpMo}(\text{O}_2)(\text{O})\text{CF}_3]$ were grown from a diethyl ether solution with slow hexane diffusion at $-30\text{ }^\circ\text{C}$.

Single-crystal X-ray structure determinations

$[\text{CpMo}(\text{CO})_3\text{CF}_3]$: yellow needle, $\text{C}_9\text{H}_5\text{F}_3\text{MoO}_3$, $M_r = 314.07$, preliminary structural data (bond lengths and angles) were retrieved from the crystal coordinate file (.res).

$[\text{CpMo}(\text{O}_2)(\text{O})\text{CF}_3]$: yellow fragment, $\text{C}_6\text{H}_5\text{F}_3\text{MoO}_3$, $M_r = 278.04$, monoclinic, space group $C2/c$ (No. 15), $a = 20.5911(3)\text{ \AA}$, $b = 6.9325(1)\text{ \AA}$, $c = 12.3919(2)\text{ \AA}$, $\beta = 117.372(1)^\circ$, $V = 1570.87(4)\text{ \AA}^3$, $Z = 8$, $\lambda(\text{Mo K}\alpha) = 0.71073\text{ \AA}$, $\mu = 1.693\text{ mm}^{-1}$, $\rho_{\text{calc}} = 2.351\text{ g cm}^{-3}$, $T = 123(1)\text{ K}$, $F(000) = 1072$, $\Theta_{\text{max}} = 25.4^\circ$, $R1 = 0.0194$ (1266 observed data), $wR2 = 0.0448$ (all 1266 data), $\text{GOF} = 1.04$, 118 parameters, $\Delta\rho_{\text{max/min}} = 0.60/-0.30\text{ e \AA}^{-3}$.

6.5 References

1. (a) W. A. Herrmann, F. E. Kühn, *Acc. Chem. Res.*, **1997**, *30*, 169; (b) C. C. Romão, F. E. Kühn, W. A. Herrmann, *Chem. Rev.*, **1997**, *97*, 3197.
2. (a) R. Wiest, T. Leiniger, G.-H. Jeung, M. Bénard, *J. Phys. Chem.*, **1992**, *96*, 10800; (b) C. Mealli, J. A. López, M. J. Calhorda, C. C. Romão, W. A. Herrmann, *Inorg. Chem.*, **1994**, *33*, 1139; (c) S. Köstlmeier, O. D. Häberlen, N. Rösch, W. A. Herrmann, B. Solouki, H. Bock, *Organometallics*, **1996**, *15*, 1872; (d) M. Lein, A. Hammerl, H. L. Hermann, P. Schwerdtfeger, *Polyhedron*, **2007**, *26*, 486.
3. (a) M. Högerl, F. E. Kühn, *Z. Anorg. Allg. Chem.*, **2008**, *634*, 1444; (b) S. Huber, M. Cokoja, M. Drees, J. Mink, W. A. Herrmann, F. E. Kühn, *Cat. Sci. Technol.*, **2012**, 1353.
4. (a) F. E. Kühn, A. M. Santos, M. Abrantes, *Chem. Rev.*, **2006**, *106*, 2455; (b) N. Grover, F. E. Kühn, *Curr. Org. Chem.*, **2012**, *16*, 16.
5. (a) D. Betz, A. Raith, M. Cokoja, F. E. Kühn, *ChemSusChem*, **2010**, *3*, 559; (b) P. Altmann, M. Cokoja, F. E. Kühn, *Eur. J. Inorg. Chem.*, **2012**, 3235.
6. R. B. King, L. W. Houk, *Can. J. Chem.*, **1969**, *47*, 2959.
7. R. B. King, M. B. Bisnette, *J. Organomet. Chem.*, **1964**, *2*, 15.
8. D. J. Parker, M. H. B. Stiddard, *J. Chem. Soc. (A)*, **1970**, 480.
9. D. J. Parker, *J. Chem. Soc. (A)*, **1970**, 1382.
10. M. Abrantes, P. Neves, M. M. Antunes, S. Gago, F. A. A. Paz, A. E. Rodrigues, M. Pillinger, I. S. Gonçalves, C. M. Silva, A. A. Valente, *J. Mol. Catal. A: Chem.*, **2010**, *320*, 19.
11. A. M. Al-Ajlouni, D. Veljanovski, A. Capapé, E. Herdtweck, J. Zhao, M. J. Calhorda, F. E. Kühn, *Organometallics*, **2009**, *28*, 639.
12. J. Mink, L. Mink, Computer program system for vibrational analysis of polyatomic molecules (in Lahey-Fujitsu Fortran Win32), Stockholm (**2004**). Available from J. Mink, e-mail: jmink@chemres.hu
13. E. Bencze, B. V. Lokshin, J. Mink, W. A. Herrmann, F. E. Kühn, *J. Organomet. Chem.*, **2001**, *627*, 55.
14. L. Hajba, J. Mink, F. E. Kühn, I. S. Gonçalves, *Inorg. Chim. Acta.*, **2006**, *359*, 4741.
15. J. Zhao, A. M. Santos, E. Herdtweck, F. E. Kühn, *J. Mol. Catal. A: Chem.*, **2004**, *222*, 265.
16. A. A. Valente, J. D. Seixas, I. S. Gonçalves, M. Abrantes, M. Pillinger, C. C. Romão, *Catal. Lett.*, **2005**, *101*, 127.
17. C. Freund, M. Abrantes, F. E. Kühn, *J. Organomet. Chem.*, **2006**, *691*, 3718.

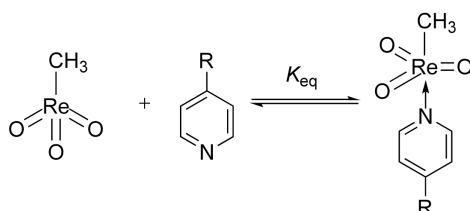
18. K. Nakamoto, *Infrared and Raman Spectra of Inorganic and Coordination Compounds-Part B*, fifth ed., Wiley, New York, **1997**.
19. E. Bencze, J. Mink, C. Németh, W. A. Herrmann, B. V. Lokshin, F. E. Kühn, *J. Organomet. Chem.*, **2002**, *642*, 246.
20. M. Abrantes, A. M. Santos, J. Mink, F. E. Kühn, C. C. Romão, *Organometallics*, **2003**, *22*, 2112.
21. F. A. Cotton, C. S. Kraihanzel, *J. Am. Chem. Soc.*, **1962**, *84*, 4432.
22. A. O. Ogweno, M. O. Onani, *Acta Cryst.*, **2012**, *E68*, 364.
23. R. B. King, *Organometallic Syntheses (Vol. 1)*, Academic Press, New York, **1965**, pp. 145.
24. F. Abugideiri, R. Poli, *Synthetic Methods of Organometallic and Inorganic Chemistry (Vol. 8)*, W. A. Herrmann, Ed., Georg Thieme, Stuttgart, **1997**, pp. 103.

7 Summary

Catalytic epoxidation of olefins, particularly in homogeneous phase, are among the best studied reactions in molecular transition metal catalysis. This thesis aimed at the experimental investigation of two catalytic transition-metal systems, namely organorhenium and organomolybdenum complexes.

7.1 Methyltrioxorhenium

A series of chromophoric Lewis base adducts of methyltrioxorhenium (MTO) was synthesised and fully characterised by UV-Vis, IR and NMR spectroscopy, single crystal X-ray diffraction and elemental analysis (Scheme 7.1). The ligands were pyridine derivatives with different sizes of the aromatic system and variable substituents, thus providing a variation of electronic and steric parameters. The investigation of these novel compounds included the determination of their stability constants in dichloromethane by means of UV-Vis spectroscopy. Furthermore, the influence of the N-donor ligands coordinated to MTO on the catalytic activity of epoxidation of 1-octene was studied. Each compound was tested twice; in a catalytic reaction under exclusion of light and in daylight. No significant differences in catalytic performance were found. Finally, the behaviour of the complexes under irradiation with UV-light was investigated by means of ^{17}O NMR and UV-Vis spectroscopy.



Scheme 7.1 Adduct formation of MTO with pyridine derivatives in solution (K_{eq} = stability constant).

The herein presented experiments aimed for probing potential beneficial effects of chromophoric N-donor ligands in MTO adducts, as they might activate the catalytic system by providing additional energy for weakening bonds that have to be broken during the catalytic cycle. With respect to the benchmark ligand *tert*-butylpyridine, however, the presented ligands do not show any advantages in the epoxidation of 1-octene, whether performed under exclusion of light or in daylight. Moreover, the chromophoric ligands do not influence the stability of the adducts under UV irradiation. Complex decomposition occurs through the reported pathway, as formation of the perrhenate anion was already observable after a short irradiation time with UV-light.

7.2 Molybdenum complexes

Monomeric organomolybdenum carbonyl complexes of the general formula $[\eta^5\text{-(C}_5\text{R}_5\text{)Mo(CO)}_3\text{X}]$ (R = H, CH₃, CH₂Ph; X = alkyl, halide) are known pre-catalysts to be applied in olefin epoxidation (Figure 7.1).

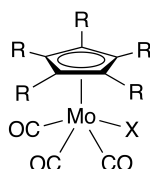
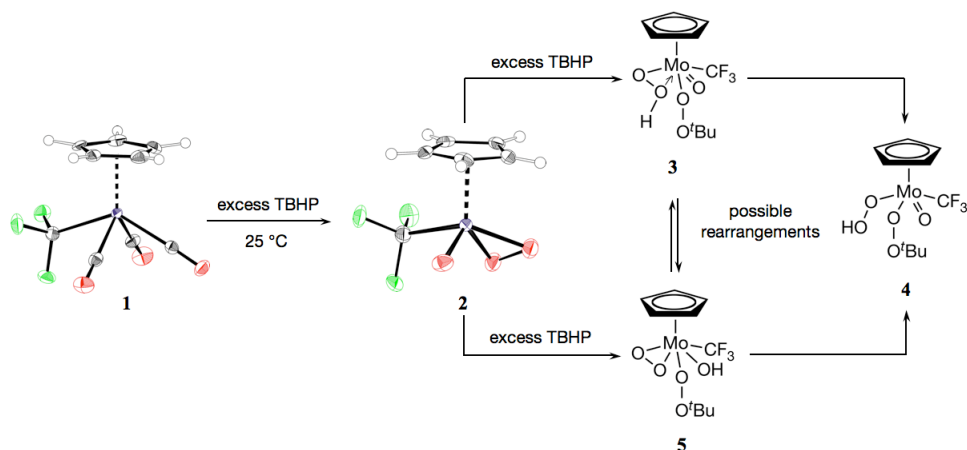


Figure 7.1 Drawing of the monomeric organomolybdenum complex with R = H, CH₃, CH₂Ph and X = alkyl, halide.

In this work, the application of a fluorinated complex, [CpMo(CO)₃CF₃] (Cp = η⁵-C₅H₅), is reported. With benzene as the solvent, the performance of [CpMo(CO)₃CF₃] in the catalytic epoxidation of cyclooctene does not surpass the performances of known analogous complexes (R = CH₃, Cl) in homogeneous epoxidation of cyclooctene. However, in a reaction medium that activates the oxidant, such as hexafluoroisopropanol, the activity of the fluorinated catalyst outperforms [CpMo(CO)₃CH₃]; in fact, a TOF of > 6300 h⁻¹ was achieved in the epoxidation of cyclooctene. Taking into account that the herein reported catalytic reactions were all performed at room temperature, this represents the highest TOF for pre-catalysts of the general formula [CpMo(CO)₃X] (X = alkyl, halide). So far, only the *ansa* compounds [Mo(η⁵-C₅H₄(CH(CH₂)_n)-η¹-CH)(CO)₃] show better performances in catalytic epoxidation of cyclooctene at room temperature. [CpMo(CO)₃CF₃] was also applied in 2-phase catalytic epoxidation reactions. The high stability of the oxidised species allows catalyst recycling for multiple catalytic runs without significant loss of activity.

The kinetic data of homogeneous olefin epoxidation was assessed for three additional mononuclear complexes ([Cp*Mo(CO)₃CH₃], [Cp*Mo(CO)₃Cl], and [CpMo(CO)₃Cl]), in order to complete the series of five pre-catalysts. Their turn-over frequencies (TOF) vary with the cyclopentadienyl substituent (η⁵-C₅H₅ or η⁵-C₅(CH₃)₅), but, more importantly, with the ligand X. It was found that the Cp moiety is more favourable than Cp*, because of the larger steric bulk of the methyl groups on the Cp*, and that the catalytic performance of the pre-catalysts decreases in the order of Cl > CH₃ > CF₃. This is more difficult to explain, as the shielding of the [CpMo(CO)₃]⁺ core increases in the order Cl < CF₃ < CH₃ (determined by ⁹⁵Mo NMR spectroscopy). It is, however, noteworthy that the formation of the catalytically active species of the CF₃ derivative, *i.e.* the decarbonylation of the precursor, is significantly slower than in the case of X = CH₃ and Cl, what influences the performance in olefin epoxidation. That is the reason why further investigations on vibrational and structural properties of the three molybdenum cyclopentadienyl tricarbonyl complexes (Figure 7.1, R = H, X = CH₃, CF₃, Cl) were carried out. The main goals of this study were to examine the influence of the X group on the spectral features and on the bond force constants, in order to elucidate the differences in reactivity in presence of an organic oxidant (*tert*-butyl hydroperoxide) as mentioned above. FT-IR, FT-FIR and FT-Raman spectra were recorded and a complete assignment of the [CpMo(CO)₃X] vibrations was proposed. Furthermore, the characteristics of the solid-state structures were compared, as it was possible to solve the only missing single crystal analysis

of the series, $[\text{CpMo}(\text{CO})_3\text{CF}_3]$. Additionally, the solution of the solid-state structure of the oxidised derivative $[\text{CpMo}(\text{O}_2)(\text{O})\text{CF}_3]$ allowed comparison with its CH_3 analogue. Both are supposed to be intermediates in the catalytic olefin epoxidation with *tert*-butyl hydroperoxide, thus, structural features provided further insight into their reactivity towards oxygen transfer reactions, supplementary to ^{19}F NMR studies and DFT-calculations (Scheme 7.2).



Scheme 7.2 Oxidation of $[\text{CpMo}(\text{CO})_3\text{CF}_3]$ (1) with excess TBHP yields $[\text{CpMo}(\eta^2\text{-O}_2)(\text{O})\text{CF}_3]$ (2) and $[\text{CpMo}(\eta^2\text{-OOH})(\text{O})(\sigma\text{-O}_2^t\text{Bu})\text{CF}_3]$ (3), $[\text{CpMo}(\sigma\text{-O}_2\text{H})(\text{O})(\sigma\text{-O}_2^t\text{Bu})\text{CF}_3]$ (4) or $[\text{CpMo}(\eta^2\text{-O}_2)(\text{OH})(\sigma\text{-O}_2^t\text{Bu})\text{CF}_3]$ (5).

8 Appendix A

This section contains supplementary information to Chapter 3:
Chromophoric Lewis Base Adducts of Methyltrioxorhenium: Synthesis, Catalysis and Photo-chemistry

Ligand characterisation

4-Styrylpyridine (1): Yield 314 mg (70 %). ^1H NMR (400 MHz, CDCl_3 , 25 °C): δ = 8.51 [d, $J_{(H,H)}$ = 4.8 Hz, 2 H, $\text{NC}_2\text{H}_2\text{C}_2\text{H}_2\text{C}-$], 7.48 [d, $J_{(H,H)}$ = 7.4 Hz, 2 H, $-\text{CC}_2\text{H}_2\text{C}_2\text{H}_2\text{CH}$], 7.35-7.24 [m, 4 H, $\text{NC}_2\text{H}_2\text{C}_2\text{H}_2\text{C}-\text{CHCH}-\text{CC}_2\text{H}_2\text{C}_2\text{H}_2\text{CH}$], 7.21 [d, $J_{(H,H)}$ = 9.8 Hz, 2 H, $-\text{CC}_2\text{H}_2\text{C}_2\text{H}_2\text{CH}$], 6.96 [d, $J_{(H,H)}$ = 15.9 Hz, 1 H, $\text{Pyr}-\text{CHCH}-\text{Ph}$] ppm. ^{13}C NMR (100.6 MHz, CDCl_3 , 25 °C): δ = 150.2 (2 C), 144.6 (2 C), 136.2 (1 C), 133.2 (1 C), 128.8 (2 C), 128.7 (2 C), 127.0 (1 C), 126.0 (2 C), 120.8 (1 C) ppm.

4-[2-(4-Methylphenyl)ethenyl]pyridine (2): Yield 386 mg (80 %). ^1H NMR (400 MHz, CDCl_3 , 25 °C): δ = 8.55 [d, $J_{(H,H)}$ = 6.0 Hz, 2H, $\text{NC}_2\text{H}_2\text{C}_2\text{H}_2\text{C}-$], 7.43 [d, $J_{(H,H)}$ = 8.0 Hz, 2 H, $\text{NC}_2\text{H}_2\text{C}_2\text{H}_2\text{C}-$], 7.34 [d, $J_{(H,H)}$ = 6.0 Hz, 2 H, $-\text{CC}_2\text{H}_2\text{C}_2\text{H}_2\text{CCH}_3$], 7.27 [d, $J_{(H,H)}$ = 13.6 Hz, 1 H, $-\text{PhCHCHPyr}-$], 7.18 [d, $J_{(H,H)}$ = 7.6 Hz, 2 H, $-\text{CC}_2\text{H}_2\text{C}_2\text{H}_2\text{CCH}_3$], 6.95 [d, $J_{(H,H)}$ = 16.0 Hz, 1 H, $-\text{PhCHCHPyr}-$], 2.37 [s, 3 H, $-\text{CC}_2\text{H}_2\text{C}_2\text{H}_2\text{CCH}_3$] ppm. ^{13}C NMR (100.6 MHz, CDCl_3 , 25 °C): δ = 150.2 [1 C, $\text{NC}_2\text{H}_2\text{C}_2\text{H}_2\text{C}-$], 144.8 [2 C, $\text{NC}_2\text{H}_2\text{C}_2\text{H}_2\text{C}-$], 138.9 [1 C, $-\text{CC}_2\text{H}_2\text{C}_2\text{H}_2\text{CCH}_3$], 133.4 [1 C, $-\text{CC}_2\text{H}_2\text{C}_2\text{H}_2\text{CCH}_3$], 133.1 [1 C, $-\text{PhCHCHPyr}-$], 129.5 [2 C, $-\text{CC}_2\text{H}_2\text{C}_2\text{H}_2\text{CCH}_3$], 126.9 [2 C, $-\text{CC}_2\text{H}_2\text{C}_2\text{H}_2\text{CCH}_3$], 124.9 [1C, $-\text{PhCHCHPyr}-$], 120.8 [2 C, $\text{NC}_2\text{H}_2\text{C}_2\text{H}_2\text{C}-$], 21.3 [1 C, $-\text{PhCH}_3$] ppm.

4-[2-(4-Bromophenyl)ethenyl]pyridine (3): Yield 503 mg (78 %). ^1H NMR (400 MHz, CDCl_3 , 25 °C): δ = 8.58 [d, $J_{(H,H)}$ = 6.0Hz, 2 H, $\text{NC}_2\text{H}_2\text{C}_2\text{H}_2\text{C}-$], 7.50 [d, $J_{(H,H)}$ = 8.4 Hz, 2 H, $-\text{CC}_2\text{H}_2\text{C}_2\text{H}_2\text{CBr}$], 7.38 [d, $J_{(H,H)}$ = 8.4 Hz, 2 H, $-\text{CC}_2\text{H}_2\text{C}_2\text{H}_2\text{CBr}$], 7.34 [d, $J_{(H,H)}$ = 5.2 Hz, 2 H, $\text{NC}_2\text{H}_2\text{C}_2\text{H}_2\text{C}-$], 7.22 [d, $J_{(H,H)}$ = 16.4 Hz, 1 H, $\text{PyrCHCH}-$], 6.98 [d, $J_{(H,H)}$ = 16.4 Hz, 1 H, $\text{PyrCHCH}-$] ppm. ^{13}C NMR (100.6 MHz, CDCl_3 , 25 °C): δ = 150.30 (2 C, $\text{NC}_2\text{H}_2\text{C}_2\text{H}_2\text{C}-$), 144.23 (1 C, $\text{NC}_2\text{H}_2\text{C}_2\text{H}_2\text{C}-$), 135.13 (1 C, $-\text{CC}_2\text{H}_2\text{C}_2\text{H}_2\text{CBr}$), 132.02 (2 C, $-\text{CC}_2\text{H}_2\text{C}_2\text{H}_2\text{CBr}$), 131.87 (1 C, $\text{PyrCHCH}-$), 128.44 (2 C, $-\text{CC}_2\text{H}_2\text{C}_2\text{H}_2\text{CBr}$), 126.76 (1 C, $\text{PyrCHCH}-$), 122.68 (1 C, $-\text{CC}_2\text{H}_2\text{C}_2\text{H}_2\text{CBr}$), 120.85 (2 C, $\text{NC}_2\text{H}_2\text{C}_2\text{H}_2\text{C}-$) ppm.

4-[2-(Biphenyl)ethenyl]pyridine (4): Yield 980 mg (83 %). ^1H NMR (400 MHz, CDCl_3 , 25 °C): δ = 8.59 [d, $J_{(H,H)}$ = 8.0 Hz, 2 H, $\text{NC}_2\text{H}_2\text{C}_2\text{H}_2\text{C}-$], 7.63 (m, 7 H, $-\text{CC}_2\text{H}_2\text{C}_2\text{H}_2\text{C}-\text{CC}_2\text{H}_2\text{C}_2\text{H}_2\text{CH}$), 7.46 [t, $J_{(H,H)}$ = 8.0 Hz, 2 H, $-\text{CC}_2\text{H}_2\text{C}_2\text{H}_2\text{CH}$], 7.39 (m, 2 H, $\text{NC}_2\text{H}_2\text{C}_2\text{H}_2\text{C}-$), 7.35 [d, $J_{(H,H)}$ = 16.0 Hz, 1 H, $\text{Pyr}-\text{CHCH}-\text{Ph}-\text{Ph}$], 7.06 [d, $J_{(H,H)}$ = 16.0 Hz, 1 H, $\text{Pyr}-\text{CHCH}-\text{Ph}-\text{Ph}$] ppm. ^{13}C NMR (100.6 MHz, CDCl_3 , 25 °C): δ = 150.20 (2 C, $\text{NC}_2\text{H}_2\text{C}_2\text{H}_2\text{C}-$), 144.62 (1 C, $\text{NC}_2\text{H}_2\text{C}_2\text{H}_2\text{C}-$), 141.51 (1 C, $-\text{CC}_2\text{H}_2\text{C}_2\text{H}_2\text{CH}$), 140.38 (1 C, $-\text{CC}_2\text{H}_2\text{C}_2\text{H}_2\text{C}-\text{CC}_2\text{H}_2\text{C}_2\text{H}_2\text{CH}$), 135.16 (1 C, $-\text{CC}_2\text{H}_2\text{C}_2\text{H}_2\text{C}-\text{CC}_2\text{H}_2\text{C}_2\text{H}_2\text{CH}$), 132.71 (1 C, $\text{Pyr}-\text{CHCH}-\text{Ph}-\text{Ph}$), 128.85 (2 C, $-\text{CC}_2\text{H}_2\text{C}_2\text{H}_2\text{CH}$), 127.58 (1 C, $-\text{CC}_2\text{H}_2\text{C}_2\text{H}_2\text{CH}$), 127.47 (4 C, $-\text{CC}_2\text{H}_2\text{C}_2\text{H}_2\text{C}-\text{CC}_2\text{H}_2\text{C}_2\text{H}_2\text{CH}$), 126.95 (2 C, $-\text{CC}_2\text{H}_2\text{C}_2\text{H}_2\text{C}-\text{CC}_2\text{H}_2\text{C}_2\text{H}_2\text{CH}$), 125.99 (1 C, $\text{Pyr}-\text{CHCH}-\text{Ph}-\text{Ph}$), 120.83 (2 C, $\text{NC}_2\text{H}_2\text{C}_2\text{H}_2\text{C}-$) ppm.

4-[2-(4-Anthracenylphenyl)ethenyl]pyridine (5): Yield 880 mg (65 %). ^1H NMR (400 MHz, CDCl_3 , 25 °C): δ = 8.63 [d, $J_{(H,H)}$ = 4.9 Hz, 2 H], 8.52 (s, 1 H), 8.06 [d, $J_{(H,H)}$ = 8.6 Hz, 2 H], 7.77 [d, $^3J_{(H,H)}$ = 8.6 Hz, 2 H], 7.69 [d, $J_{(H,H)}$ = 8.6 Hz, 2 H], 7.47 [t, $J_{(H,H)}$ = 8.6, 7.4 Hz, 7 H], 7.37 [t, $^3J_{(H,H)}$ = 7.4, 7.4 Hz, 2 H], 7.18 [d, $J_{(H,H)}$ = 15.9 Hz, 1 H] ppm.

^{13}C NMR (100.6 MHz, CDCl_3 , 25 °C): δ = 150.2 (2 C), 144.7 (1 C), 139.5 (1 C), 136.3 (1 C), 135.4 (1 C), 132.9 (1 C), 131.8 (2 C), 131.4 (2 C), 130.1 (2 C), 128.4 (1 C), 127.0 (3 C), 126.8 (1 C), 126.6 (2 C), 126.3 (2 C), 125.5 (1 C), 125.1 (2 C), 120.9 (2 C) ppm.

4-Tolylpyridine (6): Yield 193 mg (60 %). ^1H NMR (400 MHz, CDCl_3 , 25 °C): δ = 8.63 [d, $J_{(H,H)}$ = 5.4 Hz, 2 H, $\text{NC}_2\text{H}_2\text{C}_2\text{H}_2\text{C}-$], 7.53 [d, $J_{(H,H)}$ = 8.0 Hz, 2 H, $\text{NC}_2\text{H}_2\text{C}_2\text{H}_2\text{C}-$], 7.48 [d, $J_{(H,H)}$ = 6.0 Hz, 2 H, $-\text{CC}_2\text{H}_2\text{C}_2\text{H}_2\text{CCH}_3$], 7.28 [d, $J_{(H,H)}$ = 8.0 Hz, 2 H, $-\text{CC}_2\text{H}_2\text{C}_2\text{H}_2\text{CCH}_3$], 2.40 [s, 3 H, $-\text{PhCH}_3$] ppm. ^{13}C NMR (100.6 MHz, CDCl_3 , 25 °C): δ = 150.2 [2 C, $\text{NC}_2\text{H}_2\text{C}_2\text{H}_2\text{C}-$], 148.2 [1 C, $\text{NC}_2\text{H}_2\text{C}_2\text{H}_2\text{C}-$], 139.2 [1 C, $-\text{CC}_2\text{H}_2\text{C}_2\text{H}_2\text{C}(\text{CH}_3)$], 135.2 [1 C, $-\text{CC}_2\text{H}_2\text{C}_2\text{H}_2\text{C}(\text{CH}_3)$], 129.8 [2 C, $-\text{CC}_2\text{H}_2\text{C}_2\text{H}_2\text{C}(\text{CH}_3)$], 126.8 [2 C, $-\text{CC}_2\text{H}_2\text{C}_2\text{H}_2\text{C}(\text{CH}_3)$], 121.4 [2 C, $\text{NC}_2\text{H}_2\text{C}_2\text{H}_2\text{C}-$], 21.2 [1 C, $-\text{PhCH}_3$] ppm.

4-(3,5-Dimethylphenyl)pyridine (7): Yield 450 mg (66 %). ^1H NMR (400 MHz, CDCl_3 , 25 °C): δ = 8.65 [d, $J_{(H,H)}$ = 6.8 Hz, 2 H, $\text{NC}_2\text{H}_2\text{C}_2\text{H}_2\text{C}-$], 7.50 [d, $J_{(H,H)}$ = 6.8 Hz, 2 H, $\text{NC}_2\text{H}_2\text{C}_2\text{H}_2\text{C}-$], 7.27 [s, 2 H, $-\text{CC}_2\text{H}_2\text{C}_2(\text{CH}_3)_2\text{CH}$], 7.10 [s, 1 H, $-\text{CC}_2\text{H}_2\text{C}_2(\text{CH}_3)_2\text{CH}$], 2.41 [s, 6 H, $-\text{CC}_2\text{H}_2\text{C}_2(\text{CH}_3)_2\text{CH}$] ppm. ^{13}C NMR (100.6 MHz, CDCl_3 , 25 °C): δ = 150.15 [2 C, $\text{NC}_2\text{H}_2\text{C}_2\text{H}_2\text{C}-$], 148.65 [1 C, $\text{NC}_2\text{H}_2\text{C}_2\text{H}_2\text{C}-$], 138.71 [2 C, $-\text{CC}_2\text{H}_2\text{C}_2(\text{CH}_3)_2\text{CH}$], 138.18 [1 C, $-\text{CC}_2\text{H}_2\text{C}_2(\text{CH}_3)_2\text{CH}$], 130.67 [1 C, $-\text{CC}_2\text{H}_2\text{C}_2(\text{CH}_3)_2\text{CH}$], 124.86 [2 C, $-\text{CC}_2\text{H}_2\text{C}_2(\text{CH}_3)_2\text{CH}$], 121.69 [2 C, $\text{NC}_2\text{H}_2\text{C}_2\text{H}_2\text{C}-$], 21.36 [2 C, $-\text{CC}_2\text{H}_2\text{C}_2(\text{CH}_3)_2\text{CH}$] ppm.

Complex characterisation

Methyl(4-styrylpyridine)trioxorhenium (8): Yield 58 mg (76 %). ^1H NMR (400 MHz, CDCl_3 , 25 °C): δ = 8.29 [d, $J_{(H,H)}$ = 6.2 Hz, 2 H, $\text{NC}_2\text{H}_2\text{C}_2\text{H}_2\text{C}-$], 7.54 [d, $J_{(H,H)}$ = 7.4 Hz, 2 H, $-\text{CC}_2\text{H}_2\text{C}_2\text{H}_2\text{CH}$], 7.45 (m, 6 H, $\text{NC}_2\text{H}_2\text{C}_2\text{H}_2\text{C}-\text{CHCHCC}_2\text{H}_2\text{C}_2\text{H}_2\text{CH}$), 7.01 [d, $J_{(H,H)}$ = 17.2 Hz, 1 H, $\text{Pyr}-\text{CHCH}-\text{Ph}$], 2.03 (s, 3 H, $-\text{ReCH}_3$) ppm. ^{13}C NMR (100.6 MHz, CDCl_3 , 25 °C): δ = 147.2 (2 C), 135.6 (2 C), 135.5 (1 C), 129.3 (1 C), 128.9 (2 C), 127.3 (2 C), 124.7 (1 C), 121.9 (2 C), 24.7 (1 C) ppm. IR (KBr): $\tilde{\nu}$ = 1605 (vs), 1499 (w), 1449 (w), 1428 (w), 1384 (w), 1013 (m), 971 (m), 961 (w), 934 (vs), 927 (vs), 877 (w), 818 (m), 559 (w), 548 (m) cm^{-1} . $\text{C}_{14}\text{H}_{14}\text{NO}_3\text{Re}$ (430.47): calcd. C 39.06, H 3.28, N 3.25; found C 39.56, H 3.31, N 3.34.

Methyl{4-[2-(4-Methylphenyl)ethenyl]pyridine}trioxorhenium (9): Yield 53 mg (72 %). ^1H NMR (400 MHz, CDCl_3 , 25 °C): δ = 8.20 [d, $J_{(H,H)}$ = 5.4 Hz, 2 H, $\text{NC}_2\text{H}_2\text{C}_2\text{H}_2\text{C}-$], 7.42 (m, 4 H, $\text{NC}_2\text{H}_2\text{C}_2\text{H}_2\text{C}-$, $-\text{CC}_2\text{H}_2\text{C}_2\text{H}_2\text{CCH}_3$), 7.30 [d, $J_{(H,H)}$ = 16.2 Hz, 1 H, $-\text{PhCHCHPyr}$], 7.20 [d, $J_{(H,H)}$ = 7.9 Hz, 2 H, $-\text{CC}_2\text{H}_2\text{C}_2\text{H}_2\text{CCH}_3$], 6.93 [d, $J_{(H,H)}$ = 16.2 Hz, 1 H, $-\text{PhCHCHPyr}$], 2.37 (s, 3 H, $-\text{PhCH}_3$), 1.92 (s, 3 H, $-\text{ReCH}_3$) ppm. ^{13}C NMR (100.6 MHz, CDCl_3 , 25 °C): δ = 147.94 (1 C, $\text{NC}_2\text{H}_2\text{C}_2\text{H}_2\text{C}-$), 147.06 (2 C, $\text{NC}_2\text{H}_2\text{C}_2\text{H}_2\text{C}-$), 139.66 (1 C, $-\text{CC}_2\text{H}_2\text{C}_2\text{H}_2\text{CCH}_3$), 135.48 (1 C, $-\text{CC}_2\text{H}_2\text{C}_2\text{H}_2\text{CCH}_3$), 132.76 (1 C, $-\text{PhCHCHPyr}$), 129.65 (2 C, $-\text{CC}_2\text{H}_2\text{C}_2\text{H}_2\text{CCH}_3$), 127.23 (2 C, $-\text{CC}_2\text{H}_2\text{C}_2\text{H}_2\text{CCH}_3$), 123.52 (1 C, $-\text{PhCHCHPyr}$), 121.85 (2 C, $\text{NC}_2\text{H}_2\text{C}_2\text{H}_2\text{C}-$), 25.08 (1 C, $-\text{ReCH}_3$), 21.36 (1 C, $-\text{PhCH}_3$) ppm. IR (KBr): $\tilde{\nu}$ = 3434 (w), 3025 (w), 1636 (m), 1602 (vs), 1514 (m), 1428 (m), 1384 (w), 1210 (w), 1183

(w), 1013 (s), 975 (m), 936 (vs), 926 (vs), 826 (s), 736 (w), 706 (w), 624 (m), 547 (s), 502 (m) cm^{-1} . $\text{C}_{15}\text{H}_{16}\text{NO}_3\text{Re}$ (444.50): calcd. C 40.53, H 3.63, N 3.15; found C 38.55, H 3.33, N 3.16.

{4-[2-(4-Bromophenyl)ethenyl]pyridine}methyltrioxorhenium (10): Yield 68 mg (79 %). ^1H NMR (400 MHz, CDCl_3 , 25 °C): δ = 8.26 [d, $J_{(H,H)}$ = 6.2 Hz, 2 H, $\text{NC}_2\text{H}_2\text{C}_2\text{H}_2\text{C}-$], 7.52 [d, $J_{(H,H)}$ = 8.3 Hz, 2 H, $-\text{CC}_2\text{H}_2\text{C}_2\text{H}_2\text{CBr}$], 7.41 (m, 4 H, $\text{NC}_2\text{H}_2\text{C}_2\text{H}_2\text{C}-$, $-\text{CC}_2\text{H}_2\text{C}_2\text{H}_2\text{CBr}$), 7.25 [d, $J_{(H,H)}$ = 16.4 Hz, 1 H, Pyr-CHCH-], 6.98 [d, $J_{(H,H)}$ = 16.2 Hz, 1 H, Pyr-CHCH-], 1.96 (s, 3 H, $-\text{ReCH}_3$) ppm. ^{13}C NMR (100.6 MHz, CDCl_3 , 25 °C): δ = 147.3 (2 C), 147.0 (1 C), 134.5 (1 C), 134.1 (1 C), 132.1 (3 C), 128.7 (2 C), 125.4 (1 C), 123.5 (1 C), 122.0 (1 C), 24.0 (1 C) ppm. IR (KBr): $\tilde{\nu}$ = 3466 (w), 3048 (w), 2973 (w), 1895 (w), 1773 (w), 1637 (m), 1610 (vs), 1586 (s), 1497 (m), 1483 (m), 1428 (s), 1393 (m), 1385 (m), 1209 (m), 1070 (vs), 1017 (vs), 1008 (s), 975 (s), 970 (s), 928 (vs), 883 (m), 875 (m), 829 (vs), 738 (w), 674 (w), 583 (m), 557 (s), 542 (s). 496 (w) cm^{-1} . $\text{C}_{14}\text{H}_{13}\text{BrNO}_3\text{Re}$ (509.37): calcd. C 33.01, H 2.57, N 2.75; found C 32.88, H 2.53, N 2.78.

{4-[2-(Biphenyl)ethenyl]pyridine}methyltrioxorhenium (11): Yield 69 mg (80 %). ^1H NMR (400 MHz, CDCl_3 , 25 °C): δ = 8.34 [d, $J_{(H,H)}$ = 6.2 Hz, 2 H, $\text{NC}_2\text{H}_2\text{C}_2\text{H}_2\text{C}-$], 7.62 (m, 6 H, $-\text{CC}_2\text{H}_2\text{C}_2\text{H}_2\text{C}-\text{CC}_2\text{H}_2\text{C}_2\text{H}_2\text{CH}$), 7.47-7.37 (m, 5 H, $\text{NC}_2\text{H}_2\text{C}_2\text{H}_2\text{C}-$, $-\text{CC}_2\text{H}_2\text{C}_2\text{H}_2\text{CH}$), 7.36 [d, $J_{(H,H)}$ = 16.2 Hz, 1 H, Pyr-CHCH-Ph-Ph], 7.04 [d, $J_{(H,H)}$ = 16.2 Hz, 1 H, Pyr-CHCHPh-Ph], 2.13 (s, 3 H, $-\text{ReCH}_3$) ppm. ^{13}C NMR (100.6 MHz, CDCl_3 , 25 °C): δ = 147.7 (2 C), 147.0 (1 C), 142.0 (1 C), 140.2 (1 C), 140.2 (1 C), 134.6 (2 C), 128.9 (2 C), 127.7 (2 C), 127.6 (2 C), 127.0 (2 C), 124.8 (1 C), 121.7 (2 C), 24.4 (1 C) ppm. IR (KBr): $\tilde{\nu}$ = 344 (w), 3032 (w), 1600 (s), 1487 (m), 1426 (m), 1204 (w), 1195 (w), 1015 (m), 976 (m), 934 (vs), 927 (vs), 879 (w), 836 (m), 765 (m), 737 (w), 690 (m), 638 (w), 561 (m), 529 (w) cm^{-1} . $\text{C}_{20}\text{H}_{18}\text{NO}_3\text{Re}$ (506.57): calcd. C 47.40, H 3.58, N 2.77; found C 47.33, H 3.58, N 2.77.

{4-[2-(4-Anthracenylphenyl)ethenyl]pyridine}methyltrioxorhenium (12): Yield 87 mg (84 %). ^1H NMR (400 MHz, CDCl_3 , 25 °C): δ = 8.51 (s, 1 H), 8.33 [d, $J_{(H,H)}$ = 6.2 Hz, 2 H], 8.05 [d, $J_{(H,H)}$ = 8.3 Hz, 2 H], 7.76 [d, $J_{(H,H)}$ = 8.3 Hz, 2 H], 7.67 [d, $J_{(H,H)}$ = 8.7 Hz, 2 H], 7.47 (m, 7 H), 7.35 [m, $J_{(H,H)}$ = 15.6 Hz, 2 H], 7.15 [d, $J_{(H,H)}$ = 16.2 Hz, 1 H], 2.00 (s, 3 H, $-\text{ReCH}_3$) ppm. ^{13}C NMR (100.6 MHz, CDCl_3 , 25 °C): δ = 148.2 (2 C), 146.7 (1 C), 140.0 (1 C), 136.1 (1 C), 135.0 (1 C), 134.6 (1 C), 132.0 (2 C), 131.4 (2 C), 130.1 (2 C), 128.4 (1 C), 127.2 (3 C), 126.9 (1 C), 126.5 (2 C), 125.6 (2 C), 125.4 (1 C), 125.2 (2 C), 121.7 (2 C), 24.9 (1 C, $-\text{ReCH}_3$) ppm. IR (KBr): $\tilde{\nu}$ = 3434 (w), 3050 (w), 1607 (s), 1592 (m), 1443 (w), 1426 (m), 1412 (w), 1384 (m), 1066 (w), 1015 (m), 969 (w), 931 (vs), 881 (m), 827 (m), 790 (w), 735 (s), 653 (w), 635 (w), 613 (m), 568 (w), 554 (m) cm^{-1} . 541 (m), 422 (w) cm^{-1} . $\text{C}_{28}\text{H}_{22}\text{NO}_3\text{Re}$ (606.69): calcd. C 55.41, H 3.66, N 2.31; found C 55.80, H 3.72, N 2.24.

Methyl(4-tolylpyridine)trioxorhenium (13): Yield 67 mg (97 %). ^1H NMR (400 MHz, CDCl_3 , 25 °C): δ = 8.31 [d, $J_{(H,H)}$ = 6.2 Hz, 2 H, $\text{NC}_2\text{H}_2\text{C}_2\text{H}_2\text{C}-$], 7.56 [d, $J_{(H,H)}$ = 6.2 Hz, 2 H, $\text{NC}_2\text{H}_2\text{C}_2\text{H}_2\text{C}-$], 7.52 [d, $J_{(H,H)}$ = 7.9 Hz, 2 H, $-\text{CC}_2\text{H}_2\text{C}_2\text{H}_2\text{CCH}_3$], 7.30 [d, $J_{(H,H)}$ = 7.5

Hz, 2 H, -CC₂H₂C₂H₂CCH₃], 2.41 (s, 3 H, -PhCH₃), 1.97 (s, 3 H, -ReCH₃) ppm. ¹³C NMR (100.6 MHz, CDCl₃, 25 °C): δ = 151.1 (1 C), 147.1 (2 C), 140.3 (1 C), 133.8 (1 C), 130.0 (2 C), 126.9 (2 C), 122.5 (2 C), 24.8 (1 C, -ReCH₃), 21.2 (1 C, Ph-CH₃) ppm. IR (KBr): $\tilde{\nu}$ = 33445 (m), 2925 (w), 1610 (s), 492 (m), 1384 (m), 1262 (w), 1227 (w), 12211 (w), 1073 (m), 1037 (w), 1010 (m), 934 (vs), 927 (vs), 854 (w), 811 (s), 721 (m), 559 (m), 498 (m) cm⁻¹. C₁₃H₁₄NO₃Re (418.46): calcd. C 37.31, H 3.37, N 3.35; found C 37.05, H 3.41, N 3.34.

[4-(3,5-Dimethylphenyl)pyridine]methyltrioxorhenium (14): Yield 106 mg (70 %). ¹H NMR (400 MHz, CDCl₃, 25 °C): δ = 8.32 [d, $J_{(H,H)}$ = 6.4 Hz, 2 H, NC₂H₂C₂H₂C-], 7.56 [d, $J_{(H,H)}$ = 6.6 Hz, 2 H, NC₂H₂C₂H₂C-], 7.21 [s, 2 H, -CC₂H₂C₂(CH₃)₂CH], 7.11 [s, 1 H, -CC₂H₂C₂(CH₃)₂CH], 2.39 [s, 6 H, -CC₂H₂C₂(CH₃)₂CH], 1.98 (s, 3 H, -ReCH₃) ppm. ¹³C NMR (100.6 MHz, CDCl₃, 25 °C): δ = 151.4 (1 C), 147.2 (2 C), 139.0 (2 C), 136.8 (1 C), 131.5 (1 C), 125.0 (2 C), 122.8 (2 C), 24.4 (1 C), 21.3 (2 C) ppm. IR (KBr): $\tilde{\nu}$ = 3434 (w), 2916 (w), 1613 (vs), 1551 (w), 1507 (w), 1408 (w), 1385 (w), 1232 (w), 1073 (m), 1021 (m), 931 (vs), 828 (s), 664 (m), 589 (m), 561 (m), 434 (w), 418 (w) cm⁻¹. C₁₄H₁₆NO₃Re (432.49): calcd. C 38.88, H 3.73, N 3.24; found C 38.88, H 3.73, N 3.24.

Curve fittings to Eq. (2) or (3)

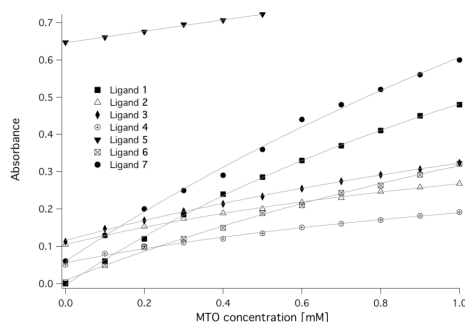
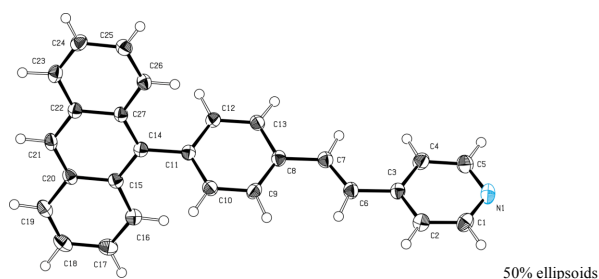


Figure S1. Curve fittings on experimental data for determination of the value of the formation constant.

Crystal Structure Determinations

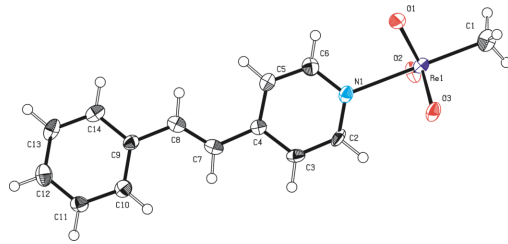
Compound 5



| | |
|------------------------|--|
| Operator: | *** Herdtweck *** |
| Molecular Formula: | C ₂₇ H ₁₉ N |
| Crystal Color / Shape: | Colorless fragment |
| Crystal Size: | Approximate size of crystal fragment used for data collection: 0.51 × 0.56 × 0.64 mm |
| Molecular Weight: | 357.43 a.m.u. |
| F ₀₀₀ : | 752 |
| Systematic Absences: | hkl: h+k≠2n; h0l: l≠2n |
| Space Group: | Monoclinic C c (I.T.-No.: 9) |
| Cell Constants: | Least-squares refinement of 9969 reflections with the programs "APEX suite" and "SAINT" [1,2]; theta range 2.38° < θ < 25.34°; Mo(K α); λ = 71.073 pm |
| | a = 1499.71(6) pm |
| | b = 1094.97(4) pm β = 114.048(2)° |
| | c = 1241.75(5) pm |
| | V = 1862.14(13) × 10 ⁶ pm ³ ; Z = 4; D _{calc} = 1.275 g cm ⁻³ ; Mos. = 0.69 |
| Diffractometer: | Kappa APEX II (Area Diffraction System; BRUKER AXS); rotating anode; graphite monochromator; 50 kV; 40 mA; λ = 71.073 pm; |
| Temperature: | (-100±1) °C; (173±1) K |
| Measurement Range: | 2.38° < θ < 25.34°; h: -18/18, k: -13/13, l: -14/14 |
| Measurement Time: | 2 × 2.50 s per film |
| Measurement Mode: | measured: 10 runs; 4003 films / scaled: 10 runs; 4003 films |
| LP - Correction: | Yes [2] |
| Intensity Correction: | No/Yes; during scaling [2] |
| Absorption Correction: | Multi-scan; during scaling; μ = 0.073 mm ⁻¹ [2] |
| Reflection Data: | Correction Factors: T _{min} = 0.6442 T _{max} = 0.7452 |
| | 33953 reflections were integrated and scaled |
| | 1043 reflections systematic absent and rejected |
| | 32910 reflections to be merged |
| | 3397 independent reflections |
| | 0.023 R _{int} : (basis F _o ²) |
| | 3397 independent reflections (all) were used in refinements |
| | 3360 independent reflections with I _o > 2σ(I _o) |
| | 99.6 % completeness of the data set |
| | 329 parameter full-matrix refinement |
| | 10.3 reflections per parameter |
| Solution: | Direct Methods [3]; Difference Fourier syntheses |
| Refinement Parameters: | In the asymmetric unit: |
| | 28 Non-hydrogen atoms with anisotropic displacement parameters |
| | 19 Hydrogen atoms with isotropic displacement parameters |
| Hydrogen Atoms: | All hydrogen atom positions were found in the difference map calculated from the model containing all non-hydrogen atoms. The hydrogen positions were refined with individual isotropic displacement parameters. |

Atomic Form Factors: For neutral atoms and anomalous dispersion [4]
 Extinction Correction: no
 Weighting Scheme: $w^1 = \sigma^2(F_o^2) + (a * P)^2 + b * P$
 with a: 0.0444; b: 0.4705; P: [Maximum(0 or F_o^2) + 2 * F_c^2]/3
 Shift/Err: Less than 0.001 in the last cycle of refinement:
 Resid. Electron Density: +0.13 e_o⁻/Å³; -0.12 e_o⁻/Å³
 R1: $\Sigma ||F_o - |F_c|| / \Sigma |F_o|$
 [F_o > 4σ(F_o)]; N=3360]; = 0.0255
 [all reflectns; N=3397]; = 0.0258
 wR2: $[\Sigma w(F_o^2 - F_c^2)^2] / \Sigma w(F_o^2)^2$ ^{1/2}
 [F_o > 4σ(F_o)]; N=3360]; = 0.0709
 [all reflectns; N=3397]; = 0.0713
 Goodness of fit: $[\Sigma w(F_o^2 - F_c^2)^2 / (\text{NO-NV})]$ ^{1/2} = 1.080
 Flack's Parameter : x = 0(2)
 Remarks: Refinement expression $\Sigma w(F_o^2 - F_c^2)^2$
 The correct enantiomere could **not** be proved by Flack's Parameter.

Compound 8

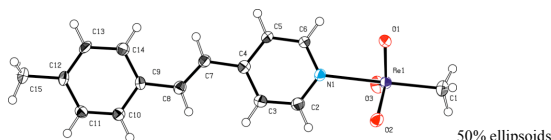


50% ellipsoids

Operator: *** Herdtweck ***
 Molecular Formula: C₁₄H₁₄N₂O₃Re
 Crystal Color / Shape: Yellow fragment
 Crystal Size: Approximate size of crystal fragment used for data collection: 0.13 × 0.18 × 0.51 mm
 Molecular Weight: 430.47 a.m.u.
 F₀₀₀: 408
 Systematic Absences: 0k0: k≠2n
 Space Group: Monoclinic P 2₁ (I.T.-No.: 4)
 Cell Constants: Least-squares refinement of 9956 reflections with the programs "APEX suite" and "SAINT" [1,2]; theta range 1.95° < θ < 25.39°;
 Mo(Kα): λ = 71.073 pm
 a = 900.54(2) pm
 b = 724.42(2) pm β = 109.3284(11)°
 c = 1107.21(3) pm
 V = 681.60(3) × 10⁶ pm³; Z = 2; D_{calc} = 2.098 g cm⁻³; Mos. = 0.72
 Kappa APEX II (Area Diffraction System; BRUKER AXS); rotating anode; graphite monochromator; 50 kV; 40 mA; λ = 71.073 pm;
 Mo(Kα)
 (-150±1) °C; (123±1) K
 Measurement Range: 1.95° < θ < 25.39°; h: -10/10, k: -7/7, l: -13/13
 Measurement Time: 2 × 5 s per film
 Measurement Mode: measured: 5 runs; 2663 films / scaled: 5 runs; 2663 films
 φ- and ω-movement; Increment: Δφ/Δω = 0.50°; dx = 55.0 mm
 LP - Correction: Yes [2]
 Intensity Correction: No/Yes; during scaling [2]
 Absorption Correction: Multi-scan; during scaling; μ = 8.916 mm⁻¹ [2]
 Correction Factors: T_{min} = 0.4026 T_{max} = 0.7452
 Reflection Data: 10807 reflections were integrated and scaled
 1 obvious wrong intensity and rejected
 10806 reflections to be merged
 2281 independent reflections
 0.059 R_{int}: (basis F_o²)
 2281 independent reflections (all) were used in refinements
 2275 independent reflections with I_o > 2σ(I_o)
 91.0 % completeness of the data set
 173 parameter full-matrix refinement
 13.2 reflections per parameter
 Solution: Direct Methods [3]; Difference Fourier syntheses
 Refinement Parameters: In the asymmetric unit:
 19 Non-hydrogen atoms with anisotropic displacement parameters
 Hydrogen Atoms: In the difference map(s) calculated from the model containing all non-hydrogen atoms, not all of the hydrogen positions could be determined from the highest peaks. For this reason, the hydrogen atoms were placed in calculated positions (d_H = 95, 98 pm). Isotropic displacement parameters were calculated from the parent carbon atom (U_H = 1.2/1.5 U_C). The hydrogen atoms were included in the structure factor calculations but not refined.
 Atomic Form Factors: For neutral atoms and anomalous dispersion [4]
 Extinction Correction: no
 Weighting Scheme: $w^1 = \sigma^2(F_o^2) + (a * P)^2 + b * P$
 with a: 0.0375; b: 0.4316; P: [Maximum(0 or F_o^2) + 2 * F_c^2]/3
 Shift/Err: Less than 0.001 in the last cycle of refinement:

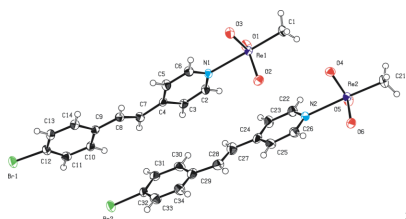
Resid. Electron Density: +2.27 e_g⁻/Å³; -2.57 e_g⁻/Å³
 R1: $\Sigma(|F_o|-|F_c|)/\Sigma|F_o|$
 [F_o > 4σ(F_o); N=2275]; = 0.0259
 [all reflctns; N=2281]; = 0.0259
 wR2: $[\Sigma w(F_o^2-F_c^2)^2]/\Sigma w(F_o^2)^2$ ^{1/2}
 [F_o > 4σ(F_o); N=2275]; = 0.0648
 [all reflctns; N=2281]; = 0.0648
 Goodness of fit: $[\Sigma w(F_o^2-F_c^2)^2/(\text{NO-NV})]^{1/2}$ = 1.091
 Refinement expression $\Sigma w(F_o^2-F_c^2)^2$
 Remarks: The correct enantiomere is proved by Flack's Parameter.
 Twin refinement (twin operation: inversion)
 BASF = 0.16(2)

Compound 9



Operator: *** Bechlers ***
 Molecular Formula: C₁₅H₁₆N O₃ Re
 Crystal Color / Shape: Yellow fragment
 Crystal Size: Approximate size of crystal fragment used for data collection: 0.15 × 0.15 × 0.43 mm
 Molecular Weight: 444.49 a.m.u.
 F₀₀₀: 848
 Systematic Absences: h0l: h+1≠2n; 0k0: k≠2n
 Space Group: Monoclinic P 2₁/n (I.T.-No.: 14)
 Cell Constants: a = 916.61(4) pm
 b = 717.41(3) pm β = 97.795(2)°
 c = 2237.72(9) pm
 V = 1457.89(11) · 10⁶ pm³; Z = 4
 Diffractometer: Kappa APEX II (Area Diffraction System; BRUKER AXS); rotating anode; graphite monochromator; 50 kV; 40 mA; λ = 71.073 pm;
 Mo(K_α)
 Temperature: (-100±1) °C; (173±1) K
 Measurement Range: 1.84° < θ < 25.36°; h: -11/11, k: -8/8, l: -26/25
 Measurement Time: 2 × 5 s per film
 Measurement Mode: measured: 4 runs; 2355 films / scaled: 4 runs; 2355 films
 q- and ω-movement; Increment: Δq/Δω = 0.50°; dx = 40.0 mm
 LP - Correction: Yes [2]
 Intensity Correction: No/Yes; during scaling [2]
 Absorption Correction: Multi-scan; during scaling; μ = 8.341 mm⁻¹ [2]
 Reflection Data: Correction Factors: T_{min} = 0.1239 T_{max} = 0.3676
 29722 reflections to be merged
 2564 independent reflections
 0.058 R_{int}: (basis F_o²)
 2564 independent reflections (all) were used in refinements
 2423 independent reflections with I_o > 2σ(I_o)
 96.2 % completeness of the data set
 183 parameter full-matrix refinement
 14.0 reflections per parameter
 Solution: Direct Methods [3]; Difference Fourier syntheses
 Refinement Parameters: In the asymmetric unit:
 20 Non-hydrogen atoms with anisotropic displacement parameters
 Hydrogen Atoms: In the difference map(s) calculated from the model containing all non-hydrogen atoms, not all of the hydrogen positions could be determined from the highest peaks. For this reason, the hydrogen atoms were placed in calculated positions (d_{C-H} = 92, 98 pm). Isotropic displacement parameters were calculated from the parent carbon atom (U_H = 1.2/1.5 U_C). The hydrogen atoms were included in the structure factor calculations but not refined.
 Atomic Form Factors: For neutral atoms and anomalous dispersion [4]
 Extinction Correction: no
 Weighting Scheme: w⁻¹ = σ²(F_o²) + (a*P)² + b*P
 with a: 0.0157; b: 8.4508; P: [Maximum(0 or F_o²) + 2*F_c²]/3
 Shift/Err: Less than 0.001 in the last cycle of refinement.
 Resid. Electron Density: +0.85 e_g⁻/Å³; -1.54 e_g⁻/Å³
 R1: $\Sigma(|F_o|-|F_c|)/\Sigma|F_o|$
 [F_o > 4σ(F_o); N=2423]; = 0.0289
 [all reflctns; N=2564]; = 0.0307
 wR2: $[\Sigma w(F_o^2-F_c^2)^2]/\Sigma w(F_o^2)^2$ ^{1/2}
 [F_o > 4σ(F_o); N=2423]; = 0.0671
 [all reflctns; N=2564]; = 0.0680
 Goodness of fit: $[\Sigma w(F_o^2-F_c^2)^2/(\text{NO-NV})]^{1/2}$ = 1.261
 Refinement expression $\Sigma w(F_o^2-F_c^2)^2$
 Remarks:

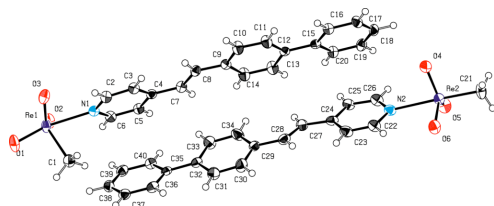
Compound 10



50% ellipsoids

Operator: *** Herdtweck ***
Molecular Formula: C₁₄H₁₃BrNO₃Re
Crystal Color / Shape: Yellow fragment
Crystal Size: Approximate size of crystal fragment used for data collection: 0.05 × 0.13 × 0.53 mm
Molecular Weight: 509.36 a.m.u.
F₀₀₀: 952
Systematic Absences: none
Space Group: Triclinic $P\bar{1}$ (I.T.-No.: 2)
Cell Constants: Least-squares refinement of 9934 reflections with the programs "APEX suite" and "SAINT" [1,2]; theta range 1.31° < θ < 25.45°;
Mo(K α); λ = 71.073 pm
a = 598.49(2) pm α = 66.0608(15)°
b = 1591.31(6) pm β = 85.8488(15)°
c = 1707.85(6) pm γ = 86.3720(14)°
V = 1481.68(9) × 10⁶ pm³; Z = 4; D_{calc} = 2.283 g cm⁻³; Mos. = 0.74
Diffractometer: Kappa APEX II (Area Diffraction System; BRUKER AXS); rotating anode; graphite monochromator; 60 kV; 50 mA; λ = 71.073 pm;
Mo(K α)
(-120±1) °C; (153±1) K
Temperature: 1.31° < θ < 25.45°; h: -6/6, k: -19/19, l: -20/20
Measurement Range: 2 × 5 s per film
Measurement Time: measured: 4 runs; 1364 films / scaled: 4 runs; 1364 films
Measurement Mode: φ- and ω-movement; Increment: Δφ/Δω = 0.50°; dx = 45.0 mm
Yes [2]
LP - Correction: No/Yes; during scaling [2]
Intensity Correction: Multi-scan; during scaling; μ = 10.903 mm⁻¹ [2]
Absorption Correction: Correction Factors: T_{min} = 0.3097 T_{max} = 0.7452
Reflection Data: 18921 reflections were integrated and scaled
18921 reflections to be merged
5188 independent reflections
0.042 R_{int}: (basis F_o²)
5188 independent reflections (all) were used in refinements
4839 independent reflections with I_o > 2σ(I_o)
94.7 % completeness of the data set
363 parameter full-matrix refinement
14.3 reflections per parameter
Solution: Direct Methods [3]; Difference Fourier syntheses
Refinement Parameters: In the asymmetric unit:
40 Non-hydrogen atoms with anisotropic displacement parameters
Hydrogen Atoms: In the difference map(s) calculated from the model containing all non-hydrogen atoms, not all of the hydrogen positions could be determined from the highest peaks. For this reason, the hydrogen atoms were placed in calculated positions (d_{calc} = 95, 98 pm). Isotropic displacement parameters were calculated from the parent carbon atom (U_{eq} = 1.2/1.5 U_C). The hydrogen atoms were included in the structure factor calculations but not refined.
Atomic Form Factors: For neutral atoms and anomalous dispersion [4]
Extinction Correction: no
Weighting Scheme: w⁻¹ = σ²(F_o²) + (a*P)² + b*P
with a: 0.0444; b: 2.0405; P: [Maximum(0 or F_o²) + 2*F_c²]/3
Shift/Err: Less than 0.002 in the last cycle of refinement:
Resid. Electron Density: +2.13 e_q⁻/Å³; -1.85 e_q⁻/Å³
R1: Δ(|F_o - F_c|)/Σ|F_o| = 0.0264
[F_o > 4σ(F_o); N=4839]; = 0.0286
[all reflctns; N=5188];
wR2: [Σw(F_o² - F_c²)²]/Σw(F_o²)^{1/2} = 0.0697
[F_o > 4σ(F_o); N=4839]; = 0.0721
[all reflctns; N=5188]; = 1.048
Goodness of fit: [Σw(F_o² - F_c²)²/(NO-NV)]^{1/2}
Remarks: Refinement expression Σw(F_o² - F_c²)²

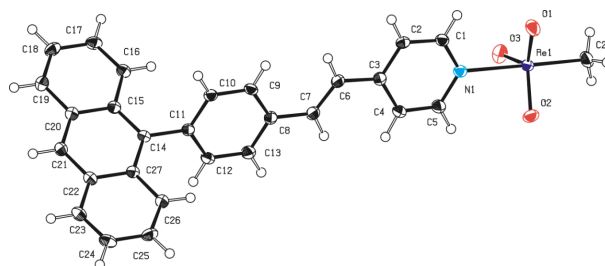
Compound 11



50% ellipsoids

| | | | |
|--|--|--|---------------------------|
| Operator: | *** Herdtweck *** | | |
| Molecular Formula: | C ₂₀ H ₁₈ N ₃ O ₃ Re | | |
| Crystal Color / Shape: | Yellow fragment | | |
| Crystal Size: | Approximate size of crystal fragment used for data collection: 0.24 × 0.35 × 0.38 mm | | |
| Molecular Weight: | 506.56 a.m.u. | | |
| F ₀₀₀ : | 976 | | |
| Systematic Absences: | none | | |
| Space Group: | Triclinic | <i>P</i> 1 | (I.T.-No.: 2) |
| Cell Constants: | Least-squares refinement of 9813 reflections with the programs "APEX suite" and "SAINT" [1,2]; theta range 0.75° < θ < 25.37°; Mo(K _α); λ = 71.073 pm | | |
| | <i>a</i> = | 572.88(3) pm | α = 82.715(3)° |
| | <i>b</i> = | 1145.64(6) pm | β = 89.200(2)° |
| | <i>c</i> = | 2741.20(14) pm | γ = 77.895(2)° |
| | <i>V</i> = 1744.74(16) · 10 ⁶ pm ³ ; <i>Z</i> = 4; <i>D</i> _{calc} = 1.929 g cm ⁻³ ; Mos. = 0.72 | | |
| Diffractometer: | Kappa APEX II (Area Diffraction System; BRUKER AXS); rotating anode; graphite monochromator; 50 kV; 40 mA; λ = 71.073 pm; Mo(K _α) | | |
| Temperature: | (-120±1) °C; (153±1) K | | |
| Measurement Range: | 0.75° < θ < 25.37°; h: -6/6, k: -13/13, l: -32/33 | | |
| Measurement Time: | 2 × 10 s per film | | |
| Measurement Mode: | measured: 9 runs; 4939 films / scaled: 9 runs; 4939 films | | |
| | φ- and ω-movement; Increment: Δφ/Δω = 0.50°; dx = 40.0 mm | | |
| LP - Correction: | Yes [2] | | |
| Intensity Correction: | No/Yes; during scaling [2] | | |
| Absorption Correction: | Multi-scan; during scaling; μ = 6.983 mm ⁻¹ [2] | | |
| Reflection Data: | Correction Factors: | T _{min} = 0.5786 | T _{max} = 0.7452 |
| | 69973 | reflections were integrated and scaled | |
| | 69973 | reflections to be merged | |
| | 6039 | independent reflections | |
| | 0.070 | R _{int} : (basis <i>F_o</i> ²) | |
| | 6039 | independent reflections (all) were used in refinements | |
| | 5347 | independent reflections with <i>I_o</i> > 2σ(<i>I_o</i>) | |
| | 94.5 % | completeness of the data set | |
| | 453 | parameter full-matrix refinement | |
| | 13.3 | reflections per parameter | |
| Solution: | Direct Methods [3]; Difference Fourier syntheses | | |
| Refinement Parameters: | In the asymmetric unit: | | |
| | 50 | Non-hydrogen atoms with anisotropic displacement parameters | |
| Hydrogen Atoms: | In the difference map(s) calculated from the model containing all non-hydrogen atoms, not all of the hydrogen positions could be determined from the highest peaks. For this reason, the hydrogen atoms were placed in calculated positions (<i>d_{C-H}</i> = 95, 98 pm). Isotropic displacement parameters were calculated from the parent carbon atom (<i>U_H</i> = 1.2/1.5 <i>U_C</i>). The hydrogen atoms were included in the structure factor calculations but not refined. | | |
| Atomic Form Factors: | For neutral atoms and anomalous dispersion [4] | | |
| Extinction Correction: | no | | |
| Weighting Scheme: | <i>w</i> ¹ = σ ² (<i>F_o</i> ²) + (<i>a</i> * <i>P</i>) ² + <i>b</i> * <i>P</i> | | |
| | with <i>a</i> : 0.0149; <i>b</i> : 3.2884; <i>P</i> : [Maximum(0 or <i>F_o</i> ²) + 2 * <i>F_c</i> ²]/3 | | |
| Shift/Err: | Less than 0.002 in the last cycle of refinement: | | |
| Resid. Electron Density: | +0.87 e _o ⁻ /Å ³ ; -0.52 e _o ⁻ /Å ³ | | |
| R1: | Σ(<i>F_o</i> - <i>F_c</i>)/Σ <i>F_o</i> | | |
| [<i>F_o</i> > 4σ(<i>F_o</i>); | N=5347]; | | = 0.0217 |
| [all reflctns; | N=6039]; | | = 0.0279 |
| wR2: | [Σw(<i>F_o</i> ² - <i>F_c</i> ²)/Σw(<i>F_o</i> ²)] ^{1/2} | | |
| [<i>F_o</i> > 4σ(<i>F_o</i>); | N=5347]; | | = 0.0507 |
| [all reflctns; | N=6039]; | | = 0.0538 |
| Goodness of fit: | [Σw(<i>F_o</i> ² - <i>F_c</i> ²)/Σw(<i>F_o</i> ²)] ^{1/2} | | |
| Remarks: | Refinement expression Σw(<i>F_o</i> ² - <i>F_c</i> ²) ² | | |

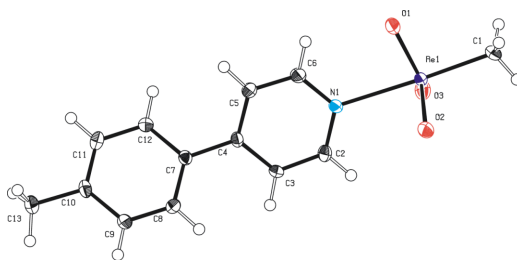
Compound 12



50% ellipsoids

| | | | |
|---|---|--|----------------------------------|
| Operator: | *** Herdtweck *** | | |
| Molecular Formula: | C ₂₈ H ₂₂ N ₂ O ₃ Re | | |
| Crystal Color / Shape: | Yellow fragment | | |
| Crystal Size: | Approximate size of crystal fragment used for data collection: 0.15 × 0.18 × 0.36 mm | | |
| Molecular Weight: | 606.68 a.m.u. | | |
| F ₀₀₀ : | 592 | | |
| Systematic Absences: | none | | |
| Space Group: | Triclinic | <i>P</i> 1̄ | (I.T.-No.: 2) |
| Cell Constants: | Least-squares refinement of 9899 reflections with the programs "APEX suite" and "SAINT" [1,2]; theta range 1.77° < θ < 25.44°; | | |
| | Mo(K _α); λ = 71.073 pm | | |
| | <i>a</i> = | 986.94(3) pm | α = 99.490(2)° |
| | <i>b</i> = | 1096.26(4) pm | β = 105.050(2)° |
| | <i>c</i> = | 1251.54(7) pm | γ = 112.906(1)° |
| | <i>V</i> = 1149.44(9) × 10 ⁶ pm ³ ; <i>Z</i> = 2; <i>D</i> _{calc} = 1.753 g cm ⁻³ ; Mos. = 0.72 | | |
| Diffractometer: | Kappa APEX II (Area Diffraction System; BRUKER AXS); rotating anode; graphite monochromator; 50 kV; 40 mA; λ = 71.073 pm | | |
| | Mo(K _α) | | |
| Temperature: | (-150 ± 1) °C; (123 ± 1) K | | |
| Measurement Range: | 1.77° < θ < 25.44°; h: -11/11, k: -13/13, l: -15/15 | | |
| Measurement Time: | 2 × 5 s per film | | |
| Measurement Mode: | measured: 9 runs; 2673 films / scaled: 9 runs; 2673 films | | |
| | <i>φ</i> - and <i>ω</i> -movement; Increment: Δ <i>φ</i> /Δ <i>ω</i> = 0.50°; dx = 40.0 mm | | |
| LP - Correction: | Yes [2] | | |
| Intensity Correction: | No/Yes; during scaling [2] | | |
| Absorption Correction: | Multi-scan; during scaling; μ = 5.316 mm ⁻¹ [2] | | |
| | Correction Factors: | <i>T</i> _{min} = 0.5292 | <i>T</i> _{max} = 0.7452 |
| Reflection Data: | 27800 | reflections were integrated and scaled | |
| | 27800 | reflections to be merged | |
| | 3955 | independent reflections | |
| | 0.039 | <i>R</i> _{int} : (basis <i>F</i> _o ²) | |
| | 3955 | independent reflections (all) were used in refinements | |
| | 3917 | independent reflections with <i>I</i> _o > 2σ(<i>I</i> _o) | |
| | 93.1 % | completeness of the data set | |
| | 299 | parameter full-matrix refinement | |
| | 13.2 | reflections per parameter | |
| Solution: | Direct Methods [3]; Difference Fourier syntheses | | |
| Refinement Parameters: | In the asymmetric unit: | | |
| | 33 | Non-hydrogen atoms with anisotropic displacement parameters | |
| Hydrogen Atoms: | In the difference map(s) calculated from the model containing all non-hydrogen atoms, not all of the hydrogen positions could be determined from the highest peaks. For this reason, the hydrogen atoms were placed in calculated positions (<i>d</i> _{C-H} = 95, 98 pm). Isotropic displacement parameters were calculated from the parent carbon atom (<i>U</i> _H = 1.2/1.5 <i>U</i> _C). The hydrogen atoms were included in the structure factor calculations but not refined. | | |
| | For neutral atoms and anomalous dispersion [4] | | |
| Atomic Form Factors: | no | | |
| Extinction Correction: | <i>w</i> ⁻¹ = σ ² (<i>F</i> _o ²) + (<i>a</i> * <i>P</i>) ² + <i>b</i> * <i>P</i> | | |
| Weighting Scheme: | with <i>a</i> : 0.0094; <i>b</i> : 1.3619; <i>P</i> : [Maximum(0 or <i>F</i> _o ²) + 2* <i>F</i> _c ²]/3 | | |
| Shift/Err: | Less than 0.002 in the last cycle of refinement: | | |
| Resid. Electron Density: | +1.12 e _o ⁻ /Å ³ ; -0.44 e _o ⁻ /Å ³ | | |
| R1: | Σ(<i>F</i> _o - <i>F</i> _c)/Σ <i>F</i> _o | | |
| [<i>F</i> _o > 4σ(<i>F</i> _o)]; | N=3917]; | | = 0.0139 |
| [all reflctns]; | N=3955]; | | = 0.0141 |
| wR2: | [Σw(<i>F</i> _o ² - <i>F</i> _c ²) ²]/Σw(<i>F</i> _o ²) ²] ^{1/2} | | |
| [<i>F</i> _o > 4σ(<i>F</i> _o)]; | N=3917]; | | = 0.0356 |
| [all reflctns]; | N=3955]; | | = 0.0358 |
| Goodness of fit: | [Σw(<i>F</i> _o ² - <i>F</i> _c ²) ² /(NO-NV)] ^{1/2} | | |
| Remarks: | Refinement expression Σw(<i>F</i> _o ² - <i>F</i> _c ²) ² | | |

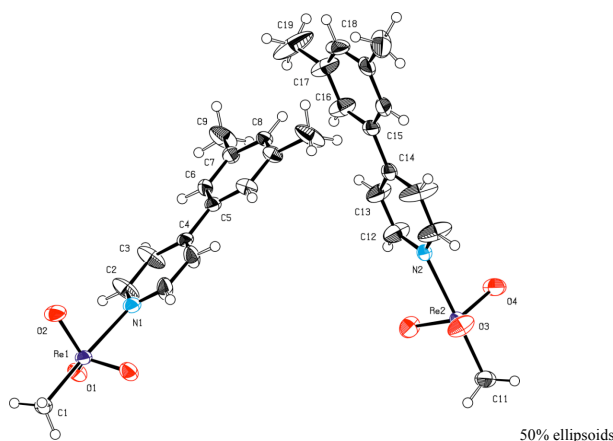
Compound 13



50% ellipsoids

| | | | |
|--|--|---|---------------------------|
| Operator: | *** Herdtweck *** | | |
| Molecular Formula: | C ₁₃ H ₁₄ N ₂ O ₃ Re | | |
| Crystal Color / Shape: | Yellow fragment | | |
| Crystal Size: | Approximate size of crystal fragment used for data collection: 0.15 × 0.20 × 0.38 mm | | |
| Molecular Weight: | 418.46 a.m.u. | | |
| F ₀₀₀ : | 792 | | |
| Systematic Absences: | h0l: l≠2n; 0k0: k≠2n | | |
| Space Group: | Monoclinic | <i>P</i> 2 ₁ / <i>c</i> | (I.T.-No.: 14) |
| Cell Constants: | Least-squares refinement of 3984 reflections with the programs "APEX suite" and "SAINT" [1,2]; theta range 1.86° < θ < 25.39°; | | |
| | Mo(Kα); λ = 71.073 pm | | |
| | <i>a</i> = | 1169.24(4) pm | |
| | <i>b</i> = | 1437.08(4) pm | β = 110.3695(14)° |
| | <i>c</i> = | 822.19(3) pm | |
| | <i>V</i> = 1295.13(8) × 10 ⁶ pm ³ ; <i>Z</i> = 4; <i>D</i> _{calc} = 2.146 g cm ⁻³ ; Mos. = 0.70 | | |
| Diffractometer: | Kappa APEX II (Area Diffraction System; BRUKER AXS); rotating anode; graphite monochromator; 50 kV; 40 mA; λ = 71.073 pm; Mo(Kα) | | |
| Temperature: | (-150±1) °C; (123±1) K | | |
| Measurement Range: | 1.86° < θ < 25.39°; h: -8/13, k: -17/15, l: -9/9 | | |
| Measurement Time: | 2 × 5 s per film | | |
| Measurement Mode: | measured: 2 runs; 421 films / scaled: 2 runs; 421 films | | |
| | φ- and ω-movement; Increment: Δφ/Δω = 0.50°; dx = 40.0 mm | | |
| LP - Correction: | Yes [2] | | |
| Intensity Correction: | No/Yes; during scaling [2] | | |
| Absorption Correction: | Multi-scan; during scaling; μ = 9.381 mm ⁻¹ [2] | | |
| Reflection Data: | Correction Factors: | T _{min} = 0.2789 | T _{max} = 0.7452 |
| | 5016 | reflections were integrated and scaled | |
| | 114 | reflections systematic absent and rejected | |
| | 4912 | reflections to be merged | |
| | 2260 | independent reflections | |
| | 0.028 | R _{int} (basis F _o ²) | |
| | 2260 | independent reflections (all) were used in refinements | |
| | 2196 | independent reflections with I _o > 2σ(I _o) | |
| | 95.5 % | completeness of the data set | |
| | 165 | parameter full-matrix refinement | |
| | 13.7 | reflections per parameter | |
| Solution: | Direct Methods [3]; Difference Fourier syntheses | | |
| Refinement Parameters: | In the asymmetric unit: | | |
| | 18 | Non-hydrogen atoms with anisotropic displacement parameters | |
| Hydrogen Atoms: | In the difference map(s) calculated from the model containing all non-hydrogen atoms, not all of the hydrogen positions could be determined from the highest peaks. For this reason, the hydrogen atoms were placed in calculated positions (d _{CH} = 95, 98 pm). Isotropic displacement parameters were calculated from the parent carbon atom (U _{CH} = 1.2/1.5 U _C). The hydrogen atoms were included in the structure factor calculations but not refined. | | |
| | For neutral atoms and anomalous dispersion [4] | | |
| Atomic Form Factors: | no | | |
| Extinction Correction: | w ¹ = σ ² (F _o ²) + (a*P) ² + b*P | | |
| Weighting Scheme: | with a: 0.0251; b: 1.0363; P: [Maximum(0 or F _o ²) + 2*F _c ²]/3 | | |
| Shift/Err: | Less than 0.002 in the last cycle of refinement: | | |
| Resid. Electron Density: | +1.12 e _p ⁻ /Å ³ ; -1.39 e _p ⁻ /Å ³ | | |
| R1: | Σ(F _o - F _c)/Σ F _o | | |
| [F _o > 4σ(F _o); | N=2196]; | | = 0.0218 |
| [all reflctns; | N=2260]; | | = 0.0225 |
| wR2: | [Σw(F _o ² - F _c ²) ² / Σw(F _o ²) ²] ^{1/2} | | |
| [F _o > 4σ(F _o); | N=2196]; | | = 0.0556 |
| [all reflctns; | N=2260]; | | = 0.0561 |
| Goodness of fit: | [Σw(F _o ² - F _c ²) ² / (NO-NV)] ^{1/2} | | = 1.144 |
| Remarks: | Refinement expression Σw(F _o ² - F _c ²) ² | | |

Compound 14



Operator: *** Herdtweck ***
Molecular Formula: C₁₄H₁₆N₂O₃Re
Crystal Color / Shape: Yellow needle
Crystal Size: Approximate size of crystal fragment used for data collection:
0.03 × 0.05 × 0.23 mm
Molecular Weight: 432.49 a.m.u.
F₀₀₀: 824
Systematic Absences: 0k0: k≠2n
Space Group: Monoclinic P 2₁/m (I.T.-No.: 11)
Cell Constants: Least-squares refinement of 9786 reflections with the programs "APEX suite" and "SAINT" [1,2]; theta range 1.08° < θ < 25.37°;
Mo(K_α); λ = 71.073 pm
a = 647.63(9) pm
b = 1165.2(2) pm β = 93.705(6)°
c = 1893.0(3) pm
V = 1425.5(4) · 10⁶ pm³; Z = 4; D_{calc} = 2.015 g cm⁻³; Mos. = 0.72
Diffractometer: Kappa APEX II (Area Diffraction System; BRUKER AXS); rotating anode; graphite monochromator; 50 kV; 40 mA; λ = 71.073 pm;
Mo(K_α)
Temperature: (-120±1) °C; (153±1) K
Measurement Range: 1.08° < θ < 25.37°; h: -7/7, k: -14/14, l: -22/22
Measurement Time: 2 × 5 s per film
Measurement Mode: measured: 6 runs; 3160 films / scaled: 6 runs; 3160 films
q- and ω-movement; Increment: Δq/Δω = 0.50°; dx = 40.0 mm
LP - Correction: Yes [2]
Intensity Correction: No/Yes; during scaling [2]
Absorption Correction: Multi-scan; during scaling; μ = 8.527 mm⁻¹ [2]
Correction Factors: T_{min} = 0.4010 T_{max} = 0.7452
Reflection Data: 35348 reflections were integrated and scaled
46 reflections systematic absent and rejected
35302 reflections to be merged
2741 independent reflections
0.047 R_{int}: (basis F_o²)
2741 independent reflections (all) were used in refinements
2592 independent reflections with I_o > 2σ(I_o)
99.9 % completeness of the data set
195 parameter full-matrix refinement
14.1 reflections per parameter
Solution: Direct Methods [3]; Difference Fourier syntheses
Refinement Parameters: In the asymmetric unit:
26 Non-hydrogen atoms with anisotropic displacement parameters
Hydrogen Atoms: In the difference map(s) calculated from the model containing all non-hydrogen atoms, not all of the hydrogen positions could be determined from the highest peaks. For this reason, the hydrogen atoms were placed in calculated positions (d_{C-H} = 95, 98 pm). Isotropic displacement parameters were calculated from the parent carbon atom (U₁₁ = 1.2/1.5 U_C). The hydrogen atoms were included in the structure factor calculations but not refined.
Atomic Form Factors: For neutral atoms and anomalous dispersion [4]
Extinction Correction: no
Weighting Scheme: w⁻¹ = σ²(F_o²) + (a*P)² + b*P
with a: 0.0000; b: 3.9102; P: [Maximum(0 or F_o²) + 2*F_c²]/3
Shift/Err: Less than 0.002 in the last cycle of refinement:
Resid. Electron Density: +1.09 e_p⁻/Å³; -1.30 e_p⁻/Å³
R1: Σ||F_o - |F_c|| / Σ|F_o| = 0.0186
[F_o > 4σ(F_o); N=2592]; = 0.0200
[all reflctns; N=2741];
wR2: [Σw(F_o² - F_c²)² / Σw(F_o²)²]^{1/2} = 0.0410
[F_o > 4σ(F_o); N=2592]; = 0.0416
[all reflctns; N=2741]; = 1.099
Goodness of fit: [Σw(F_o² - F_c²)² / (NO - NV)]^{1/2}
Remarks: Refinement expression Σw(F_o² - F_c²)²

References

- [1] APEX suite of crystallographic software. APEX 2 Version 2008.4. Bruker AXS Inc., Madison, Wisconsin, USA (2008).
- [2] SAINT, Version 7.56a and SADABS Version 2008/1. Bruker AXS Inc., Madison, Wisconsin, USA (2008).
- [3] Altomare, A.; Casciaro, G.; Giacovazzo, C.; Guagliardi, A.; Burla, M. C.; Polidori, G.; Camalli M. **SIR92**, *J. Appl. Cryst.* **1994**, *27*, 435-436.
- [4] International Tables for Crystallography, Vol. C, Tables 6.1.1.4 (pp. 500-502), 4.2.6.8 (pp. 219-222), and 4.2.4.2 (pp. 193-199), Wilson, A. J. C., Ed., Kluwer Academic Publishers, Dordrecht, The Netherlands, 1992.
- [5] Sheldrick, G. M. "SHELXL-97", University of Göttingen, Göttingen, Germany, (1998).
- [6] Spek, A. L. "PLATON", A Multipurpose Crystallographic Tool, Utrecht University, Utrecht, The Netherlands, (2009).
- [7] L. J. Farrugia, "WinGX (Version 1.70.01 January 2005)", *J. Appl. Cryst.* **1999**, *32*, 837-838.

9 Appendix B

This section contains supplementary information to Chapter 6:
The $[\eta^5\text{-(C}_5\text{H}_5)\text{Mo(CO)}_3\text{R}]$ Compound Class: Similarities and Differences

=====

S U P P L E M E N T A R Y M A T E R I A L

=====

Table S1 - Crystal Data and Details of the Structure Determination
for: **HauSi4-AP7073-123**

| Crystal Data | | | |
|---|------------|---------------------------|-------------|
| Formula | | C6 H5 F3 Mo O3 | |
| Formula Weight | | 278.04 | |
| Crystal System | | Monoclinic | |
| Space group | | C2/c | (No. 15) |
| a, b, c [Angstrom] | 20.5911(3) | 6.9325(1) | 12.3919(2) |
| alpha, beta, gamma [deg] | 90 | 117.372(1) | 90 |
| V [Ang**3] | | | 1570.87(4) |
| Z | | | 8 |
| D(calc) [g/cm**3] | | | 2.351 |
| Mu(MoKa) [/mm] | | | 1.693 |
| F(000) | | | 1072 |
| Crystal Size [mm] | | 0.08 x 0.09 x | 0.34 |
| Data Collection | | | |
| Temperature (K) | | | 123 |
| Radiation [Angstrom] | | MoKa | 0.71073 |
| Theta Min-Max [Deg] | | | 2.2, 25.4 |
| Dataset | | -24: 24 ; -8: 8 ; -14: 14 | |
| Tot., Uniq. Data, R(int) | | 8754, 1447, | 0.032 |
| Observed data [I > 2.0 sigma(I)] | | | 1266 |
| Refinement | | | |
| Nref, Npar | | | 1447, 118 |
| R, wR2, S | | 0.0194, 0.0448, | 1.04 |
| w = 1/[s^2^(Fo^2)+(0.0193P)^2+2.5435P] where P=(Fo^2+2Fc^2)/3 | | | |
| Max. and Av. Shift/Error | | | 0.00, 0.00 |
| Min. and Max. Resd. Dens. [e/Ang^3] | | | -0.30, 0.60 |

A clear intense yellow fragment-like specimen of C6H5F3MoO3, approximate dimensions 0.077 mm x 0.085 mm x 0.343 mm, was used for the X-ray crystallographic analysis. The X-ray intensity data were measured.

A total of 2194 frames were collected. The total exposure time was 3.05 hours. The frames were integrated with the Bruker SAINT software package using a narrow-frame algorithm. The integration of the data using a monoclinic unit cell yielded a total of 8754 reflections to a maximum θ angle of 25.40° (0.83 Å resolution), of which 1447 were independent (average redundancy 6.050, completeness = 99.9%, Rint = 3.18%, Rsig = 2.38%) and 1266 (87.49%) were greater than 2 σ (F2). The final cell constants of a = 20.632(11) Å, b = 6.947(3) Å, c = 12.417(6) Å, β = 117.377(9)°, volume = 1580.(4) Å³, are based upon the refinement of the XYZ-centroids of 90 reflections above 20 σ (I) with 8.882° < 2 θ < 52.04°. Data were corrected for absorption effects using the multi-scan method (SADABS). The ratio of minimum to maximum apparent transmission was 0.926.

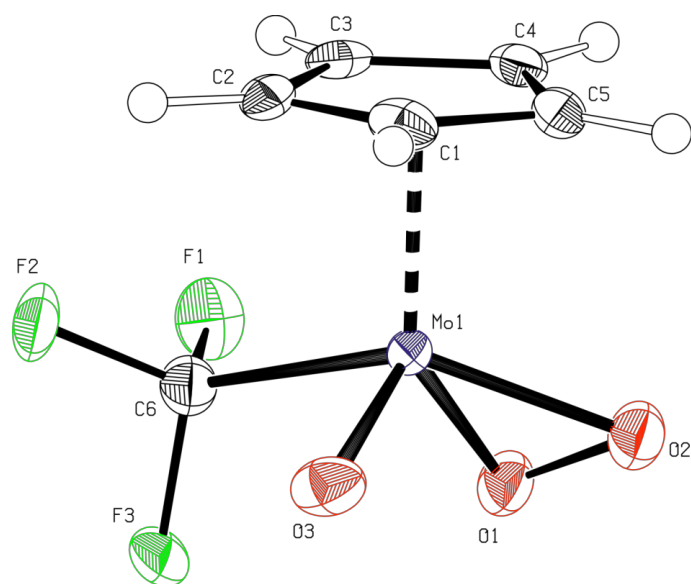
Table S2 - Bond Distances (Angstrom) for: **HauSi4-AP7073-123**

| | | | | | |
|-----|-----|-----------|----|-----|-----------|
| Mo1 | -O1 | 1.922 (2) | O1 | -O2 | 1.440 (3) |
| Mo1 | -O2 | 1.933 (2) | C1 | -C2 | 1.390 (4) |
| Mo1 | -O3 | 1.689 (2) | C1 | -C5 | 1.413 (4) |
| Mo1 | -C1 | 2.401 (2) | C2 | -C3 | 1.441 (5) |
| Mo1 | -C2 | 2.378 (3) | C3 | -C4 | 1.390 (4) |
| Mo1 | -C3 | 2.395 (3) | C4 | -C5 | 1.420 (4) |
| Mo1 | -C4 | 2.415 (3) | C1 | -H1 | 0.9500 |
| Mo1 | -C5 | 2.359 (2) | C2 | -H2 | 0.9500 |
| Mo1 | -C6 | 2.197 (3) | C3 | -H3 | 0.9500 |
| F1 | -C6 | 1.350 (4) | C4 | -H4 | 0.9500 |
| F2 | -C6 | 1.354 (3) | C5 | -H5 | 0.9500 |
| F3 | -C6 | 1.356 (4) | | | |

Table S3 - Bond Angles (Degrees) for: **HauSi4-AP7073-123**

| | | | | | | | |
|-----|------|-----|-------------|-----|-----|-----|------------|
| O1 | -Mo1 | -O2 | 43.88 (9) | Mo1 | -O2 | -O1 | 67.68 (12) |
| O1 | -Mo1 | -O3 | 110.21 (10) | Mo1 | -C1 | -C2 | 72.20 (16) |
| O1 | -Mo1 | -C1 | 155.26 (10) | Mo1 | -C1 | -C5 | 71.13 (14) |
| O1 | -Mo1 | -C2 | 148.47 (11) | C2 | -C1 | -C5 | 107.7 (3) |
| O1 | -Mo1 | -C3 | 114.28 (10) | Mo1 | -C2 | -C1 | 73.97 (17) |
| O1 | -Mo1 | -C4 | 102.23 (10) | Mo1 | -C2 | -C3 | 73.07 (17) |
| O1 | -Mo1 | -C5 | 120.75 (9) | C1 | -C2 | -C3 | 108.1 (3) |
| O1 | -Mo1 | -C6 | 76.86 (10) | Mo1 | -C3 | -C2 | 71.79 (18) |
| O2 | -Mo1 | -O3 | 108.15 (10) | Mo1 | -C3 | -C4 | 74.02 (18) |
| O2 | -Mo1 | -C1 | 115.94 (9) | C2 | -C3 | -C4 | 107.8 (3) |
| O2 | -Mo1 | -C2 | 140.91 (10) | Mo1 | -C4 | -C3 | 72.40 (17) |
| O2 | -Mo1 | -C3 | 117.46 (10) | Mo1 | -C4 | -C5 | 70.53 (17) |
| O2 | -Mo1 | -C4 | 86.74 (10) | C3 | -C4 | -C5 | 107.8 (3) |
| O2 | -Mo1 | -C5 | 85.10 (9) | Mo1 | -C5 | -C1 | 74.36 (14) |
| O2 | -Mo1 | -C6 | 120.58 (10) | Mo1 | -C5 | -C4 | 74.90 (14) |
| O3 | -Mo1 | -C1 | 88.48 (11) | C1 | -C5 | -C4 | 108.4 (2) |
| O3 | -Mo1 | -C2 | 96.99 (11) | Mo1 | -C6 | -F1 | 115.1 (2) |
| O3 | -Mo1 | -C3 | 131.20 (10) | Mo1 | -C6 | -F2 | 115.5 (2) |
| O3 | -Mo1 | -C4 | 145.30 (9) | Mo1 | -C6 | -F3 | 109.4 (2) |
| O3 | -Mo1 | -C5 | 113.70 (10) | F1 | -C6 | -F2 | 105.8 (3) |
| O3 | -Mo1 | -C6 | 93.85 (12) | F1 | -C6 | -F3 | 105.3 (2) |
| C1 | -Mo1 | -C2 | 33.83 (11) | F2 | -C6 | -F3 | 104.8 (3) |
| C1 | -Mo1 | -C3 | 57.12 (10) | Mo1 | -C1 | -H1 | 122.00 |
| C1 | -Mo1 | -C4 | 56.99 (10) | C2 | -C1 | -H1 | 126.00 |
| C1 | -Mo1 | -C5 | 34.52 (10) | C5 | -C1 | -H1 | 126.00 |
| C1 | -Mo1 | -C6 | 119.22 (10) | Mo1 | -C2 | -H2 | 119.00 |
| C2 | -Mo1 | -C3 | 35.14 (11) | C1 | -C2 | -H2 | 126.00 |
| C2 | -Mo1 | -C4 | 56.99 (10) | C3 | -C2 | -H2 | 126.00 |
| C2 | -Mo1 | -C5 | 57.10 (10) | Mo1 | -C3 | -H3 | 120.00 |
| C2 | -Mo1 | -C6 | 85.94 (11) | C2 | -C3 | -H3 | 126.00 |
| C3 | -Mo1 | -C4 | 33.59 (9) | C4 | -C3 | -H3 | 126.00 |
| C3 | -Mo1 | -C5 | 57.04 (9) | Mo1 | -C4 | -H4 | 123.00 |
| C3 | -Mo1 | -C6 | 77.95 (11) | C3 | -C4 | -H4 | 126.00 |
| C4 | -Mo1 | -C5 | 34.58 (10) | C5 | -C4 | -H4 | 126.00 |
| C4 | -Mo1 | -C6 | 105.43 (12) | Mo1 | -C5 | -H5 | 117.00 |
| C5 | -Mo1 | -C6 | 134.97 (12) | C1 | -C5 | -H5 | 126.00 |
| Mo1 | -O1 | -O2 | 68.45 (12) | C4 | -C5 | -H5 | 126.00 |

Figure F1 - Ortep drawing with 50% ellipsoids for: **HauSi4-AP7073-123**



Scientific contributions

Journal publications

1. Simone A. Hauser, Valentina Korinth, Eberhardt Herdtweck, Mirza Cokoja, Wolfgang A. Herrmann, Fritz E. Kühn, *Eur. J. Inorg. Chem.*, **2010**, 4083-4090. (Chromophoric Lewis Base Adducts of Methyltrioxorhenium: Synthesis, Catalysis and Photochemistry)
2. Simone A. Hauser, Mirza Cokoja, Markus Drees, Fritz E. Kühn, *J. Mol. Catal. A*, **2012**, 363-364, 237-244. (Catalytic Olefin Epoxidation with a Fluorinated Organomolybdenum Complex)
3. Simone A. Hauser, Mirza Cokoja, Fritz E. Kühn, *Cat. Sci. Technol.*, **2013**, accepted. (Epoxidation of Olefins with Homogeneous Catalysts – *quo vadis?*)
4. Simone A. Hauser, Janos Mink, Alexander Pöthig, Fritz E. Kühn, *manuscript in preparation*. (The $[\eta^5\text{-}(\text{C}_5\text{H}_5)\text{Mo}(\text{CO})_3\text{R}]$ Compound Class: Similarities and Differences)
5. Simone A. Hauser, Marlene Möller, Mirza Cokoja, Alexander Pöthig, Fritz E. Kühn, *manuscript in preparation*. (Immobilisation of molecular molybdenum complexes on different solid supports: Investigation of the performance in heterogeneous olefin epoxidation and comparison to homogeneous catalysts)

Presentations and posters at conferences

1. Mechanistic Studies of the Epoxidation of Olefins Catalyzed by Molecular Molybdenum Complexes.
Simone A. Hauser, Mirza Cokoja, Wolfgang A. Herrmann, Fritz E. Kühn, 241st American Chemical Society National Meeting, March 27-31, 2011, Anaheim, CA, USA.
2. Mechanistic Studies of the Epoxidation of Olefins Catalyzed by Molecular Molybdenum Complexes.
Simone A. Hauser, Mirza Cokoja, Fritz E. Kühn, XIX EuCheMS Conference on Organometallic Chemistry, July 3-7, 2011, Toulouse, France.
3. Catalytic Olefin Epoxidation with a Fluorinated Organomolybdenum Complex.
Simone A. Hauser, Mirza Cokoja, Markus Drees, Fritz E. Kühn, XXV International Conference on Organometallic Chemistry, September 2-7, 2012, Lisbon, Portugal.
4. Immobilisation of Molecular Olefin Epoxidation Catalysts on Functionalised Metal-Organic Frameworks.
Simone A. Hauser, Marlene Möller, Mirza Cokoja, Fritz E. Kühn, MOF2012, September 16-19, 2012, Edinburgh, United Kingdom.

Echinger Straße 9a
80805 München
Deutschland

Geburtsdatum: 24. Januar 1985
Heimatorte: Wädenswil und Zürich (CH)

AUSBILDUNG

- 06.2009 - 11.2012 Technische Universität München (Deutschland), Promotion an der Fakultät für Chemie mit dem Titel: „Organorhenium and Organomolybdenum Oxides: Synthesis and Application as Olefin Epoxidation Catalysts”
- 08.2008 - 02.2009 Universität Lund (Schweden), Masterarbeit mit dem Titel: „Catalytic potential of transition metal carbonyl compounds containing ferrocenyl based phosphine ligands in asymmetric synthesis”
(Note: 5.50/6)
- 09.2007 - 02.2009 Eidgenössische Technische Hochschule Lausanne (EPFL, Schweiz), Master-Studium in Molekularer und Biologischer Chemie
(Note: 5.35/6)
- 10.2004 - 07.2007 Eidgenössische Technische Hochschule Lausanne (EPFL, Schweiz), Bachelor-Studium in Chemie und Chemieingenieurwesen
(Note: 5.24/6)
- 08.1998 - 06.2004 Gymnasium in Zug (Schweiz), Maturität MAR Latein/Englisch
(Note: 5.61/6)
- 08.1992 - 07.1998 Primarschule in Zug (Schweiz)

SPRACHKENNTNISSE

Deutsch: Muttersprache
Französisch: fließende Konversation, schriftlich fehlerfrei
Englisch: fließende Konversation, schriftlich fehlerfrei

STIPENDIEN

- 09.2009 - 12.2012 Promotionsstipendium des Elitenetzwerks Bayern, Doktorandenkolleg NanoCat
- 27.06. - 02.07.2010 Teilnahme als Nachwuchswissenschaftlerin an der 60. Nobelpreisträgertagung Lindau
- 08.2008 - 12.2008 Erasmus-Stipendium der EPFL für einen Forschungsaufenthalt an der Universität Lund (Schweden)